AN ABSTRACT OF THE DISSERTATION OF

Erin Madeen for the degree of Doctor of Philosophy in Toxicology presented on September 1, 2015.

Title: Translational Studies of the High Molecular Weight Polycyclic Aromatic Hydrocarbon, Dibenzo[*def,p*] Chrysene; Carcinogenesis and Metabolism

Abstract approved:

_____

David E. Williams

The objective of this work is to add to the body of translational data between high dose animal model research and the environmentally relevant human metabolism of the persistent pollutant dibenzo[*def,p*]chrysene (DBC). We furthered the knowledge of gene/exposure interactions by determining the carcinogenesis risk based on Cyp1b1 genotype following *in utero* DBC exposure in mice, finding no difference in lung carcinogesis by genotype. Cyp1b1 wild-type mice suffered mortality due to aggressive T-Cell Accute Lymphoblastic Leukemia (T-ALL), while Cyp1b1 null and CYP1B1 transgenic mice lack susceptibility to T-ALL. We also determined a link for Cyp1b1 status and fertility status, with a particular vulnerability in Cyp1b1 wild-type male mice fetally exposed to DBC. Female mice were found to have depleted primordial and primary follicle reserves in both Cyp1b1 wild-type and Cyp1b1 null mice. Further research will determine if the extent of depletion is similar across genotypes.

In addition, sensitive accelerator mass spectrometry (AMS) was utilized to detect the metabolism of DBC (and BaP) by human volunteers following environmentally relevant exposures. The human PK of DBC validated rodent based PB/PK models generated to represent human metabolism for risk assessment. DBC appeared quickly in plasma, with the majority eliminated quickly over 24 hours and a slower elimination period to 72 hours. The PD of DBC provided evidence that DBC is rapidly biotransformed to metabolites circulating in plasma. The products of three or more bio-transformations (tetrols and beyond) were not present in the plasma, indicating that they are quickly converted to conjugated species and eliminated from the plasma compartment. Urine contained primarily DBC metabolites that had undergone two transformations or more (diols, tetrols, and a putative dione). The majority of these species exist as conjugated metabolites in urine.

This body of work furthers the field of PAH translation by addressing disease and disease prevention endpoints from PAH exposure in rodent laboratory research models. Additionally, we are addressing human risk by removing the translation element and directly measuring PAH metabolism in humans from the oral route of exposure by taking a FDA IND “phase 0” approach to pharmacokinetics and pharmacodynamics.

Translational Studies of the High Molecular Weight Polycyclic Aromatic Hydrocarbon, Dibenzo[*def,p*] Chrysene; Carcinogenesis and Metabolism

by
Erin Madeen

A DISSERTATION

submitted to

Oregon State University

in partial fulfillment of
the requirements for the
degree of

Doctor of Philosophy

Presented September 1, 2015
Commencement June 2016

Doctor of Philosophy dissertation of Erin Madeen presented on September 1, 2015

APPROVED:

Major Professor, representing Toxicology

Head of the Department of Environmental and Molecular Toxicology

Dean of the Graduate School

I understand that my dissertation will become part of the permanent collection of Oregon State University libraries. My signature below authorizes release of my dissertation to any reader upon request.

Erin Madeen, Author

ACKNOWLEDGEMENTS

It has been a privilege for which I am very grateful to have been trainee of the Superfund Research Program (SRP). The support, resources, training, and opportunities that the SRP provides to students have been invaluable. The awareness of global environmental pollution and research to address that pollution has been inspiring and has helped me keep focus during the more challenging periods of my graduate career.

The unconditional support of Dr. David Williams, the most laid back PI a student could ask for, has provided me the freedom to explore and pursue projects that interest me as I have found my niche in the broad field of toxicology. All AMS analyses was completed on site at Lawrence Livermore National Laboratory with continuous support and guidance from Teressa Castro and Drs. Ken Turteltaub and Graham Bench. LNNL analysis was under the mentorship of Dr. Ted Ognibene, who deserves sainthood for his patience and grace. Expert pharmacokinetic/ pharmacodynamic training and assistance has been provided by Drs. Rick Corley and Mark Christensen. Histomorphological and reproductive toxicology training were provided by Drs. Christiane Löhr and Ulrike Luderer, both of whom have spent countless hours bouncing ideas, in person training, and providing mentorship and counsel.

My graduate committee, including Drs. William Baird, Christiane Löhr, Emily Ho, Ramesh Sagili, and David Williams, provided support and mentorship as well as much needed reality checks on pertinent matters such as time line and the need for focus. I'm grateful for the advice and recommendations that they have provided.

The open door/open lab layout of the Linus Pauling Institute has provided an excellent training and working environment. Dr. Balz Frei was quick to provide help and references. Lisbeth Siddens has provided detailed technical training and friendship. Tammie McQuistan and Drs. Sharon Krueger and Pat Iverson made the challenge of FDA IND compliance possible and successful. It was a pleasure to work with Dr. Tod Harper as my go-to "How do I do this?" reference on all things. Our lab super students Hannah You, David Sampson, Alex Van Scoyk, and Jessica Hummel thought that they were getting training and mentorship, but in reality, they probably provided me with more training and experience than they received in return.

My professional training would not have been possible without the grounding and perspective provided by the freaks and misfits that I've called friends. It has been said that "When the going gets weird, the weird turn professional" [1]. It has been comforting to be surrounded by so many passionate professionals who have maintained a childlike enthusiasm and a wonder for the natural world as it exists outside of Microsoft Office Suite ® ©.

CONTRIBUTION OF AUTHORS

Chapter 2: Christiane Löhr provided detailed histomorphological analysis. Hannah You provided mouse husbandry, generated cDNA data, and helped with necropsy and tissue collections. Lisbeth E. Siddens helped with mouse gavage, tissue collections, study design, and Cyp1b1 expression analysis. Sharon K. Krueger provided study design, experimental animal generation, and ensuring compliance. Roderick H. Dashwood and Emily Ho provided study design support. Frank J. Gonzalez generated the Cyp1b1 null and CYP1B1 humanized mouse lines. William M. Baird provided biochemical advice on DBC metabolism. Lisa Bramer provided detailed statistical analysis of data from study endpoints. Katrina M. Waters provided assistance with interpretation of statistical data. David E. Williams assisted with manuscript writing, study design and technical advice.

Chapter 3: Richard A. Corley and Susan Crowell provided training and advice on pharmacokinetic analysis. Kenneth Turteltaub, Ted Ognibene, and Mike Malfatti provided AMS analysis. Tammie J. McQuistan provided sample preparation support. Mary Garrard provided clinical coordination and clinical nursing support. Dan Sudakin provided medical supervision as a licensed medical doctor. David E. Williams provided study design, technical advice, and manuscript preparation assistance.

Chapter 4: Ted Ognibene provided AMS analysis and data analysis. Rick Corley provided pharmacokinetic assistance. Mark Christensen provided pharmacodynamics training and analysis. Tammie McQuistan provided sample preparation assistance. Ken Turteltaub and David E. Williams provided study design and project support.

TABLE OF CONTENTS

TABLE OF CONTENTS (Continued)

Page

TABLE OF CONTENTS (Continued)

Page

LIST OF FIGURES

Figure Page

LIST OF FIGURES (Continued)

Figure Page

LIST OF TABLES

CHAPTER 1

GENERAL INTRODUCTION

1.1 DBC Chemistry and Mechanisms of Biological Action

Dibenzo[*def,p*]chrysene (DBC), also known as dibenzo[*a,l*]pyrene (DBP), is a high molecular weight (302.4 g/mol) polycyclic aromatic hydrocarbon (PAH) that has been found to be highly genotoxic, with a BaP equivalence factor (BaPeq) of 10-30 [2]. It is a six ring PAH with both a bay and a fjord region [3]. DBC is highly lipophilic with a K_{ow} of 7.71, and is non-volatile with a Henry's Law Constant of $1.41X10^{-8}$ atm m^3/mole [4,3]

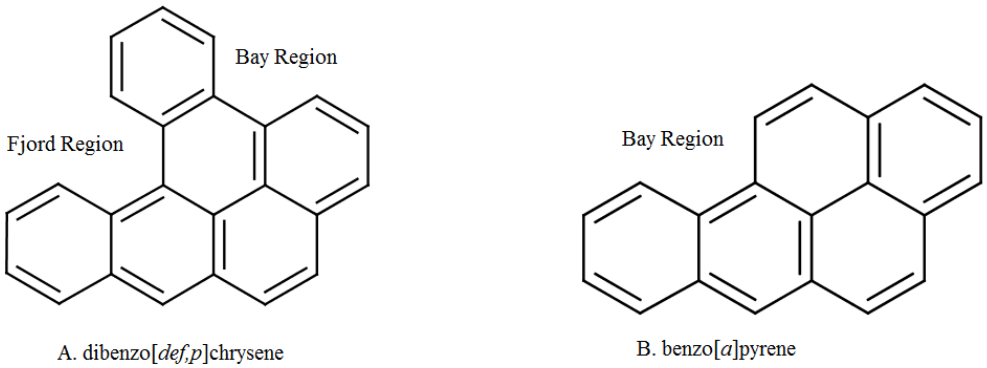

Fig.1.1: DBC and B[a]P Structure

Both DBC and B[a]P are bay region containing PAHs. DBC additionally contains a deeper fjord region that leads to a bent conformation.

The bay and fjord regions introduce steric hindrance in PAHs, leading to a bent confirmation relative to the planar PAHs lacking these regions. X-ray diffraction of DBC shows that the molecule is considerably distorted so that it is non-planar with an angle of 27.6 degrees between the outermost rings and a widening of C-C-C bond

angles in the fjord region [3]. The bay region of DBC is distorted by up to 6 degrees. The resulting molecular crowding can create a slight dipole. In a new-born mouse model, the tumorigenicity of PAH diol-epoxides were found to be enhanced by steric constraints present when the epoxide ring is part of a fjord region or is attached to a fused ring system [5].

Due to high potency in preclinical models, DBC has often been utilized as a carcinogen [5, 6]. DBC, and other carcinogenic PAHs do occur in complex mixtures in the environment [7]. Major sources of preventable PAH exposures are tobacco smoking and indoor non-ventilated solid fuel stove cooking and heating [8, 9]. In non-smokers, PAH exposure can occur via dermal, inhalation, and oral routes [10]. Exposure to low molecular weight PAHs, those with three rings and below, occurs primarily through dermal and inhalation due to relatively high volatility [11]. Exposure to high molecular weight PAHs, those with four rings and above, occurs primarily through the oral route as a contaminate of food or bound to particulate matter [12, 13]. Dietary exposure was summarized by the International Agency for Research on Cancer (IARC). Food was determined to be the major source of intake of PAHs for the general population. Estimates of PAH intake from food vary widely, ranging from a few nanograms to a few micrograms per person per day. Sources of PAHs in the diet include barbecued/grilled/broiled and smoke cured meats; roasted, baked and fried foods (high temperature heat processing); breads, cereals and grains (at least in part from gas/flame drying of grains); and vegetables grown in

contaminated soils or with surface contamination from atmospheric fallout of PAHs [14].

Neonatal exposures in human were assessed from a risk assessment perspective utilizing molecular epidemiology. PAH adduct levels are correlated with environmental PAH exposure and molecular biomarkers [15-17]. Children exposed as fetuses were found to have reduced weight and head circumference, risk factors for several adult onset-diseases [18, 19]. Increasing PAH exposure correlates with increasing chromosome aberrations in fetal cord blood, indicating risk for carcinogenesis later in life [20, 21]. Prenatal exposures to environmental PAHs lead to changes in brain white to grey matter ratios in early childhood, indicative of lower cognitive potential [22].

Techniques to reliably synthesize and distinguish DBC from dibenzo[*a*,*e*]fluoranthene were not available until 1968 [23, 24]. DBC is potent carcinogen by dermal, oral, and transplacental exposures [25-28]. In controlled rodent transplacental DBC exposures, offspring develop T-cell acute lymphoblastic leukemia (T-ALL). The American Cancer Society estimates that in 2015 about 6,250 new cases of ALL (3,100 in males and 3,150 in females) and about 1,450 deaths from ALL (800 in males and 650 in females) will occur [29]. The risk for developing ALL is highest in children younger than 5 years of age. The risk then declines slowly until the mid-20s, and begins to rise again slowly after age 50. Overall, about 4 of every 10 cases of ALL are in adults. The average person’s lifetime risk of getting ALL is less

than 1 in 750. The risk is slightly higher in males than in females, and higher in whites than in African Americans. Most cases of ALL occur in children, but most deaths from ALL (about 4 out of 5) occur in adults [29]. ALL is divided into several sub-classes, believed to be of different origins, that are treated with different therapies [30]. FBXW7 and PTEN were identified as commonly deleted genes both in murine lymphomas and in human T-cell acute lymphoblastic leukaemia/lymphoma (T-ALL). The murine cancers acquire widespread recurrent amplifications and deletions targeting loci syntenic to those not only in human T-ALL but also in diverse human haematopoietic, mesenchymal and epithelial tumors. This indicates that murine and human tumors experience common biological processes driven by similar genetic events in their progression [31].

1.2 *in utero* DBC Exposure Mouse Models Of Carcinogenesis

Maternal oral exposure and subsequent transplacental fetal exposures has been found to generate adult onset diseases/cancers in mice [32, 33]. The mouse *in utero* model of DBC induced carcinogenesis includes an F_1 generation containing both genotypes of aryl hydrocarbon receptor (Ahr), Ahr^{d} is less responsive to dioxin than the $Ahr^{b\text{-}1}$ allele [34-36]. The F_1 is generated by crossing B6/129 ($Ahr^{b\text{-}1/d}$) dams with 129SF ($Ahr^{d/d}$) sires. Gestation day 0 is determined by identification of a vaginal plug. On gestation day 17, the dam is administered an oral gavage of DBC, typically 15 mg/kg bw. The offspring are born on gestation day 19. Litters are comprised of a 50:50 mix of $Ahr^{b\text{-}1/d}$ and $Ahr^{d/d}$ pups. Starting at 12 weeks of age, pups begin to succumb to an aggressive T-cell lymphoblastic leukemia (T-ALL). The remaining pups are collected

at various time points for analysis with a terminal 10 month time point for carcinogenesis analysis including cancers/diseases of the lungs, thymus, liver, and gonad.

In a B6129SF1/J mouse model, DBC pharmacokinetics were compared between naïve and pregnant mice exposed to 15 mg/kg by oral gavage [37]. The C_{max} values of DBC, diol, and tetrol metabolites were found to be higher in pregnant mice verses naïve mice and peak concentrations were reached between 2 to 4 hours, with the exception of fat, which reached maximal concentrations between 12 to 24 hours [37]. Peak concentrations of DBC were elevated in blood (3.72-fold), liver (3.75-fold), and lung (1.35 fold) in pregnant animals compared to naïve mice, resulting in higher area under the curves (AUCs) for these tissues in pregnancy of, 2.2, 2.8, and 1.3 fold, respectively. The half-life of DBC elimination in all tissues was reduced in pregnant vs naïve mice [37]. DBC-11,12-diol concentrations were elevated in pregnant vs naïve mice in blood, lung, and fat. DBC-11,12,13,14-tetrol maximal concentrations were similar between pregnant and naïve animals, while naïve mice had a greater AUC. There was a 2-10-fold reduction in enzymatic activity across over 30 PAH metabolizing enzymes in pregnant vs naïve mice [37].

Maternal verses fetal DBC distribution was assessed utilizing ^{14}C-DBC (15 mg/300 µCi/kg bw) dosed by gavage on gestation day 17 [38]. The distribution of DBC in maternal and pup tissues was determined at 2, 4, 6, and 8 hour post dosing. The maternal feces had the highest concentration of DBC at 9% of that administered at 8

hours. Maternal plasma maintained 1500 ng DBC/µL from 2-6 hours before decreasing to 560 ng DBC/µL at 8 hours. All analyzed maternal tissues, with the exception of placenta, followed the time course of maintaining or increasing in concentration until a decrease at 8 hours. Placenta reached a C_{max} of 3200 ng/g at 8 hours. Fetal plasma reached a C_{max} of 320 ng/mL at 6 hours before a dramatic decrease in concentration at 8 hours. The remaining fetal tissues plateaued or increased from 6 to 8 hours [38].

In an HPLC analysis of pharmacokinetics, fetal tissues were found to be 1 to 2 orders of magnitude below maternal tissues for DBC, but closely resembled maternal concentrations for metabolites [37]. DBC maximum concentrations were reached in the placenta and fetus at 3 hours while the DBC-11,12-diol peaked at 6 hours. DBC concentrations were found to be 10-fold higher in the placenta than the fetus, while DBC-11,12-diol was 2 fold higher in placenta. Fetal concentrations of DBC were found to be 1-100 x lower than maternal blood, while DBC-11,12-diol was similar or elevated relative to maternal blood. In summary, it was determined that the fetus exhibits delayed tissue absorption relative to the maternal dam and that the total ng DBC/g tissue concentrations of the fetus was approximately 10 fold less than that of the dam [38].

Maternal Cyp1b1 activity in liver was assessed on gestation day 17, following dietary intervention with caffeine, green tea, decaffeinated green tea, or EGCG [39]. Over a two-fold increase in Cyp1b1 activity was found relative to control with caffeinated

green tea ($p = 0.01$) and caffeine ($p = 0.024$). A proposed mechanism of phytointervention with these compounds is the increase in Cyp1b1 expression in the maternal liver, reducing bioavailability to the fetus.

Lactational exposure was also assessed in this model. Pups were born to mothers gavaged at DBC 15 mg/kg bw or corn oil controls. At birth, pups were cross-fostered to one of three groups, DBC: corn oil, DBC: DBC, or corn oil: DBC. The percent survival of DBC:DBC, DBC: corn oil, and corn oil: DBC was 25.5, 60.0, and 91.1, respectively [32]. Of the animals that survived to 10 months of age, the DBC: DBC, DBC: corn oil, corn oil: DBC groups developed 14, 11, and 3 lung tumors, respectively per animal. This same fetal: lactational cross-foster experiment was recreated with the dam receiving 15 mg/300 μCi/kg bw ^{14}C-DBC. The pups were collected at 21 days postpartum and tissues were analyzed by ^{14}C via scintillation counting. No significant differences were found between groups, indicating that by 21 days the majority of ingested DBC had been eliminated from tissues [38]. In summary, the majority of exposure is believed to be from transplacental origin, occurring in the 48 hour window between maternal dosing on gestation day 17 and birth on gestation day 19. However, sufficient lactational exposure to initiate disease may have occurred due to the 0.9% mortality and average of 3 lung tumors per animal in the corn oil: DBC group, no significance was determined as there was no corn oil: corn oil group for comparison [32].

The effect of the "responsive" Ahr^{b-1} allele (expressed as a hemizygote $Ahr^{b-1/d}$) vs the "non-responsive" "human like" $Ahr^{d/d}$ allele on DBC mortality and carcinogenesis has been assessed in several studies. Ahr binding is one mechanism proposed for PAH activation that results in induction of cytochrome P4501b1 and increased PAH activation [40]. $Ahr^{d/d}$ pups born to $Ahr^{b-1/d}$ mothers had the lowest mortality from T-ALL, presumably due to maternal metabolism of DBC reducing the amount of DBC available to cross the placental barrier and the reduced activation by the less responsive pup $Ahr^{d/d}$ for any DBC that does cross the placenta. Differential metabolism based on fetal Ahr status was not detected in pharmacokinetic analysis [37]. In conclusion, the role of Ahr status in DBC response is unclear.

The survival endpoint was typically assessed from a 15 mg/kg DBC dose with or without phytointervention. Mortality is from an aggressive T-Cell lymphoblastic leukemia (T-ALL) starting at 6 weeks of age, with the majority of mortality from approximately 12 to 16 weeks of age. Pups with $Ahr^{d/d}$ alleles were found to have reduced mortality when the maternal alleles were $Ahr^{b-1/d}$ [33]. When the maternal allele was $Ahr^{b-1/d}$ and the fetal allele was $Ahr^{b-1/d}$ there was 10-20% less survival relative to pup $Ahr^{d/d}$ following *in utero* and/or lactational exposure [32]. When a DBC dose of 3.75 mg/kg was administered on each of four gestation days 5, 9, 13 and 17, T-All and subsequent mortality did not occur in any genotype [38]. When the $Ahr^{b-1/d}$ dam was dosed with 15 mg/kg DBC, the fetal Ahr genotype at times led to a differential mortality response [32, 33, 41], and at times did not [42, 43]. Offspring mortality was reduced with the supplementation of maternal diet with caffeine,

caffeinated green tea, chlorophyllin (co-gavage), or indole-3-carbinole [39, 41, 42]. When the B6129 model was null for cyp1b1, appreciable T-ALL and mortality did not occur [44].

The incidence of lung nodules, histologically determined to be adenoma, hyperplasia, or adenocarcinoma, following DBC *in utero* exposure was assessed. When the maternal dose was 15 mg/kg without intervention, the percent incidence of lung nodules was consistently over 95%, regardless of Ahr status in survivors of T-ALL [32, 33, 41, 42, 44]. When the maternal dose was 3.75 mg/kg on each of gestation days 5, 7, 9, and 13, the offspring presented with 80% incidence of lung nodules [38]. A maternal dose of 1 mg/kg on gestation day 17 resulted in a 25.6% tumor incidence and 50 mg/kg benzo[a]pyrene (BaP) on gestation day 17 resulted in 40.3% incidence [44]. There was not a reduction of lung tumor incidence by intervention with sulforaphane, indole-3-carbinol (I3C), Brussels sprouts, or broccoli sprouts [43], green tea, decaffeinated green tea, caffeine [39], chlorophyll, chlorophyllin, or spinach [41].

The number of lung nodules were reported as lung tumor multiplicity. When DBC is administered without intervention, the average multiplicity in these studies were found to range from 15 to 24 [39, 41]. Relative to DBC-only controls, intervention was found to reduce multiplicity by 40% with EGCG, by 27% with caffeine, by 32% with green tea, and by 36% with decaffeinated green tea [39]. A co-gavage of chlorophyll with DBC at gestation day 17 resulted in a 51% reduction of lung lesions

relative to control [41]. Intervention with I3C resulted in a dose dependent inverse relationship (p=0.019) for average multiplicities of 17.6, 12.4, and 11.3 tumors at 100, 500, and 1000 ppm I3C, respectively [43]. Cyp1b1 null mice were found to have half the multiplicity (5.0) relative to wild type mice (9.3) with a 15 mg/kg DBC dose at gestation day 17 [44].

1.3 Translational Studies of PAHs, Human Relevance

DBC exposure, metabolism, and risk in humans is poorly understood. PAHs occur in mixtures, of which DBC is a minor component [45]. DBC is not one of the EPA 16 priority PAH pollutants [46], resulting in its exclusion from common environmental analytic chemistry identification libraries. DBC has been determined to be an IARC class 2A carcinogen, or a compound believed, but not conclusively proven, to induce cancer in humans [14]. Due to the genotoxicity and carcinogenicity in animal models, understanding the human metabolism from environmentally relevant DBC concentrations is important to understanding risk from compound PAH mixtures.

Physiologically based pharmacokinetic (PBPK) models of human exposure to BaP and DBC exposures have been developed [47]. These models scale high dose animal exposure experiments to low dose human metabolism predictions and risk estimates. A criticism of PBPK models is that they include many scaling factors and algorithms to predict human metabolism, but often these predictions are not or cannot be validated for accuracy.

Building upon the PBPK model of Crowell et al. [47], we addressed the human metabolism of an environmentally relevant dose of DBC. Volunteers were given a dose of ^{14}C-DBC (29 ng/5Ci), determined to be environmentally relevant and predicted to be of *de minimus* risk (dissertation ch.3). This was possible due to ultra-sensitive accelerator mass spectrometry (AMS) available through collaborators at the Center for Accelerator Mass Spectrometry (CAMS) at Lawrence Livermore National Laboratory (LLNL).

1.4 Accelerator Mass Spectrometry Analysis

AMS has traditionally been used in carbon dating and geologic applications [48, 49]. During AMS, carbon, or other target atoms, are ionized [50] prior to acceleration through sheets of thin gas to sheer carbon containing molecules to atoms [51]. The flight path and energy permit only the atom and isotope of interest to reach the particle detector for highly sensitive and accurate quantitation. The concentration of the isotope is then related to the starting material for an isotopic ratio used in carbon dating.

1.5 Biological Accelerator Mass Spectrometry and Historic Studies

The sensitivity of AMS allowed the new field of Bio-AMS, permitting researchers to safely administer doses of radiolabeled compounds to humans without appreciable risk from radiation or chemical exposure.

Previously, AMS was instrumental in determining the distribution, metabolism, adduction (DNA and protein), and translation of the human dietary carcinogens, heterocyclic amines. A ^{14}C label was utilized to determine the distribution and metabolism of 2-amino-1-methyl-6-phenylimidazo 4,5-b pyridine (PhIP) in female rats and their pups at dietary human relevant doses [52]. The metabolism of heterocyclic amines 2-amino-3,8-dimethylimidazo[4,5-f]quinoxaline (MeIQx) and PhIP was compared between animal models and humans [53]. Covalent binding of MeIQx to albumin and hemoglobin was compared between human subjects and F344 rats at environmentally relevant doses [54].

In humans, DNA and protein adduct formation in colon and blood were quantitated after exposure to a dietary-relevant dose of PhIP [55]. Urinary biomarkers to predict colon DNA adducts following low dose human exposure were determined by AMS based on the metabolite profile of the dietary carcinogen PhIP [56]

Dietary chemoprotection was evaluated with intervention and quantitation of adduct formation *in vitro* and *in vivo*. Sulforaphane and quercetin were found to modulate PhIP-DNA adduct formation in human HepG2 cells and primary hepatocytes [57]. The chemopreventive potential of diets supplemented with phenethylisothiocyanate (PEITC), genistein, chlorophyllin, or lycopene were assessed with regard to adduct formation following a low dose of the heterocyclic amines PhIP and 2-Amino-3methylimidazo[4,5-f]quinoline (IQ) and phase II hepatic enzymes, PEITC and chlorophyllin were found to be effective [58]. The effect of

dietary constituents curcumin, garlic, grapeseed extract, tea polyphenols, vitamin C, and vitamin E were assessed in nictotine-DNA adduct formation, all reduced adduction [59].

Additionally, the adduction and carcinogenesis of the dietary contaminate aflatoxin B_1 (AFB_1) was assessed following human dietary levels of exposure in rats and humans [60]. The human uptake and pharmacokinetics of $AFB_{1,}$ with and without chlorophyll and chlorphyllin, was determined [61]. Chlorophyll was found to decrease the plasma and urine concentrations of AFB_1, believed to be through a reduction in bioavailability.

1.6 Recent Bio-AMS Advances

Recently, the majority of published biomedical AMS studies have focused on pharmacokinetics and pharmaceutical absorption, distribution, metabolism, and elimination (ADME) studies in humans, utilizing a microdose, defined as a dose 100-fold below that which would be expected to yield a pharmacological effect. Microdose studies are under FDA Investigational New Drug phase 0 regulations, or extrapolatory guidelines [62, 63].

The comparative pharmacokinetics were analyzed between a microdose and therapeutic dose for clarithromycin, sumatriptan, propafenone, paracetamol (acetaminophen), and phenobarbital in human volunteers [64] to determine if

microdoses provide linear scaling to therapeutic doses. For all drugs analyzed, a microdose detected by AMS predicted the PK for a therapeutic dose detected by HPLC. Additionally, the same compounds were assessed as a ^{14}C-labeled IV microdose, with and without co-treatment of an oral therapeutic dose. This resulted in no deviation in microdose disposition or PK, indicating that any change in linearity with increasing dose is a result of the absorption process [64].

A variety of pharmaceutical therapies have been evaluated for traditional absorption, distribution, and elimination parameters following sub-therapeutic doses of various drugs or drug candidates, including pasireotide [65], GSK2251052 (a boron containing antibiotic) [66], tenofovir diphosphate and zidovudine triphosphate antiretrovirals [67], darapladib (an arthrosclerosis treatment) [68], the cancer chemotherapeutic sonidegib [69], and the epigenetic modulator SRT2104 [70]. Functional modification was found to increase PK efficiency in osteoprotegerin therapy in rats utilizing AMS [71].

The sub-therapeutic safety and low beta particle radiation exposure required of AMS detection permits safe administration for especially sensitive populations. In a recent study, ursodiol, a cholesterol preventative, was safely administered to newborn infants for pharmacokinetic analysis [72]. Additionally, metabolic differences, with respect to genotype (pharmacogenomics), can be assessed as a personalized medicine approach to therapy. A recent example is a pharmacogenetic study of tolbutamide, a

potassium channel blocker, for which CYP2C9*3 allelic variance significantly alters metabolism [73].

A challenge in traditional methods for studying ADME, is that the limit of detection from traditional instruments is not sensitive enough to detect environmentally relevant doses of contaminants. Providing a dose high enough to detect in biofluids may be putting volunteers at risk for toxicity. Absolute bioavailability and mass balance analysis for drug absorption and distribution are essential in determining therapeutic dosing and administration methods. This is potentially a risk in human volunteers as absolute bioavailability requires intravenous injection of a therapeutic compound as a baseline to relative to other modes of administration [74]. Heterogeneity of human populations and imperfect translational models make estimation of appropriate safe intravenous injection concentrations potentially risky. A benefit of microdosing is the ability to perform absolute bioavailability and mass balance in human volunteers with minimal potential for toxicity.

AMS assisted absolute bioavailability and disposition studies have been conducted recently for pharmaceuticals including; the diabetic therapeutics saxagliptin and dapagliflozin [75], tofogliflozin [76], beta-sitosterol, used for the treatment of prostate hyperplasia [77], anti-cancer agents trametinib [78], vismodegib [79, 80], antimicrobial drug candidate (GP-4) [81], and cerlapirdine, targeted to Alzheimer’s disease [82].

The evaluation of potential therapies requires mode of action and safety assessment. Chemotherapeutics, by design, are cytotoxic, often through adduction. Such adducts can be evaluated by AMS for specific nucleotide adduction, mode of action, and specificity of targets. Recently, several candidate/current chemotherapeutics have been evaluated via AMS, including; debio0507 [83], adriamycin and daunomycin [84], carboplatin [85], and gemcitabine [86]. Protein binding of the antidiabetic drug troglitazone and cancer therapeutic flutamide were evaluated in a humanized mouse model [87]. Tamoxifen, a common breast cancer therapeutic and potential preventative, was found to generate human colon DNA adducts following a single ^{14}C dose [88], raising questions about the safety of chronic, long term treatment of women with tamoxifen [89].

Additionally, chemical and toxicology assessments at low and environmentally relevant levels are important to risk assessment and environmental protection. The personal care product and emerging environmental pollutant, triclocarban, was recently assessed for protein adduction and metabolism [90]. The genotoxicity and carcinogenicity of the heterocyclic hydrocarbon furan was evaluated in rats [91]. The fuel additive ethyl tertiary butyl ether was found to have genotoxic effects following sub-chronic exposure in mouse liver [92]. Aluminum intake from drinking water is being evaluated as a causative agent in Alzheimer's Disease [93].

Bioaccumulation and dispersement of nanoparticles is becoming an increasing concern with increasing usage. The sensitivity of AMS was able to detect SiO_2

particles over a time course in mice. The particles were eliminate quickly in most compartments, except for the macarophage system, where they persisted for eight weeks [94]. Complex engineered nanoparticles are comprised of surface functional groups and a particle core. Recently, isotopically labeled fractions of surface functional groups and particle core were traced for distribution and degradation in multiple rat biological matrices [95].

Currently, AMS bomb pulse biology, utilizing endogenous isotopes, is being applied to disease progression and biological molecule anabolism/catabolism. Calcium isotopes were utilized to study osteoclast resorbion with and without strontium ranelate therapy [96]. Aneurysm progression and development was measured and characterized with carbon isotopes [97, 98].

Building from previous forensic application of AMS, such as clandestine remains dating, atomic analysis for the origin and age of isotopes can aid in security and point of origin contamination. For example, *Bacillus* spore proteins were assessed for bomb pulse age relative to nuclear arms testing, used to determine if a store of bioagent material is from before the nuclear era or from the modern era via specific ^{14}C endogenous content [99]. A method was developed to detect plutonium and neptunium from urine with accuracy and precision for national security applications [100]. Additionally point of origin food contamination was determined utilizing carbon isotope content. The origin of phthalate contamination in food was determined to be from human sources, with additional contributions from natural sources [101].

1.7 Accelerator Mass Spectrometry for PAH Analysis and Risk Assessment

AMS has been utilized for several PAH research experiments, mostly focusing on PAH adduction to DNA and proteins. Benzo[a]pyrene-DNA adducts were successfully quantified by AMS following post-labeling with ^{14}C-acetic anhydride and accelerator mass spectrometry [102]. ^{14}C-Naphthalene-protein adducts [103] were measured with free flow electrophoresis separation and AMS quantitation. In human breast cancer patients, tissue biopsies were analyzed for DNA adduction following administration of ^{14}C labeled PhIP and B[a]P [104]. Human microdosing for AMS detection is a vehicle to determine the distribution, pharmacokinetics, and adduction of PAHs in humans and for translation studies. We address AMS as a technique to generate such data in chapters 3 and 4, and in appendix 3.

1.8 Hypothesis and Specific Aims

The objective of this work is to add to the body of translational data between high dose animal model research and the environmentally relevant human metabolism of the persistent pollutant dibenzo[*def,p*]chrysene (DBC). A murine model was utilized to investigate the effect of Cyp1b1 metabolism on DBC induced cancer. In addition, sensitive AMS is utilized to detect the metabolism of DBC by human volunteers at environmentally relevant levels of exposure.

Specific Aim 1 (chapter 2): Determine the effects of Cyp1b1 genotype status of wild-type, null, or “humanized” CYP1B1 transgenic mice on carcinogenesis and

tumogenesis in an *in utero* exposure model following a maternal oral dose of 6.5 mg/kg DBC or 12 mg/kg DBC.

Specific Aim 2 (Chapter 3): Determine the human pharmacokinetics of an environmentally relevant oral dose of 26 ng DBC utilizing the sensitivity of AMS.

Specific Aim 3 (Chapter 4): Utilize a novel HPLC-AMS interface to determine the pharmacodynamics of DBC from human volunteers administered an environmentally relevant dose.

Chapter 2.

Cyp1b1 Status and PAH Dibenzo[*def,p*]chrysene Transplacental Exposure: Effects of Wild Type, Null and Transgenic Human *CYP1B1* Genotype on Adult On-Set Carcinogenesis in B6129F1 Mice.

Erin P. Madeen[1-3], Christiane Löhr[2-4], Hannah You[2], Lisbeth E. Siddens[1,2], Sharon K. Krueger[2,3], Roderick H. Dashwood[5], Frank J. Gonzalez[6], William M. Baird[1,3], Emily Ho[2,7], Lisa Bramer[3,8], Katrina M. Waters[3,8], David E. Williams[1-3]

[1]Department of Molecular and Environmental Toxicology, Oregon State University, Corvallis, Oregon, 97331, USA
[2]Cancer Protection and Prevention Program, Linus Pauling Institute, Oregon State University, Corvallis, Oregon, 97331, USA
[3]Superfund Research Program, Oregon State University, Corvallis, Oregon, 97331, USA
[4]College of Veterinary Medicine, Oregon State University, Corvallis, Oregon, 97331, USA
[5]Center for Epigenetics and Disease Prevention, M.D. Anderson Cancer Center, Houston, TX, 77030, USA
[6]Center for Cancer Research, National Cancer Institute, Bethesda, Maryland, 20810, USA
[7]School of Biological:Population Health Sciences, Oregon State University, Corvallis, Oregon, 97331, USA
[8]Biological Sciences Division, Pacific Northwest National Laboratory, Richland, Washington, 99352, USA

Short Title: CYP1B1 status and PAH induced carcinogenesis

* To whom correspondence should be addressed. Tel: +1 541 737 3277; Fax: +1 1541 737 0497; Email: david.williams@oregonstate.edu

In submission to Molecular Carcinogenesis

2.1 Abstract

The cytochrome P450 (CYP) 1 family metabolizes numerous environmental pollutants, including polycyclic aromatic hydrocarbons (PAHs). Using *Cyp1b1*-null and *CYP1B1*-transgenic "humanized" mouse models the hypothesis was tested that human CYP1B1 (hCYP1B1) is important for dibenzo[*def,p*]chrysene (DBC) transplacental carcinogenesis. Wild-type (m*Cyp1b1*), *Cyp1b1*-null, *CYP1B1*-humanzed mice were assessed, containing either the aryl hydrocarbon receptor (*AhR)*$^{b\text{-}1/d}$ or *AhR*$^{d/d}$ alleles. Pregnant mice were gavaged on gestation day 17 with 6.5 or 12 mg/kg of DBC, and compared to corn oil-treated controls. The offspring, born on gestation day 19, were evaluated at 10 months of age for mortality, general health, lymphatic diseases, and lung tumor incidence and multiplicity. Wild-type mice were 59% more likely to succumb to T-cell Acute Lymphoblastic Leukemia (T-ALL). The *AhR* genotype was not a significant factor in lung tumor incidence, multiplicity, or mortality. Gender was not a significant factor in lung tumor incidence or mortality, males exhibited a significantly greater lung tumor multiplicity. The h*CYP1B1*

genotype did not impact lung tumor multiplicity, but lung tumor incidence was greater in *Cyp1b1*-nulls compared to wild-type mice. *CYP1B1*-humanzied mice were more likely to develop lung tumors than *mCyp1b1* wild-type mice but this did not reach statistical significance ($p = 0.07$).

2.2 Introduction

Endogenous Role of *CYP1B1:*

CYP1B1 is constitutively expressed in human extra-hepatic tissue in both the adult and fetus [105-110]. However, there is a significant intra-individual variation in expression in the same tissue and between tissues of the same individual [111]. CYP1B1 contributes to ocular development and differentiation, and mutations in *CYP1B1* are associated with primary congenital glaucoma [112, 113]. Among the endogenous substrates, CYP1B1 is active in the 4-hydroxylation of 17β-estradiol [114-116] a metabolite linked to estrogen-dependent carcinogenesis [115, 116]. CYP1B1 and polymorphisms of CYP1B1 have been linked to several hormone-induced cancers, including prostate, breast, endometrial, and ovarian cancers [113]. In the present study we investigated the response of Cyp1b1 wild-type, Cyp1b1 null, and CYP1B1-transgenic "humanized" mice to environmental pollutants.

Exogenous Substrates:

The mouse and human CYP1 families, consisting of CYP1A1, CYP1A2, and CYP1B1, metabolically activate polycyclic aromatic hydrocarbons (PAHs), to phenols, dihydrodiols or quinones that can be conjugated by detoxification enzymes such as UDP-glucuronosyltransferase (UGT) and sulfotransferase (SULT) for renal elimination [117] . Often, high molecular weight PAHs, (with at least 5 aromatic rings) are pro-carcinogens, and following occupational or environmental exposures and activation by CYP1 enzymes, produce reactive intermediates capable of DNA binding and/or redox cycling

resulting in cancer development [10, 118-121]. Previous work employed a transplacental model of cancer utilizing dibenzo[*def,p*]chrysene (DBC), also known as dibenzo[*a,l*]pyrene, and documented an aggressive T-cell acute lymphoblastic leukemia (T-ALL) in offspring beginning at 12-18 weeks of age, as well as adult onset cancers of the reproductive system, liver, and lung [32, 38, 44]. *Cyp1b1*-null mice did not develop T-ALL, but was susceptible to lung tumors in a transplacental model [44]. Lung tumor multiplicity in *Cyp1b1*-null mice was reduced by half compared to mice possessing one or both *Cyp1b1* alleles [44].

Role of the *AhR:*

The endogenous roles of AhR appear to include cell cycle control, response to oxidative stress and apoptosis regulation [122]. Mouse strains can vary widely in response to AhR ligands, attributable to inbred strain allelic differences. B6 mice are homozygous for the "responsive" AhR^{b-1} allele, whereas D2 mice possess two copies of the less responsive AhR^{d} allele [34-36]. The AhR^{b-1} allele is dominant and $AhR^{b-1/d}$ mice are "responsive" to PAH-induced activation of the AhR target gene network. Interestingly, the human AhR affinity toward a single substrate can vary up to 12-fold without a clear genetic polymorphic explanation [123]. It is generally accepted that the "human like" mouse receptor is the less responsive AhR^{d} allele, however a mouse transgenic for human *AhR* was paradoxically found to be less responsive to TCDD in liver than either wild-type AhR^{d} or AhR^{b-1} mice [124].

PAHs, as with other CYP1 substrates, are capable of up-regulating their own metabolism by acting as AhR ligands [40]. Previous studies on PAH-dependent transplacental carcinogenesis have shown that susceptibility is greatest with a maternal "non-responsive ($AhR^{d/d}$) allele and a fetal responsive allele ($AhR^{b\text{-}1/d}$) [33]. The hypothesis is that a non-responsive dam does not metabolize PAHs as readily thus making the carcinogen more available to the fetus. A responsive AhR in the fetus is thought to enhance risk as the ratio of bioactivation to detoxication is higher than in adults likely due to the fact that phase two detoxication enzymes such as UGT, SULT and glutathione-S-transferase (GST) are not yet fully developed in the fetus [33].

CYP1B1-humanized Mice:

While CYP enzymes are highly conserved across species, amino acid sequence and subsequently substrate recognition and response can vary (fig. 2.1). For this reason, mouse models expressing human CYP enzymes have been developed. *CYP*-humanized mouse models have been valuable for assessing the contribution of CYP3A4 and CYP2D6 in drug metabolism *in vivo* [125, 126]. A trans-activator-controlled *CYP1B1* transgenic mouse, also expressing mouse CYP1B1, was developed to assess response to anti-androgens [127]. A *CYP1B1*-humanized mouse model, null for *Cyp1b1*, was developed and successfully used to assess the role of CYP1B1 and SCD1 in obesity [128]. This study tested the hypothesis that mouse and human CYP1B1 will exhibit differential carcinogenesis when exposed to DBC.

2.3 Materials and Methods

Chemicals and Reagents:

DBC was purchased from Midwest Research Institute (Kansas City, MO), TCDD was purchased from Cambridge Isotope Laboratories, Inc. (Tewksbury, MA.). Biolase™ buffers, DNA polymerase, and Polymate™ were from Bioline (Taunton MA.), Trizol reagent, proteinase K, Superscript III reverse transcriptase kit, Novex™ TBE gels, and dNTPS were purchased from Life Technologies (Grand Island, NY.). DirectPCR® Lysis Reagent was from Viagen Biotech (Los Angeles, CA.) SYBER green polymerase master mix was from Qiagen (Valencia, CA.) . Western Lightning® Plus ECL was from PerkinElmer (Richmond, CA.). Zymoclean™ DNA Gel Recovery kit was from Zymo Research (Irvine, CA.) Commercial antibodies were purchased from Santa Cruz Biotechnology (Dallas, TX.) All other reagents were purchased through VWR Scientific (Radnor, PA.)

Animal Care and Housing:

Animal subject research was approved by the Oregon State University Institutional Animal Care and Use Committee (IACUC), in accordance with Oregon State University's Association for the Assessment and Accreditation of Laboratory Care (AAALAC) International accreditation. Animal housing rooms were maintained on a 6:30 AM-6:30 PM 12 hour light/dark cycle, 21-23^{o}C temperature, 30-70% humidity, utilizing CareFresh bedding. Mice were fed AIN93G diet from mating through pup weaning 21 days postpartum, at which time pups were separated by sex and housed up to 5 siblings per micro isolator cage. Pups remained on AIN93G until 3 months of

age at which time diet was changed to AIN93M; all diet and water was *ad libitum*. Animals were checked twice daily for health until termination of the study. At signs of distress, such as lethargy, anemia, or heavy breathing, mice were preemptively euthanized. The mice were euthanized by CO_2 asphyxiation followed by cervical dislocation, in accordance with AAALAC guidelines.

CYP1B1-humanized Mice:

The *CYP1B1*-humanized mouse was incorporated into the *in utero* DBC exposure scenario previously found to induce T-ALL and lung cancer [32, 33, 38, 43, 44]. The *CYP1B1*-humanized mouse was generated by pronuclear injection of ovulated mouse eggs on a *Cyp1b1* null background with a *CYP1B1*-containing bacterial artificial chromosome (BAC) clone as previously described [128]. *CYP1B1*-humanized hemizygous C57BL6 dams on a *Cyp1b1*-null background were shipped to Oregon State University (OSU) from the colony maintained at the National Cancer Institute in order to establish a breeding colony for this study. Incoming transgenic dams were bred with matched null male mice from a colony at OSU. For rederivation, following natural birth, offspring were cleaned and placed with foster dams as part of an OSU-mandated procedure when importing mice from non-commercial facilities. All subsequent mating for colony maintenance was limited to C57BL6 m*Cyp1b1* null mice where at least one parent had at least one copy of the transgene (Fig. 2.2).

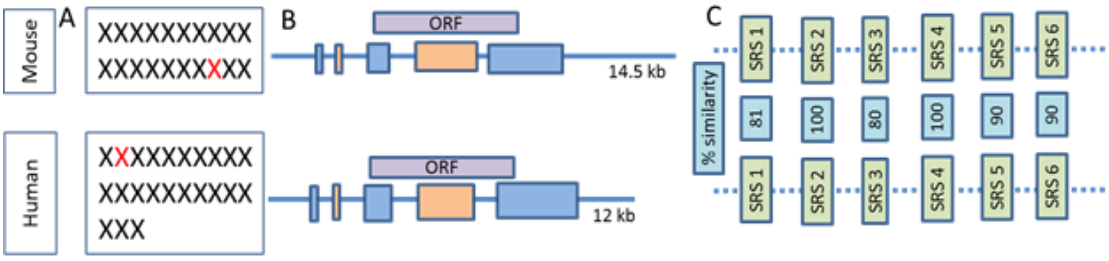

Figure 2.1: Mouse Cyp1b1 homology to Human CYP1B1

Cyp1b1 is located on mouse chromosome 17 [129] whereas *CYP1B1* is located on human chromosome 2 at the 2p21-22 region [105, 130]. Pronuclear injection is not location- or copy number-specific, therefore the *CYP1B1*-humanized mouse contains an unknown copy number and chromosomal location. The *Cyp1b1* and *CYP1B1* genes have the same number of exons and introns and open reading frames (ORFs) and sequence similarity is quite high (Figure 2.1) [130]. Both ORFs start in the second exon and continue into the third exon. *Cyp1b1* exons 1, 2, and 3 (Figure 2.1, blue boxes) are 371, 1042, and 3780 bp, respectively, whereas *CYP1B1* exons 1, 2, and 3 are 371, 1044, and 3707 bp, respectively. *Cyp1b1* introns 1 and 2 (Figure 2.1, orange) are 376 and 2591 bp in length compared to 390 and 3032 bp, respectively for *CYP1B1* [105, 129, 131, 132]. Both mRNAs are 5.2 kb and both proteins are 543 amino acids (AA) in length [112, 131]. The six substrate responsive sites (SRS) of the enzyme have a similar AA sequence and alignment as follows: SRS1, AA 116-139, 81%; SRS2, AA 224-236, 100%; SRS3, AA 259-263, 80%; SRS4, AA 330-343, 100%; SRS5, AA 392-401, 90%; SRS6, AA 503-513, 90% [129, 133] (Figure 2.1).

Breeding of Experimental Animals:

We modified a previous transplacental DBC exposure model [33, 38, 44] to include a transgenic *CYP1B1*-humanized group. All experimental *CYP1B1*-humanized (C57BL6) and *Cyp1b1*-null mice (C57BL6 and 129S genetic background) were maintained and bred at OSU. One generation was needed to produce null B6129F1 dams and a second generation was needed to produce the offspring from DBC-treated B6129F1 dams (Suppl. Figure 1). Control wild-type *Cyp1b1* B6129F1/J dams and 129S/J sires were purchased from Jackson.

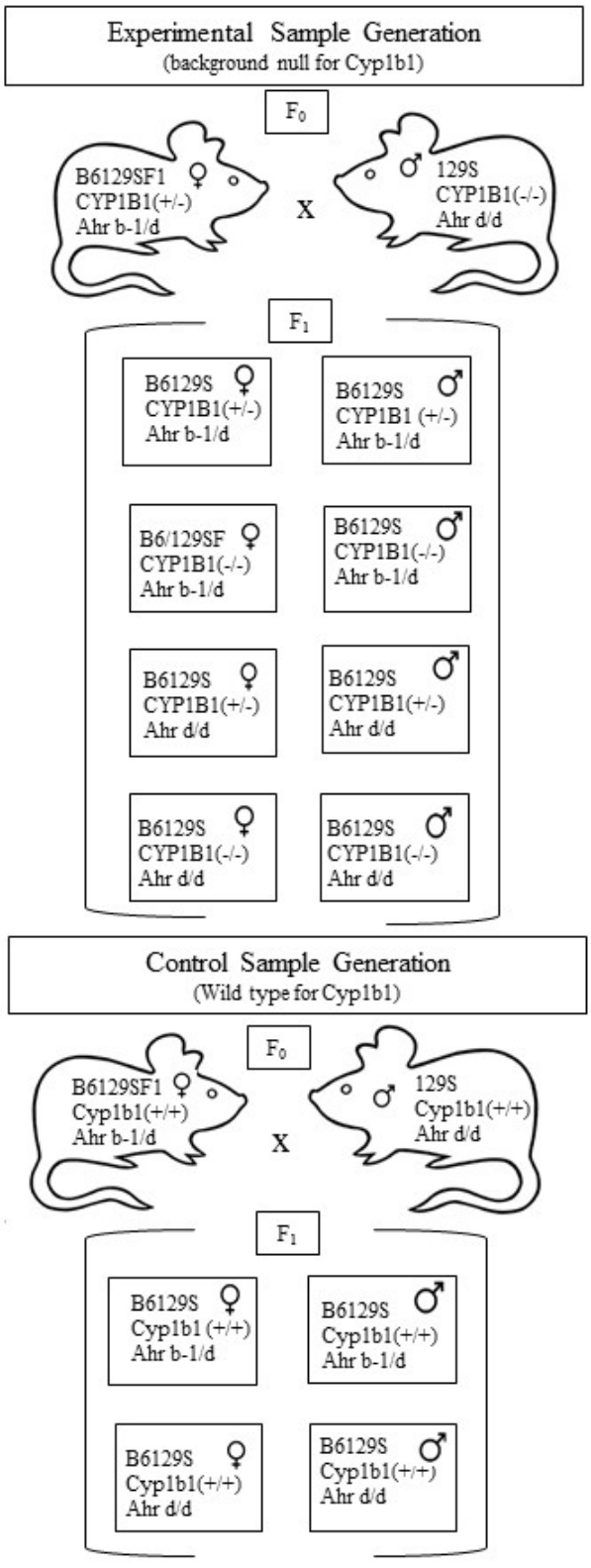

Figure 2.2: Experimental Mouse Breeding Scheme

Carcinogenesis and Mortality:

Health checks were conducted twice daily for general health. T-ALL mortality was evident beginning at about 12 weeks of age and continued until study termination at 10 months of age. At the first sign of distress, such as heavy breathing, lethargy, or lack of responsiveness, animals identified as morbid were euthanized and accounted in the mortality curve. Gross morphological observations were made of the entire body, with close focus on thymus, spleen, lymph nodes of the throat and chest, lungs, liver, gonads, and spleen. These tissues were fixed in 10% neutral buffered formalin. Histopathology and gross anatomy were utilized to determine cause of death. Lung tumor multiplicity was compared between animals surviving to the 10 month terminal endpoint by analysis of the entire surface of the 10% neutral buffered formalin fixed lung. At gross necropsy, using a dissecting microscope, lung tumors were identified and counted over the entire surface of the lung and confirmed, along with identification of tumor type by histopathology of the fixed tissue, as previously described [33].

Genotyping:

h*CYP1B1*$^{(-/-)}$ and h*CYP1B1*$^{(+/-)}$ F_1 pups were genotyped as shown in Figure 1A. h*CYP1B1*$^{(-/-)}$ and h*CYP1B1*$^{(+/-)}$ F_1 pups are identified by genotyping experimental offspring in each litter. Ear punches, 0.2 cm, were digested in 49 µL DirectPCR™ Lysis Reagent with 1 µL Proteinase K (20 mg/mL) overnight at 55^{o}C. Primers were diluted to 5 µM in Tris buffer and utilized at a 1:1 ratio of forward and reverse

primers. Each PCR reaction mix included: 2 µL 10x Biolase™ buffer, 0.8 µL 50 mM $MgCl_2$, 0.4 µL 10 mM dNTPs, 1.6 µL h*CYP1B1* mix, 1.6 µL m*FMO1* primer mix (positive control), 0.8 µL Biolase™ polymerase (5 U/µL), 10 µL Polymate™ and 1 µL 200 ng tissue lysate. PCR conditions were: Step 1, 95°C for 5 min; Step 2, (95°C for 30 sec → 55 °C for 30 sec → 72 °C for 45 sec) × 35 cycles followed by Step 3, 72°C for 10 min. Gel separation was achieved in a 2% agarose/1x TAE gel spiked with 4 µL GelRed™ (10,000x) per 100 mL gel. Wells were loaded with 18 µL amplicon and 3 µL loading dye and electrophoresis conducted at 130 V for 45 min, then 100 V for 15 min. The h*CYP1B1* product is 201 bp in length while the m*Fmo1* (positive control) product is 99 bp. The h*CYP1B1* primer sequences were:

h*CYP1B1*-f	CCA ACC TGC CCT ATG TCC T
h*CYP1B1*-r	CTG GAT CAA AGT TCT CCG GG

The forward and reverse primers for mFmo1 were:

m*Fmo1*-197f	AAG TGA GTT TGC ATG GCG CAG C
m*Fmo1*-198r	CCC TTT AGC CCC TTC CCT CTG

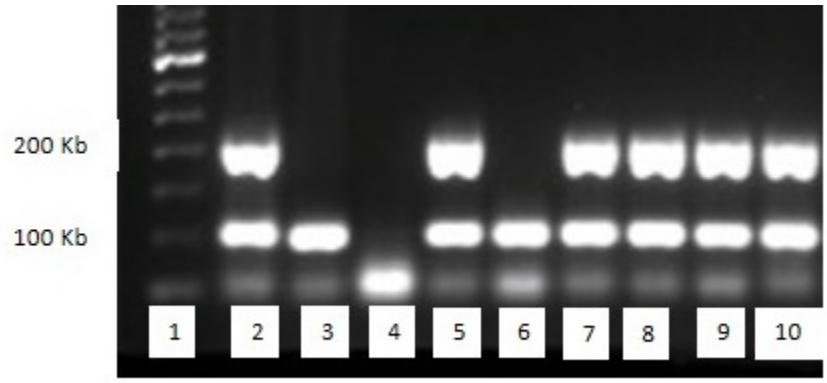

Figure 2.3: CYP1B1 Genotyping Gel

Lane 1: reference ladder, lane 2: positive control transgenic 1B1 mouse DNA (FMO 100kb, CYP1B1 200kb), Lane 3: negative control wild type mouse DNA (FMO 100kb), Lane 4: blank control, Lanes 5-10: experimental samples

AhR$^{b\text{-}1/d}$ and *AhR*$^{d/d}$ genotyping (Figure 1B), was modified from a method previously described [33]. Lysates of 0.2 cm ear punches were digested overnight at 55^{o}C in 49 µL DirectPCR™ Lysis Reagent with 1 µL Proteinase K (20 mg/mL). *AhR* primers were diluted to 5 µM in Tris buffer and utilized at a 2:1:2 mix of *AhR*546-f:*AhR*596$^{b\text{-}1}$-r:*AhR*596^{d}-r: Each PCR reaction mix included: 1 µL 10x Biolase™ buffer, 0.5 µL 50 mM $MgCl_2$, 0.2 µL 10 mM each dNTPs, 2.0 µL primer mix, 0.2 µL Biolase™ enzyme, 5.1 µL Polymate™ and 1 µL 200 ng tissue lysate. PCR conditions were as follows: Step 1, 95 °C for 10 min; Step 2, (95 °C for 45 sec → 58 °C for 45 sec → 68 °C for 1 min) (repeat 14 times); Step 3, (95 °C for 45 sec → 58 °C for 45 sec → 68 °C for 2 min) (repeat 17 times); Step 4, 68 °C for 10 min. Gel separation was performed with 0.4 µL PCR amplicon, 1.6 µL water, and 2 µL loading dye per well on an 8% Novex™ TBE gel at 200 V for 54 min prior to imaging with GelRed™ stain. The *AhR*$^{b\text{-}1}$ product is 158 bp and the *AhR*^{d} product is 148 bp. The primers sequences were:

*AhR*546-f	5'-GAA GCA TGC AGA ACG AGG AG
*AhR*596$^{b\text{-}1}$-r	5'-caa gct tat aTG CTG GCA AGC **C**GA GTT CA**G**
*AhR*596^{d}-r	5'- TG CTG GCA AGC **G**GA GTT CA**T**

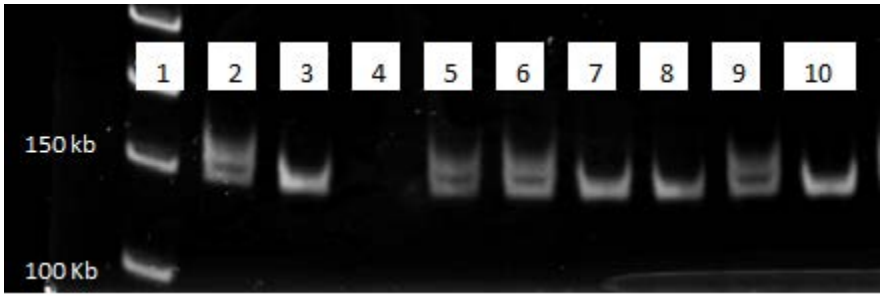

Figure 2.4: AhR Genotyping Gel

Lane 1: reference ladder, Lane 2: $b^{-1/}$d allele control (158 bp), Lane 3: d/d allele control (148 bp) Lane 4: Water lane, Lane 5-10: Experimental samples

Constitutive mRNA Expression:

Total RNA Isolation: Both *CYP1B1* and *Cyp1b1* mRNA were quantified at the 3 month time point via qRT-PCR in lung, thymus, liver, and gonad tissues collected from F_1 progeny and snap frozen prior to storage at -80^{o}C. Male mice genotyped as $AhR^{b\text{-}1/d}$ or $AhR^{d/d}$, were chosen for analysis of lung, liver, and thymus. Analysis of gonads included both male and female $AhR^{b\text{-}1/d}$ and $AhR^{d/d}$ tissues. For all tissues and both genotypes, analysis was with 3 pups from 3 separate litters. Total RNA was isolated using TRIzol® .RNA isolate was analyzed via a Bioanalyzer 2100 (Agilent Technologies, Sanata Clara, CA.), with a minimum RNA Integrity Number (RIN) of 8. cDNA was synthesized with a Superscript III First-Strand cDNA Synthesis Kit per manufacturer's instructions. Each reaction included 240 ng RNA, 1 µL 50 mM poly dT oligo, 1 µL annealing buffer, 10 µL 2X first strand reaction mix, and 2 µL Rnase OUT in a reaction volume of 20 µL. PCR conditions were 50 min 50^{o}C, 5 min 85^{o}C, hold 20^{o}C.

Real-time Quantitative PCR:

Twenty microliter reactions were run for each of the three genes, each respective forward primer (h*CYP1B1*: AAGTTCTTGAGGCACTGCGAA, 150 nM) (m*Cyp1b1*: TTG ACC CCA TAG GAA ACT GC, 75 nM) (GAPDH: TCT CCC TCA CAA TTT

CCA TCC CAG, 75 nM), reverse primer (h*CYP1B1*: GGCCGGTACGTTCTCCAAAT, 150 nM) (m*Cyp1b1*: GCT GTC TCT TGG TAG GAG GA, 75 nM) (GAPDH: GGG TGC AGC GAA CTT TAT TGA TGG, 75 nM), 10 µl 2X SYBER Green master mix (containing buffers, DNA polymerase, and dNTPs) and, 3.6 µl of water. Amplifications were done on a BioRad iQ5 thermocycler (Hercules, CA.) with the following conditions: 95^{o}C 10 minutes, 40 cycles of 95^{o}C for 15 sec, to denature, followed by 58.8^{o}C for 1 min, melt curve cycles, 10^{o}C hold. The primer efficiency cut off was 90%. Standards were generated by PCR amplification of pooled cDNA using gene specific primer pairs. Products were separated by gel electrophoresis and purified with a Zymoclean™ Gel Recovery Kit. Using a relative quantitation method, CT values were related to starting quantity of mRNA via a standard curve. The quality control for instrument and technical consistency included a CT value standard error cutoff of ≤ 0.5 between biological replicates and among the average GAPDH values across genotypes of a specific tissue type (i.e., all *AhR* m*Cyp1b1*, and h*CYP1B1* groups were ≤ 0.5 standard error within a tissue type).

Western Blot:

To assess the induction of the human CYP1B1 transgenic protein, 12 mg/kg DBC, 0.1 µg/kg TCDD, or 6.5 mL/kg corn oil were administered by oral gavage once daily for 3 days prior to collection 24 hours post final gavage. Microsomes from control, DBC- and TCDD-treated h*CYP1B1* transgenic mice, 6 weeks of age, were isolated from liver homogenate by centrifugation at 100,000*g* [134]. The positive control was

human CYP1B1 supersomes (Corning Life Sciences, Corning, NY) and the negative control was from a mouse hepa1 cell homogenate treated with TCDD for induction of mCyp1a1 (provided by Edward O'Donnell, Oregon State University). A human CYP1B1-specific antibody, previously described [135], was provided by Dr. Craig Marcus (Oregon State University) and used at a 1:1000 dilution. Goat anti-rabbit IgG secondary antibody was employed at a 1:2000 dilution with Western Lightening® Plus ECL chemiluminescent detection with a BioRad ChemiDoc® imaging system (Hercules, CA.).

Statistics:

Biostatistics were assessed for the outcomes of mortality/morbidity, lung tumor incidence and lung tumor multiplicity across the experimental parameters of gender, *AhR* and *CYP1B1* or *Cyp1b1* genotype, as well as DBC dose. Pairwise comparisons of probability were used to assess experimental factors in the probability of disease outcome using a proportional hazards model [136] and significance was attributed to p values <0.05. Due to the few numbers of animals remaining in some treatment groups, a Monte Carlo test for independence [137] was conducted instead of Chi-squared approximation, thus the usual Pearson's Chi-squared Test for independence could not be used to assess a possible litter effect. Based on the Monte Carlo test, the litter was found to have a statistically significant effect on tumor incidence ($p <0.001$). The litter effect was included as a random effect in the following models. T-ALL mortality results were verified with analysis of variance, the Wald chi-square test statistics and p values for the main effects, based on the Type III sums of squares. The

estimated odds ratios for the comparisons and p values were adjusted for multiple comparisons using the single-step method [138]. The assessment of influence by multiple factors (gender, *AhR* status, *Cyp1b1* and CYP*1B1* genotypes) was assessed by Cox proportional hazards regression parameter estimates. Multiplicity data was assessed with a reduced Poisson model based on the Type III sums of squares from the 6.5 and 12 mg/kg DBC groups. The 0 mg/kg dose control was excluded due to insufficient numbers of samples containing tumors.

2.4 Results:

Characterization of the CYP1B1 and AhR Treansgenic mice:

Offspring born to *CYP1B1*$^{+/-}$ dams, crossed to *CYP1B1*$^{-/-}$ sires, were genotyped as shown in Figure 1A. The *Ahr*^{b}and the m*Cyp1b1*$^{b\text{-}1/d}$ and *Ahr*$^{d/d}$ alleles were readily identified (Figure 1A and B). Constitutive expression of *CYP1B1* mRNA from 3-month-old transgenic mice was evaluated and compared to *Cyp1b1* mRNA from wild-type mice in lung, thymus, liver, ovary and testis. In transgenic samples, less than 0.01 pg/µL qRT-PCR amplicon was present in all tissues analyzed (Suppl. Figure 3). The level of *Cyp1b1* mRNA expression in these tissues was about four orders of magnitude higher than h*CYP1B1* mRNA (Figure 2.4).

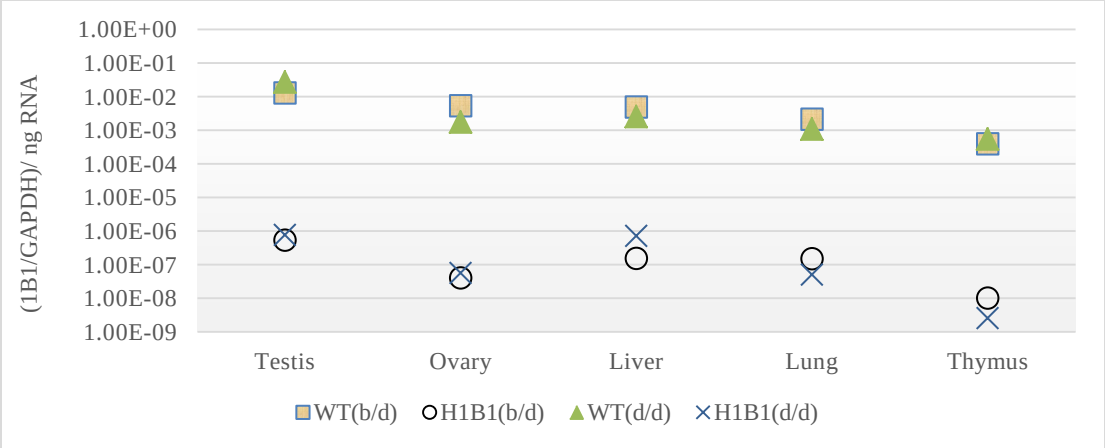

Figure 2.5: cDNA Concentrations of Constitutively Expressed hCYP1B1 and mCyp1b1

The constitutively expression of mCyp1b1 cDNA in wild-type mice was found to be four orders of magnitude greater than the hCYP1B1 cDNA expression in humanized mice.

The recombinant CYP1B1 standard (Figure 2.6, lane 2) and CYP1B1 from 40 µg microsomal protein of *CYP1B1*-humanized mice (Figure 2.6 lanes 8-10) both had an estimated MW of 55 kD. Constitutive expression of CYP1B1 is low to non-detectable (Figure 2.6 lane 4). The human *CYP1B1* gene is therefore capable of being induced in liver from this *CYP1B1*-humanized mouse by the high-affinity AhR ligand TCDD. Conversely, DBC (Figure 2.6 lanes 5-7) did not induce CYP1B1 levels above that of corn oil controls (Figure 2.6 lane 4). Inclusion of a mouse CYP1A1 standard (Figure 2.6 lane 3) confirmed that there was no cross-reaction of this human CYP1B1-specific antibody with CYP1A1.

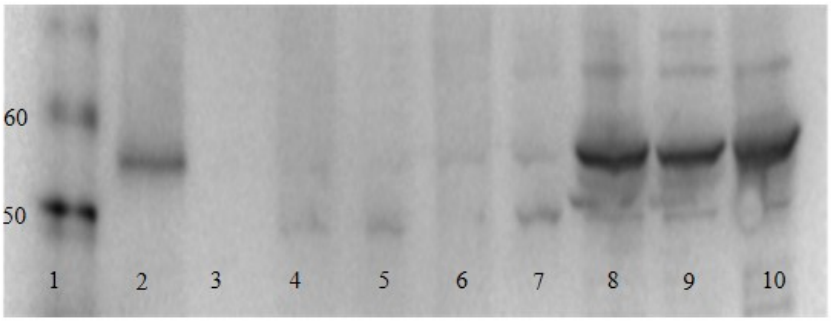

Figure 2.6: Western Blot of CYP1B1 Induction

Lane 1: CYP1B1 negative control. Lane 2: CYP1B1 positive control. Lane 3: blank control. Lane 4: humanized CYP1B1 control treated liver. Lane 5-7: humanized CYP1B1 livers induced with 12 mg/kg DBC. Lane 8-10: humanized CYP1B1 livers induced with 0.1 µg/kg TCDD.

T-ALL- Induced Mortality:

Dose-dependent T-ALL-induced mortality was observed for wild-type (m*Cyp1b1*$^{+/+}$) mice treated with 6.5 and 12 mg/kg DBC (Figure 2.7). In addition to T-ALL, other diseases of the lymphoid system were present, such as splenomegaly and enlarged lymph nodes of the neck and axillary areas, as was bone marrow (anemia). The only groups significantly ($p<0.001$) expressing lymphoid diseases were wild-type mice (Figure 2.7, panels C and F). Gender and *AhR* status were not significant predictors of mortality for T-ALL. Wild-type mice were 75-times more likely ($p<0.001$) to

experience mortality, relative to *Cyp1b1*-null mice (Figure 2.7, panels A and D), whereas the *CYP1B1*-humanized mice did not differ significantly from *Cyp1b1*-null mice (Figure 2.7, panels B and E).

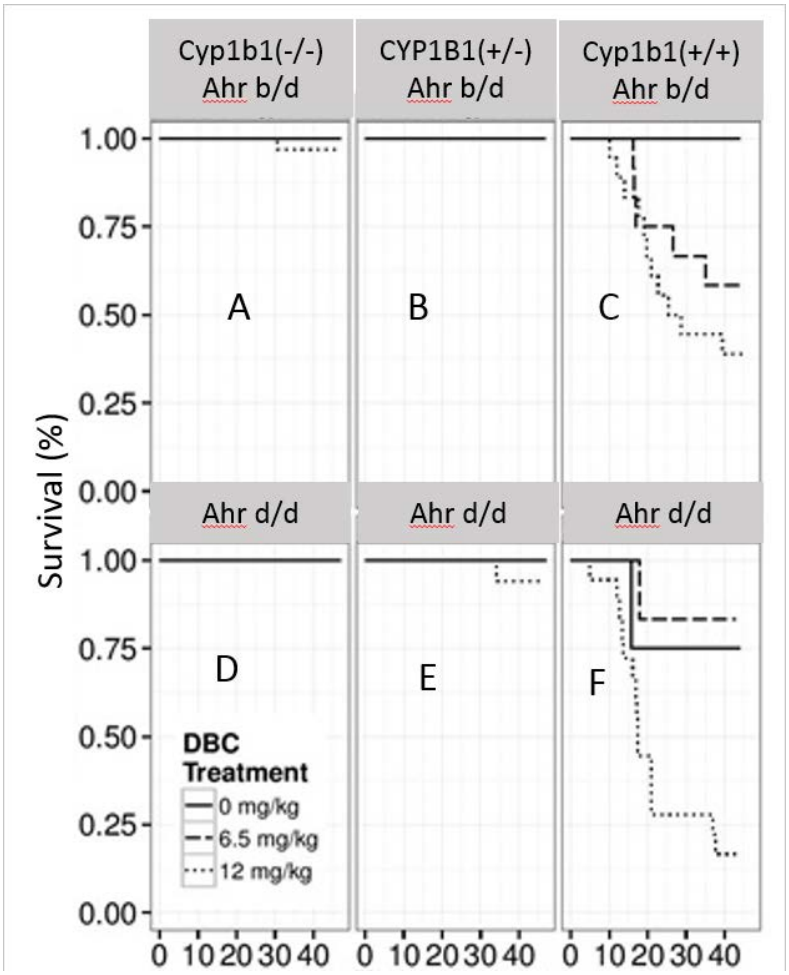

Figure 2.7: Survival Over 40 Weeks Following *in utero* DBC Exposure

The survival of Cyp1b1 wild-type mice was significantly reduced with a negative correlation with increasing DBC dose (panel C and F). Cyb1b1 null mice did not have significant mortality (Panel A and D), neither did CYP1B1 humanized mice (Panel B and E).

Lung Tumor Incidence:

Lung tumor incidence was assessed in offspring surviving to 10 months of age. The incidence, across all genotypes, of lung tumor development was 5.5% in controls (consistent with the spontaneous lung tumor incidence at 10 months previously observed in this model [32, 33, 43, 44]), 97% in mice born to mothers dosed with 6.5 mg/kg DBC, and 95% at a maternal dose of 12 mg/kg DBC. *Cyp1b1*-null mice exhibited a higher spontaneous tumor incidence, compared to wild-type mice, at 10 months. At the highest maternal DBC dose, a similar difference was observed, although these mice are survivors that did not succumb to DBC-induced T-ALL mortality and thus do not reflect the true population. *AhR* status and gender had no significant effect on lung tumor incidence. Excised tumors were analyzed and categorized from a subset (n=7 or 8) of mice with tumors (multiplicity of 6-9 tumors/tumor-bearing mouse). Samples from 5/7 wild-type mice contained a single adenocarcinoma and 1/7 two adenocarcinomas. Lungs from 5/8 *Cyp1b1*-null and 3/8 *CYP1B1*-humanized mice had two or more adenocarcinomas. Adenomas were more common in *CYP1B1*-humanized mice than in wild-type or *Cyp1b1*-null mice.

Lung Tumor Multiplicity:

Among the mice surviving to 10 months of age, the lung tumor multiplicity was increased in a dose-dependent manner with mean values of 1.5, 8.1 and 12.5 (Figure: 2.8) consistent with previous studies [32, 33, 43, 44]. In examining all mice with lung tumors, males had a slightly greater, but statistically significant ($p<0.05$), multiplicity

than females (8.5 and 7.2, respectively). Lung tumor multiplicity was not affected by *CYP1B1*, *Cyp1b1* or *AhR* genotype.

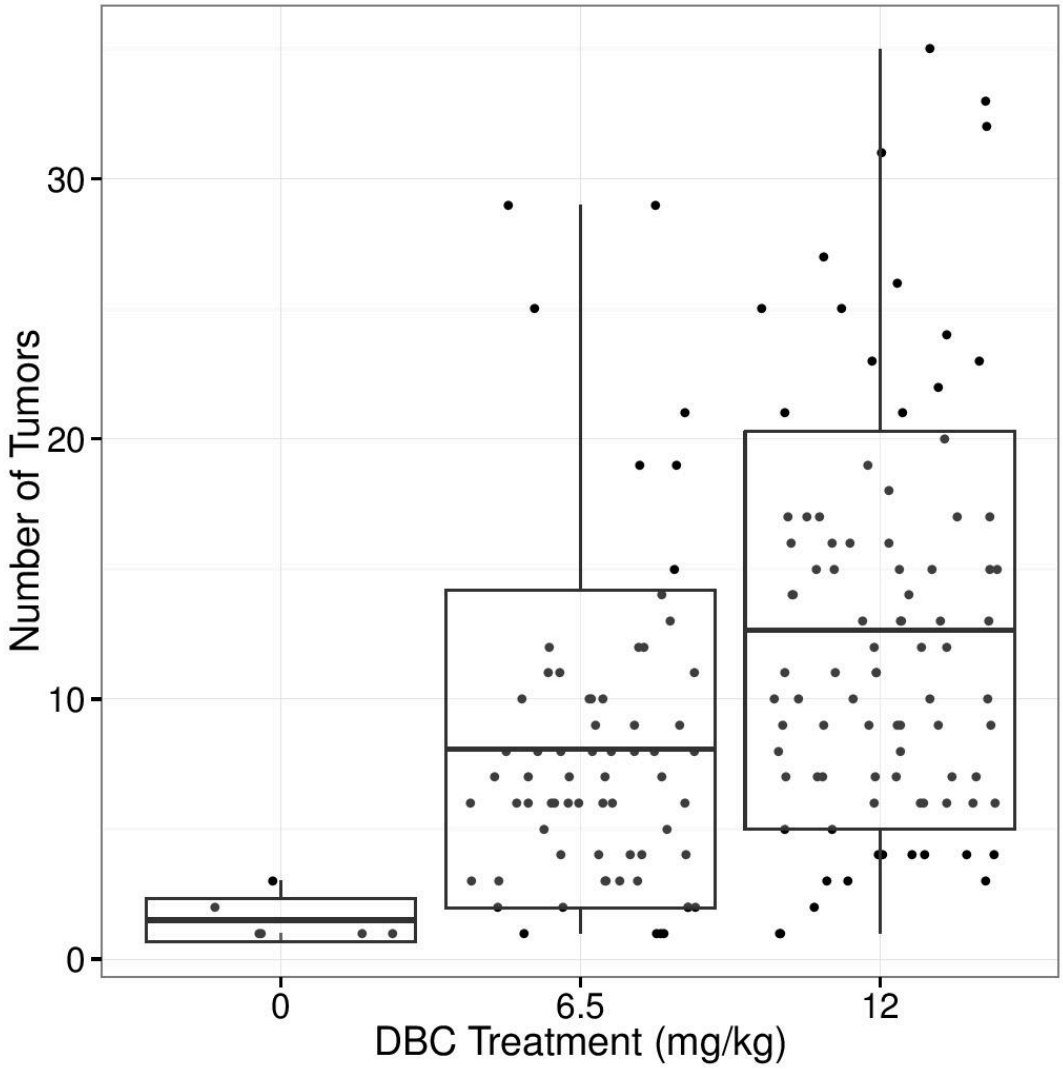

Figure 2.8: DBC Induced Lung Tumor Multiplicity

Lung tumor multiplicity had a positive correlation relative to the DBC dose administered across all CYP1B1 genotypes.

2.5 Discussion:

AhR Genotype:

Studies pioneered by Anderson and Miller used maternal exposure of pregnant mice to 3-methylcholanthrene that were either AhR "responsive" (B6D2F1) or "non-responsive" (D2), crossed with D2 males (resulting in litters with a 1:1 ratio of responsive versus non-responsive pups [139, 140]. A maternal non-responsive AhR phenotype enhanced the risk of the offspring for development of lung cancer (the B6D2F1xD2 cross did not develop T-ALL); conversely the risk was enhanced in AhR-responsive offspring irrespective of maternal AhR status [140]. AhR offspring phenotype has yielded conflicting results with respect to impact on the generation of T-ALL in previous studies [32, 33, 43, 44]. DBC is rapidly metabolized in the pregnant B6129F1 mouse (T½=5.3 hours in maternal liver and 6.3 hours in the fetus) [141]. The result may be low to no induction of CYP1B1 protein. Expression of constitutive *Cyp1b1* mRNA in adult wild-type female mice is independent of AhR "responsiveness" as is the case for the *CYP1B1*-humanized mice (Suppl. Figure 3). The expression of constitutive CYP1B1 protein in female *CYP1B1*-humanized mice is below the detection limits and not inducible by DBC. However, these same mice exhibit marked induction of hCYP1B1 protein upon treatment with TCDD.

In the fetus, CYP1B1 expression is required for DBC-induction of T-ALL mortality and maximum lung multiplicity at 10 months of age [44]. Unlike

maternal tissues, the ratio of DBC-11,12-dihydrodiol (the precursor to the ultimate carcinogenic metabolite (DBC-11,12-dihydrodiol-13,14-epoxide)) is higher than the parent compound from 0-36 hours following maternal dosing with DBC [37]. Thus, it is likely that fetal constitutive expression of CYP1B1 in lung is responsible for the potency of DBC as a transplacental lung carcinogen. A recent study using a mouse dermal model, documented that DBC appears to differ from benzo[*a*]pyrene (BaP), and other PAHs in that DBC carcinogenesis involved pathways regulated by p53/cMyc, whereas BaP carcinogenesis impacted genes regulated by AhR and Nrf2 as well as Sp1[142]. The lack of CYP1B1 up-regulation by DBC, compared to robust induction by TCDD, indicates that the AhR may not be the primary pathway for DBC carcinogenesis in the transplacental model. BaP, at maternal doses up to 50 mg/kg, does not induce T-ALL [32] and $p53^{-/-}$ mice develop T-ALL with a time course and pathology remarkably similar to transplacental DBC [142].

Mouse Cyp1b1 vs Human CYP1B1-Potential Implications:

CYP1B1-humanized mice were not susceptible to CYP1B1 protein induction following DBC exposure, or to T-ALL mortality. Additionally, they were not significantly different in response to DBC than *Cyp1b1*-null mice. Potentially, the developmental- and tissue-specific expression (as well as epigenetic mechanisms of expression) of a select gene product in a transgenic model are not representative of that of the host species, requiring technically challenging validation of transgenic

models. An alternative approach would be to employ a CRISPR/Cas9 approach to minimize off-target effects with respect to expression [143].

For translational studies, the kinetics of metabolism and metabolic profiles with carcinogenic PAHs between mouse models and humans needs to be determined. As with other CYPs, mouse and human CYP1B1 can exhibit distinct substrate specificities and enzyme kinetics, although studies *in vitro* with expressed mCyp1b1 and hCYP1B1 indicate similar kinetics toward most PAHs including DBC [107, 116]. Additionally, DBC metabolism was comparatively assessed in hamster cell lines transfected with species specific CYP genes (human, fish, rat). The human CYP1B1 enzyme was found to metabolize DBC to the greatest extent, and rat Cyp1a1 the least. All Cyp1A1 isoforms metabolized DBC by K-region transformations to (-/-)dihydrodiol-DBC, while CYP1B1 did not generate this ultimate carcinogen. CYP1A1 generated the highest genotoxicity, while CYP1B1 generated the lowest genotoxicity [144].

When considering DBC carcinogenic risk to humans, one must also consider genetic polymorphisms, such as leu432val, asn453ser, arg48gly, and ala119ser. For example, the *CYP1B1*3* (leu432val) polymorphism has been linked to an increased risk of lung cancer [145]. It is well documented that human genetic polymorphisms can significantly alter cancer risk, but little is understood regarding inter-species non-homology and divergent enzyme kinetics with respect to risk. Future work is needed

on species/strain specific substrate specificity and kinetics in preclinical models for PAH (and other environmental carcinogens) human risk assessment.

Funding:

Funding was provided by PHS NIH grants P01CA90890, P42ES016465 and T32ES07060 (EPM).

Acknowledgements:

The authors would like to thank the following individuals for their contributions. Jamie Pennington assisted with handling and dosing of mice while Dr. Nancy Kerkvliet (Oregon State University) provided expertise and TCDD used for dosing. Tissue collection and preparation assistance was provided by David Sampson, Jessica Phillips, Dr. Tod Harper, and Melissa McDougal. The hCYP1B1 antibody was provided by Dr. Craig Marcus and the mCyp1a1 protein control was provided by Dr. Edward O'Donnell (both, Oregon State University). Pacific Northwest National Laboratory is a multi-program national laboratory operated by Battelle Memorial Institute for the DOE under contract number DE-AC05-76RLO1830.

CHAPTER 3

Human Pharmacokinetics of High Molecular Weight Polycyclic Aromatic Hydrocarbon, Dibenzo[*def*,*p*]chrysene (DBC), Following Oral Micro-Doses of [^{14}C]-DBC

Erin Madeen [1], Richard A. Corley [2], Susan Crowell [2], Kenneth Turteltaub [3], Ted Ognibene [4], Mike Malfatti [4], Tammie J. McQuistan [1], Mary Garrard [5], Dan Sudakin [1,5], and David E. Williams [1,5]

[1]Department of Environmental and Molecular Toxicology, Oregon State Univeristy, Corvallis, OR 97330, United States
[2]Systems Toxicology & Exposure Science, Pacific Northwest National Laboratory, Richland, Washington 99354, United States
[3]Biology and Biotechnology Research Division, Lawrence Livermore National Laboratory, Livermore, California 94550, United States
[4]The Center for Accelerator Mass Spectrometry, Lawrence Livermore National Laboratory, Livermore, California 94550, United States
[5]Environmental Health Sciences Center, Oregon State University, Corvallis, Oregon 97331, United States

Chemical Research in Toxicology

Volume 28, Issue 1 pages 126–134

January 2015

3.1 Abstract

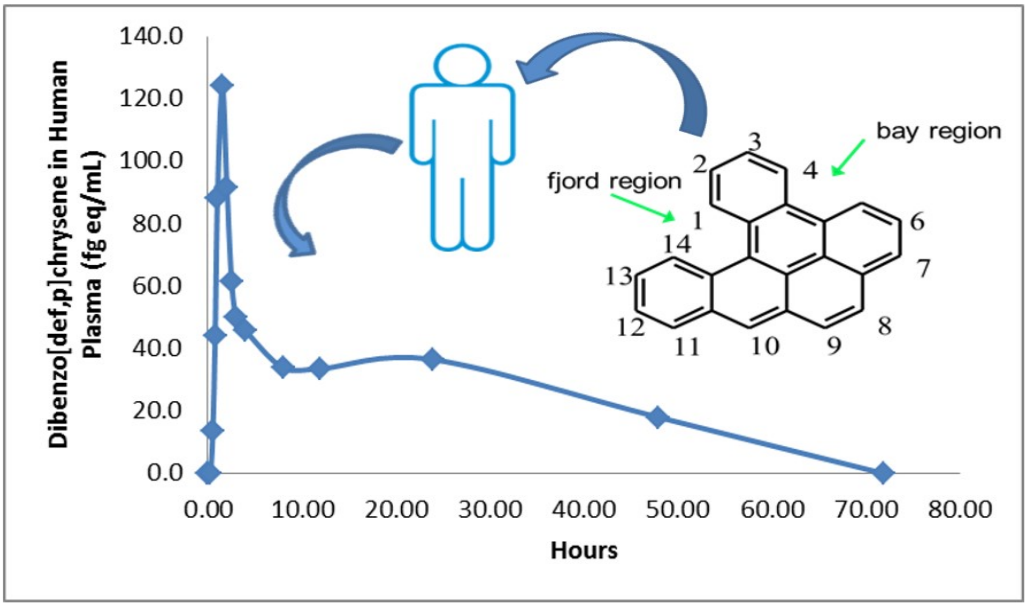

Figure 3.1: Graphical Abstract

Dibenzo(*def,p*)chrysene (DBC), (also known as dibenzo[*a,l*]pyrene), is a high molecular weight polycyclic aromatic hydrocarbon (PAH) found in the environment, including food, produced by the incomplete combustion of hydrocarbons. DBC, classified by IARC as a 2A probable human carcinogen, has a relative potency factor (RPF) in animal cancer models 30-fold higher than benzo[*a*]pyrene. No data are available describing disposition of high molecular weight (>4 rings) PAHs in humans to compare to animal studies. Pharmacokinetics of DBC was determined in 3 female

and 6 male human volunteers following oral micro-dosing (29 ng, 5 nCi) of [^{14}C]-DBC. This study was made possible with highly sensitive accelerator mass spectrometry (AMS), capable of detecting [^{14}C]-DBC equivalents in plasma and urine following a dose considered of *de minimus* risk to human health. Plasma and urine were collected over 72 hours. The plasma C_{max} was 68.8 ± 44.3 fg*mL^{-1} with a T_{max} of 2.25 ± 1.04 h. Elimination occurred in two distinct phases; a rapid (α)-phase, with a $T_{1/2}$ of 5.8 ± 3.4 h and apparent elimination rate constant (K_{el}) of 0.17 ± 0.12 fg*h^{-1} followed by a slower (β)-phase, with a $T_{1/2}$ of 41.3 ± 29.8 h and apparent K_{el} of 0.03 ± 0.02 fg*h^{-1}. In spite of the high degree of hydrophobicity (log K_{ow} of 7.4), DBC was eliminated rapidly in humans, as are most PAHs in animals, compared to other hydrophobic persistent organic pollutants such as, DDT, PCBs and TCDD. Preliminary examination utilizing a new UHPLC-AMS interface suggests the presence of polar metabolites in plasma as early as 45 min following dosing. This is the first *in vivo* dataset describing pharmacokinetics in humans of a high molecular weight PAH and should be a valuable addition to risk assessment paradigms.

3.2 INTRODUCTION

Polycyclic aromatic hydrocarbons (PAHs) are produced by the incomplete combustion of carbon and are of concern as environmental toxicants/carcinogens [14]. The most recent list of the priority chemicals at remediation sites by the Agency for Toxic Substances Disease Registry (ATSDR) include individual PAHs or PAH mixtures as three of the top ten chemicals of concern [146]. Major sources of environmental exposure include wood smoke, creosote, and burning of fossil fuels and tobacco [14]. PAHs comprised of four rings or less constitute the low molecular weight, volatile class. These PAHs tend to be less toxic and are typically classified as level 3 or insufficient weight of evidence as carcinogens in humans [14]. The major route of exposure to low molecular weight PAHs, such as naphthalene, pyrene, and phenanthrene, is inhalation. The high molecular weight PAHs include five or more aromatic rings. The majority of exposure (>95%), to high molecular weight PAHs in non-smokers is through the diet in a variety of foods including breads and cereal grains, vegetables, and smoke-cured or barbequed meats [13, 24, 147]. The high molecular weight group contains the majority of the carcinogenic PAHs, including benzo[*a*]pyrene (BaP, class 1, known human carcinogen) and dibenzo[*def,p*]chrysene (DBC, CAS 191-30-0, class 2A, probable human carcinogen) [14].

Dietary intake of total PAHs in the U.S. has been estimated to be between 160-1600 ng/day [148]. Some studies have reported intake levels of BaP alone at 40-2800 ng/day [12, 149]. A 2005 report from the FAO/WHO Joint Expert Committee on Food Additives and Contaminants listed a mean BaP daily dietary intake of 280 ng

per 70 Kg individual with 700 ng considered as a high-level intake [150]. Finally, a report by Menzie et al., estimated total PAH intake at 3120 ng/day for a non-smoking male, 19-50 years of age, of which 96.2% was from the diet [151]. The European Union established a maximum limit for BaP in smoked meats at 5,000 ng/kg fresh weight [24]. Data on DBC contamination of food is scarce. Veyrand et al., addressed DBC (also known as dibenzo[*a,l*]pyrene) as a component of food from a French market, estimating a daily exposure of 0.129 ng/kg BW in French adults and 0.208 ng/kg BW in French children [7].

Crowell et al., developed a physiologically based pharmacokinetic (PBPK) model for DBC and BaP, relying upon previous studies of *in vitro* (human and rodent liver) BaP metabolism and the metabolic profile *in vivo* following oral gavage in rodents [47]. Administering an oral dose of 15 mg/kg DBC to mice resulted in a T_{max} between 2-4 h, with detectable DBC in blood 48 hours post gavage. The $T_{1/2}$ was found to be between 3.4-4.8 h [37]. The higher log K_{ow} of DBC (7.4), compared to BaP (6.1), is believed to contribute to a prolonged sequestration in blood and other tissues. The DBC model development relied heavily upon BaP due, in part, to the lack of available data on DBC metabolism.

Accelerator mass spectrometry (AMS) measures the ratio of ^{14}C:^{12}C with ^{14}C detection limits in the attomole range per mg total carbon [152, 153], allowing the use of a “micro-dose”, defined as a dose at least 2 orders of magnitude below that which would be expected to yield a pharmacological effect. AMS is increasing being

utilized by pharmaceutical companies to assess pharmacokinetic parameters, metabolism and excretion in humans during drug development (Phase 0 trials) [154-156]. These studies almost exclusively utilized ^{14}C as the radiolabel and doses of 100 μCi have been standard [155]. AMS is an attractive method to determine human pharmacokinetics, DNA binding and other potential biomarkers of importance in risk assessment of compounds with potential toxicity. For example, AMS has been utilized to determine DNA binding of [^{14}C]- labeled amino acid pyrolysis products, or cooked meat mutagens, MeIQ, PhIP, MeIQx [53-55, 157], as well as BaP [104] and the pharmacokinetics of the potent human dietary hepatocarcinogen, aflatoxin $B_{1\ [61]}$. The sensitivity provided by AMS allows for safe micro-dosing of human volunteers with chemical carcinogens, such as DBC, at environmentally relevant doses, providing pharmacokinetic parameters for risk assessment that do not rely solely on high-dose animal studies.

In this study, we determined the human *in vivo* pharmacokinetics of DBC, following micro-dosing, utilizing AMS. Total elimination of DBC_{eq} (parent and metabolites), detected as [^{14}C] are used to determine pharmacokinetics in plasma and urine. Solid sample AMS is not able to distinguish between labeled parent compound and metabolites. Total plasma distribution and urinary elimination is compared to total plasma distribution and urinary elimination scaled from rodent models.

3.3 Materials and Methods

Human volunteers:

All protocols and procedures, including plans for recruitment and volunteer informed consent documents, were approved by the OSU Institutional Review Board. The use of radioisotopes was reviewed and approved by an OSU Radioactive Use Agreement under the oversight of the Oregon Health Authority. Healthy adult males and infertile (post-menopausal or tubally ligated) females, between the ages of 20-65 were recruited for this study. To protect confidentiality, all specimens were de-identified at the time of collection.

Additional inclusion criteria were as follows: good general health; non-smoking; not using medications that can affect gut motility; no history of gastrointestinal surgeries; kidney or liver disease; gastrointestinal diseases such as Crohn's, ulcerative colitis, or gastritis. A medical examination was conducted by a licensed physician. The screening assessment included a careful menopausal history and a urine pregnancy test for all women. Women who were pregnant or capable of becoming pregnant were excluded from the study in an abundance of caution, due to the proven transplacental toxicity of DBC in high dose rodent models [32, 33, 38, 39, 41, 42, 44]. A total of 9 volunteers were enrolled. Individual body weight, height, BMI, age, gender, ethnicity and race were recorded (Table 3.1).

Table 3.1. Volunteer Demographics

	BW (kg)	Ht (cm)	BMI	Age	Gender	Ethnicity	Race
V1	85	173	28	45	F	Non-Hispanic	Asian
V3	99	188	28	45	M	Non-Hispanic	Caucasian
V5	86	158	34	65	F	Non-Hispanic	Caucasian
V6	94	196	24	47	M	Non-Hispanic	Caucasian
V8	78	180	24	26	M	Non-Hispanic	Caucasian
V9	78	156	32	56	F	Non-Hispanic	Caucasian
V10	71	174	23	20	M	Non-Hispanic	Caucasian
V11	113	180	35	43	M	Non-Hispanic	Caucasian
V13	124	191	34	36	M	Non-Hispanic	Caucasian

Justification of dose used in this study

The 29 ng DBC dose utilized in this study is equivalent to the BaP content of a 5.2 oz serving of smoked meat at the European Union maximum legal limit [24], or 28% of the average daily dietary PAH intake [151]. This chemical dose was chosen to be relevant to typical dietary exposure in humans. The specific activity of [l-ring-U-^{14}C]-DBC was 51.4 nCi/nmol, resulting in 5 nCi of [^{14}C] in a 29 ng dose. This beta particle radiation dose of 5 nCi can be compared to the internal radiation of consuming 5 bananas, each containing 1 nCi [^{40}K] [158]. It would require a dose of 200 study capsules to equal the radioactive dose of a single [^{14}C]-urea diagnostic test for *Helicobacter pylori* [159]. The radioactive dose was chosen to be detectable by AMS without appreciable risk to volunteers consistent with the policy of utilizing doses as low as Reasonably Achievable (ALARA) or Practical (ALARP) [160].

Chemicals:

Dibenzo[*def,p*]chrysene (formerly known as dibenzo[*a,l*]pyrene) [l-ring-U-^{14}C], MRI Part No. U479C, 51.4 mCi/mmol, was obtained from the NCI Chemical Carcinogen Standards Reference Repository, Midwest Research Institute (Kansas City, MO). The reagents used include: Ultima Flo M scintillation cocktail, sulfuric acid, HPLC grade acetonitrile, milliQ water, ethyl acetate, potassium sulfate, 95% ethanol (PCCA 50-3161), lactose monohydrate (PCCA 30-3329) and size 0 cellulose capsules (Spectrum, Irvine CA). Chromatography utilized a Luna 3 µm particle C_{18} 100 Angstrom 150 x 3 mm Phenomenex HPLC column with a C_{18} 2 mm guard column on an Agilent 1100 HPLC with UV detector.

[^{14}C]-DBC dosing solution:

A portion of the stock solution of [^{14}C]-DBC (1.11 mCi/ml, 6.53 mg/mL benzene) was blown to dryness under argon and then purified, prior to preparation of dosing solutions, to ≥99% radiochemical purity via reverse phase-HPLC. HPLC elution conditions were isocratic 90% ACN, 10% H_2O with a flow rate of 1 mL/min at a column temperature of 35^{o}C. The A_{280} peak containing purified [^{14}C]-DBC (6.0 to 6.5 min retention time) was collected over several HPLC runs. The pooled eluent was evaporated to dryness under a stream of argon, and resuspended in ethanol thrice to produce dosing solution. An HPLC run of the dosing solution was collected in 15-s fractions for scintillation counting to assess radioactive purity (≥ 99%). The dosing solution was diluted with additional ethanol to 0.16 nCi/µL, representing a final target

dose of 29 ng DBC/30 µL dose incorporated into each cellulose capsule. The stock solution was stored at -80^{o}C under argon and protected from light. All neat DBC powder was handled by a trained carcinogen specialist in an enclosed glove box, per OSU Extreme Carcinogen handling protocol. DBC solutions were stored in a locked laboratory dedicated to carcinogens and all waste was discarded in accordance with OSU radiation safety and hazardous material protocols.

Capsule manufacturing and quality control:

Capsules were prepared by filling empty cellulose capsules with pharmaceutical grade lactose monohydrate. Thirty µL of 0.16 nCi/µL dosing solution was applied to the capsule and sealed, each batch manufactured included a dosing capsule per volunteer plus at least 3 extra for quality control. Capsules were stored at -20^{o}C until time of use and utilized within 5 days of preparation. Quality control was performed by scintillation counting 3 randomly chosen capsules per batch, individually dissolved by vortex in 5 mL of water prior to the addition of 15 mL scintillation cocktail. The variability between capsules per batch was $\leq$ 5%. The exact dosage a volunteer received, measured by scintillation, is included in Table 2.

Table 2. Total ng [^{14}C]-DBC$_{eq}$ eliminated in urine during each collection interval.

	0 – 6 h	6- 12h	12- 24 h	24- 48 h	48- 72 h	Elim. Total	Oral Dose DBC (ng)	% excreted
V1	0.085	0.049	0.044	0.046	0.006	0.230	23.9	0.96
V3	0.044	0.109	0.038	0.029	0.000	0.220	24.5	0.90
V5	0.033	0.184	0.123	0.119	0.073	0.532	25.2	2.11
V6	0.179	0.075	0.107	0.056	0.024	0.441	29.8	1.48
V8	0.071	0.046	0.111	0.058	0.000	0.285	23.9	1.20
V9	0.052	0.028	0.063	0.043	0.014	0.200	28.5	0.70
V10	0.237	0.104	0.097	0.027	0.028	0.494	25.6	1.93
V11	0.113	0.059	0.052	0.056	0.017	0.297	29.7	1.00
V13	0.124	0.056	0.045	0.033	0.005	0.263	28.5	0.92
Average								1.24
SD								0.49

[^{14}C]-DBC$_{eq}$ elimination (ng) per total urine volume in a given pooled time point. The % excreted is reported as total urine elimination divided by total oral dose.

Dosing and sample collection protocol:

At 8 AM volunteers who had fasted overnight were orally administered a cellulose capsule containing ^{14}C-DBC (target dose of 29 ng DBC, 5 nCi ^{14}C) swallowed with 100 mL water. Food and water were made available at 10 AM. Blood was drawn by a registered nurse at 0, 0.25, 0.5, 0.75, 1.0, 1.5, 2.0, 2.5, 3, 4, 8, 12, 24, 48 and 72 h post consumption and collected into glass vacutainer tubes containing the anticoagulant, EDTA. An indwelling IV catheter was used for the first 4 h of blood collection; the remaining time points were collected by needle sticks. Initial studies using whole blood for AMS analysis resulted in high signal to noise based upon background endogenous ^{12}C that obscured the ^{14}C attributable to [^{14}C]-DBC. Therefore, whole blood was centrifuged for 10 min at 1,000 x g and 0.75 mL plasma aliquots transferred to glass culture tubes containing 0.75 g K_2SO_4, to prevent emulsion and stored at 4°C until extracted for AMS analysis. Urine contains low

endogenous carbon, allowing AMS analysis directly without extraction. Additional plasma and urine specimens were stored at -80°C for archiving.

All urine voided during the 72-h cycle was collected. Urine was pooled by 0– 6, 6–12, 12-24, 24-48 and 48-72 h batches for homogenized sampling and volume record by pool. Glass urine containers were provided for *as voided* collection. Coded plasma and plasma extracts and urine samples were stored at -20^{o}C prior to shipment to Lawrence Livermore National Laboratory (LLNL) for analysis by AMS. Archived samples were stored at -80^{o}C at OSU.

Extraction of plasma and collection of urine:

Plasma samples were extracted according to the method of Crowell *et al*., [47] . The samples were acidified with 0.75 mL 0.9 M H_2S0_4, vortexed for 20 s, then extracted thrice with 1 mL ethyl acetate and centrifugation at 750 g for 10 min. The combined extracts were evaporated under argon to dryness in an 8 mL amber glass vial with a PTFE cap liner, then stored at -20^{o}C until shipped on dry ice to LLNL for AMS analysis. As PAHs can adsorb to plastic, care was taken to use glass containers (amber when possible) for protection from light, and argon or nitrogen capping to prevent oxidation of samples. Urine was aliquoted in 1 mL volumes for shipping, requiring no additional processing prior to AMS preparation.

Extraction efficiency:

The extraction efficiency for [^{14}C]-DBC from plasma was determined by spiking plasma with known amounts of [^{14}C]-DBC using dilutions of the [^{14}C]-DBC micro-dosing ethanol stock solution. Following ethyl acetate extraction and reconstitution with 50:50 methanol:water (v:v) used for AMS analysis (described below) the recovery was 51 ± 10% (n=3) as determined by AMS. In a separate test of extraction efficiency, fresh or thawed frozen plasma, 0.75 mL, was spiked with 1.25 nCi [^{14}C]-DBC solution prior to extraction resulting in 55 ± 7 % recovery of [^{14}C]-DBC as detected by scintillation counting. This process was repeated with several [^{14}C]-DBC concentrations, and with detection by AMS and scintillation counting. Overall, across a number of concentrations, 55 ± 7% (at the low end of previously reported recoveries of 61-101% in human studies with pharaceuticals [156], perhaps due to the much lower mass of the dose utilized in this study), was the average DBC recovery when reconstituted in methanol:water, this value was used for efficiency corrections in the PK parameters reported below. Recent work by Crowell et al., [141] had determined this to be the optimal extraction method for DBC, as well as the diol, and tetraol metabolites.

AMS of plasma and urine samples:

Upon arrival at LLNL, samples were stored at -80°C until processing. Plasma extract samples were reconstituted with 100 µL 50:50 methanol:water and converted to graphite by the method of Ognibene et al.,[161]. Urine samples (100 µl) were converted, without prior processing , by the same graphitization method. Briefly, the

samples were evaporated and flame sealed in a quartz tube containing Cu(II) and combusted to 900°C, producing CO_2. The CO_2 was then transferred to a septa sealed glass tube containing Zn and Co and heated to 525°C, producing graphite on the Co catalyst upon cooling. The graphite was then removed and loaded into an aluminum sample holder for AMS analysis.

AMS analysis was conducted on the 1 MV AMS, constructed and maintained by the Center for Accelerator Mass Spectrometry at LLNL. The current AMS operating conditions are optimized to determine the ratio of ^{14}C:^{12}C with a precision of 3% and sensitivity of 0.4 attomol ^{14}C per mg of total carbon [162]. Solid sample standards containing a known $^{14}C/^{12}C$ content are measured 4–7 times with the collection of at least 10,000 ^{14}C counts or for 30 s, to assess the ionization and counting efficiency of BioAMS prior to sample analysis [163].

Determination of pharmacokinetic parameters:

Pharmacokinetic analysis of data utilized an Excel based add-on developed at Allergan, Inc. (Irvine, CA) [164]. Briefly, the formulae rely on non-compartmental analysis of six functions: peak concentrations in plasma (C_{max}), time of peak plasma concentration (T_{max}), plasma elimination half-life ($T_{1/2}$), apparent elimination rate constant (k_{el}) and area under the plasma concentration curve (AUC_{0-t} and $AUC_{0-\infty}$) using standard regression techniques [165]. Alpha and beta phase classifications were based on peak to trough values. Urinary clearance (CL, mL/min) was calculated by dividing the cumulative amount of ^{14}C eliminated in the urine over 72 h by the plasma AUC_{0-72h}.

3.4 RESULTS

We were able to empirically determine the environmentally relevant *in vivo* pharmacokinetics of [^{14}C]-DBC, in human volunteers utilizing AMS. The pool of nine volunteers included both sexes and was characterized by an age range from 20 to 65 years of age and BMIs from 23 to 35 (Table 1). No recruitment selection was made by volunteer physical characteristics. This study was intended to assess the range of pharmacokinetics in a cross section of human volunteers; as such it is not statistically powered to assess parameters such as gender, age, or BMI. Differences in age could lead to differences in gut motility possibly resulting in changes in absorption. The range of BMI likely results in a range of blood volumes and distribution. Due to a necessary change in plasma collection and processing method, three volunteers were excluded from the plasma pharmacokinetic analysis (Table 3.3); however, urine data from all nine volunteers is included (Table 3.2, Figure 3.2).

The pattern of absorption/excretion was similar between individuals (Figures 3.1 and 3.2). Levels of [^{14}C] in plasma rose rapidly following oral administration of [^{14}C]-DBC to volunteers that had been fasted overnight (Tables 3.3 and 3.4, Figure 3.2).

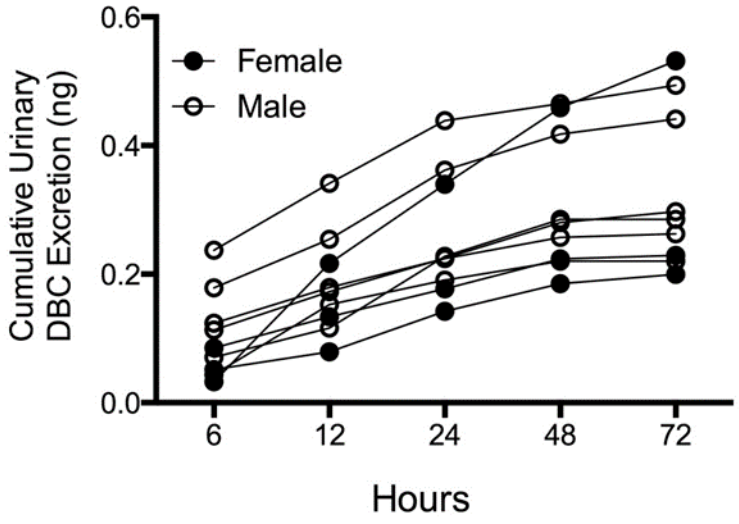

Figure 3.2. Cumulative Urinary Elimination of [^{14}C]-DBC$_{eq}$ Over Time for Six Volunteers.

All voided urine was collected over the 72 h of the study. A volumetric measurement was taken of urine pooled by time. A sample of 1 mL of urine was measured for [^{14}C]-DBC$_{eq}$ by AMS per pool, as described in Experimental Procedures. Volumetric corrections were made for total [^{14}C]-DBC$_{eq}$ elimination per pool. Results are recorded cumulatively

Figure 2

A.

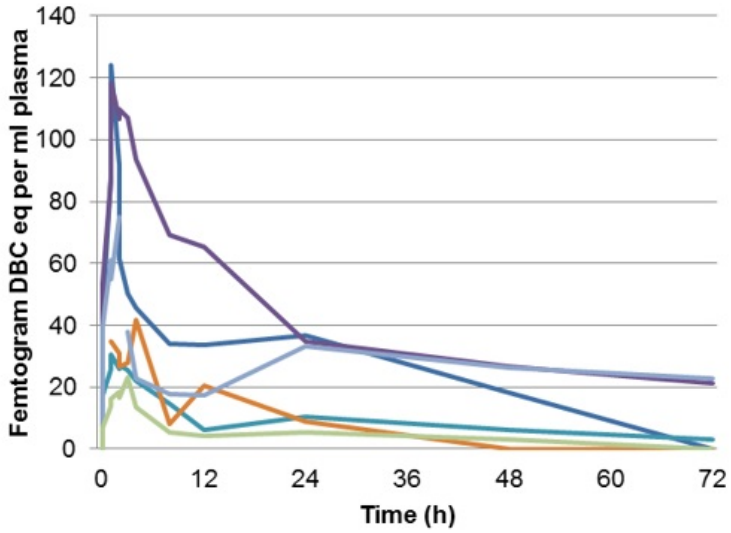

B.

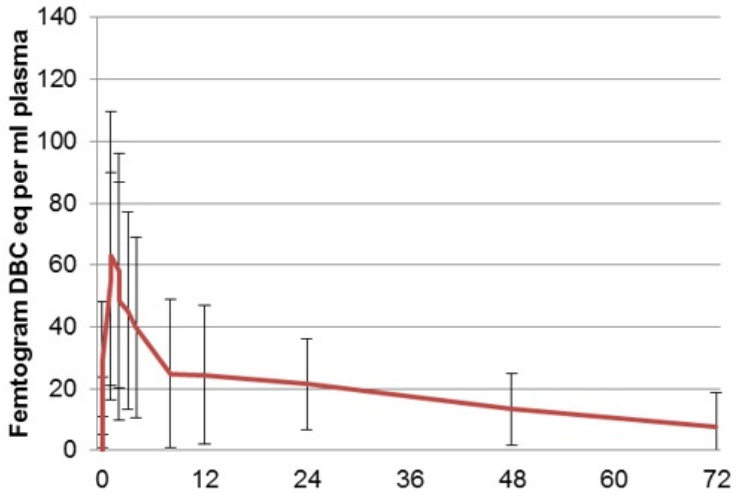

Figure 3.3: [^{14}C]-DBC$_{eq}$ Plasma Elimination Curve in 6 Volunteers

(A) Plasma levels of [^{14}C]-DBC$_{eq}$ over time are depicted for 6 individual volunteers as measured by AMS as described in Experimental Procedures. (B) This graph depicts the average and standard deviation of [^{14}C]-DBC$_{eq}$ in plasma for the same 6 volunteers as in (A).

A T_{max} at 2.25 h was observed, followed by a rapid α-phase elimination prior to a slower β-phase elimination. This study was limited to the appearance and disappearance of ^{14}C-labeled DBC_{eq} from plasma and the levels appearing with time in urine (a true mass balance study would have required fecal analysis as well as determination of tissue levels (not possible in a human study without subsequent diagnostic surgery). Considering differences in absorption based on motility, distribution based on BMI, and metabolism based on polymorphisms, the pharmacokinetics were notably consistent.

Plasma DBCeq as Determined by AMS (fg DBC/mL plasma)

Time (h)	0.00	0.25	0.50	0.75	1.0	1.5	2.0	2.5	3.0	4.0	8.0	12.0	24.0	48.0	72.0
V1	0.0	0.0	13.8	44.1	88.4	124	91.7	61.5	50.1	45.7	33.8	33.6	36.5	18.0	0.0
V6	0.0	0.0	27.9	53.7	87.3	118	107	110	107	93.4	69.3	65.1	34.9	26.5	21.2
V8	0.0	0.4	6.7	17.4	25.9	30.4	25.7	26.9	25.6	22.1	14.8	6.1	10.3	6.2	3.2
V9	0.0	0.0	0.4	15.4	N.D	34.7	30.8	26.5	27.9	41.6	8.1	20.4	9.0	0.0	0.0
V10	0.0	8.9	23.7	39.5	61.1	54.8	75.0	N.D.	37.8	22.6	17.6	17.3	33.0	26.1	22.7
V13	0.0	0.0	1.4	7.1	13.9	16.1	18.6	16.5	23.3	13.4	5.2	4.3	5.5	3.2	0.0
mean	0.0	1.5	12.3	29.5	55.3	63.1	58.1	48.2	45.3	39.8	24.8	24.5	21.5	13.3	7.8
SD	0.0	3.6	11.6	18.7	34.4	46.7	37.8	38.4	31.9	29.0	24.0	22.6	14.7	11.7	11.0

N.D., no detect

Table 3.4: Plasma DBCeq fg DBC/mL plasma

Recovery of urinary ^{14}C over 72 h yielded 1.24 ± 0.49% of the dose administered (Table 3.2). Due to the high hydrophobicity (log K_{ow} 7.4), the majority of DBC is likely unabsorbed and eliminated in the feces. Oral bioavailability could be expected to be strongly linked to the fat content of vehicle administered at dosing[166]. The fasted volunteers administered a dosing capsule with water likely limited bioavailability. Previous high dosing studies of BaP in rodents have resulted in minimal elimination in urine, 0.22-0.35% and 0.10-0.08% of oral dose administered, detected as known metabolites [167, 168]. Oral gavage of mice with 15 mg/kg of DBC with corn oil vehicle yielded 4.9 to 7% urinary excretion of the total oral dose [37]. Administering an oral dose of 15 mg/kg DBC to mice resulted in a T_{max} between 2-4 h, with detectable DBC in blood 48 h post gavage.

3.5 Discussion

As environmental PAHs occur in complex mixtures, ingestion/elimination kinetics in humans from PAH exposures are difficult to discern. The translation of high dose animal experiment data for human risk assessment is often criticized as being of questionable relevance for human exposures. Due to the sensitivity of AMS we are able to assess the *in vivo* human metabolic parameters of one of the most carcinogenic PAHs in animal models, DBC, while maintaining risk to volunteers at a *de minimus* level. Our pharmacokinetic dataset following human DBC exposure at environmentally relevant levels will provide a translational and validation tool for agencies charged with risk assessment and modeling to humans of high molecular weight, carcinogenic PAHs.

PAHs are pro-carcinogens, requiring enzymatic activation to electrophilic metabolites such as epoxides, dihydrodiol-epoxides and quinones [117, 119]. These electrophiles have numerous nucleophilic targets in the cell including DNA. In the case of DBC, cytochrome P450 (P450)-dependent 11,12- epoxygenation followed by hydrolysis (epoxide hydrolase) and a second epoxygenation produces the 11,12-dihydrodiol-13,14-epoxide (DBCDE). Of the four possible enantiomers, the (-)-*anti*-11*R*,12*S*-dihydrodiol-13*S*,14*R*-epoxide or (-)-*anti*-DBCDE is thought to be the most efficient at forming DNA adducts at a number of sites on purine bases [169] especially at N^6-dA and N^2-dG. Understanding the extent of metabolism, both bioactivation and detoxication (conjugation by SULTs, UGTs and GSTs), following exposure to environmentally relevant doses would greatly add to the impact of Bio-AMS studies such as this one. The same is true for determination of the extent and identity of DNA adducts in peripheral blood mononucleocytes following micro-dosing.

A current strength and drawback to the solid sample Bio-AMS technology employed in this study is that only total [^{14}C] label is detected. While providing sensitivity in the attomole range, this method is not capable of speciation, i.e., chemical identification and quantification of parent compound and metabolites. Previously, to identify metabolites, plasma extracts would have to be separated by HPLC and collected as discrete fractions, based on the retention time of metabolite standards, prior to graphitization [152]. This approach is burdened with the same limitations of HPLC fraction collection for uncoupled traditional MS. HPLC fraction selection is

based on the retention time of commercially available standards for downstream MS analysis. Only select fractions can be analyzed due to study limitations, including manual sample preparation.

New instrumentation at LLNL provides liquid sample AMS through the interface of UHPLC and AMS and determination of the metabolite profile [170]. Moving wire coupled UPLC-Bio-AMS (liquid sample Bio-AMS) technology combusts column eluent to $^{14}CO_{2,}$ prior to AMS carbon isotope detection across an entire chromatographic run. Parent, metabolite, and all conjugated species present from a biological matrix such as plasma, urine, or isolated DNA adducts can be detected and quantitated. Standards are necessary for identification based on retention time, but all species resulting from metabolism would be represented in the ^{14}C tracing. Future work will focus on utilizing liquid sample Bio-AMS to identify the species and concentration of PAH metabolites over time and examination of inter-individual differences such as genetics or previous environmental exposures, elucidating gene-environmental interactions at micro-doses. One such study is currently underway in our laboratory. A targeted total of 75 enrolles will be dosed with 5 nCi (46 ng) of [^{14}C]-BaP. Plasma and urine levels of parent [^{14}C]-BaP and [^{14}C]-BaP metabolites will be assessed over a 72 h period employing UHPLC-AMS [152] (FDA IND #117175; OSU IRB #5644). Preliminary results to date (Figure 3.4) show that the majority of the ^{14}C counts co-elute with the [^{14}C]-DBC standard with minor amounts of both the [^{14}C]-DBC-11,12-dihydrodiol and the [^{14}C]-DBC-11,12,13,14-tetraol

(hydrolysis product of the unstable DBCDE); again, tentatively identified by co-elution with standards. The apparent peak eluting early (2-2.5 min) is unknown.

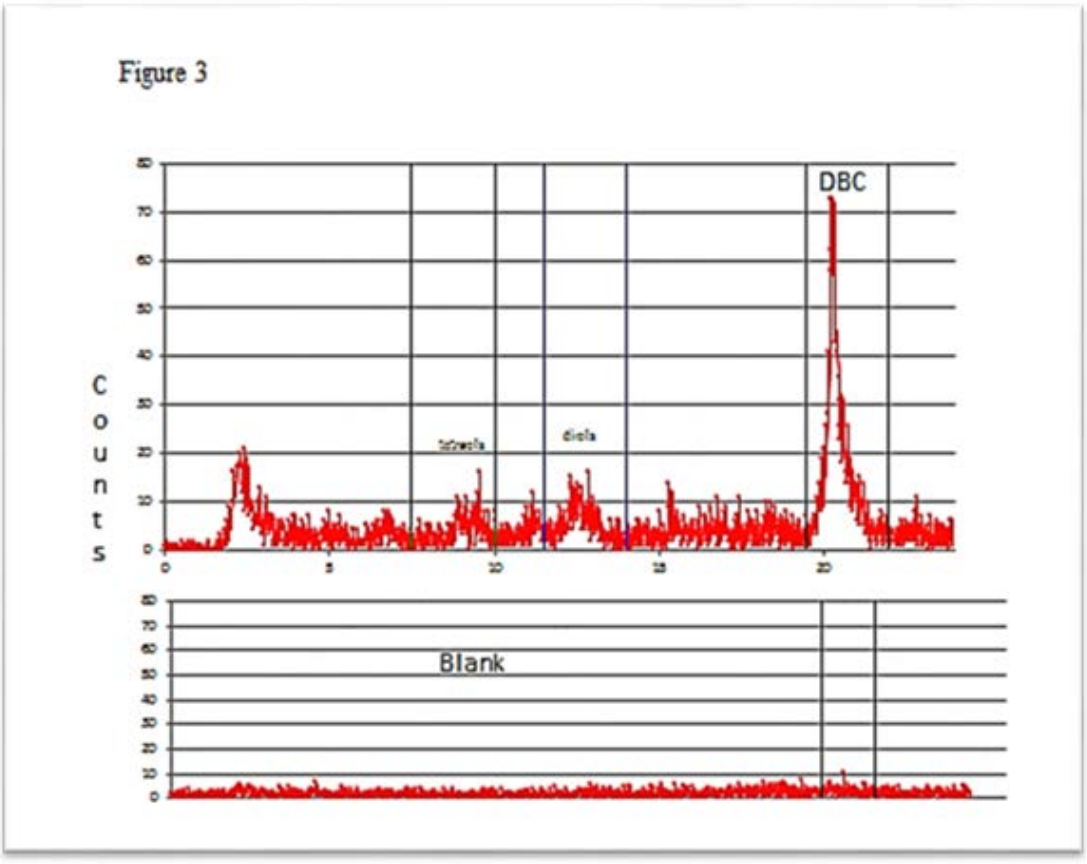

Figure 3.4: UHPLC-AMS of [^{14}C]-DBC and Putative Metabolites from Plasma of Volunteer 6 0.75 Hours Following Dosing.

Five µL of plasma extract (volunteer 6, 0.75 hour after dosing) was injected onto a Phenomenex Kinetex^{TM} 2.6 µm C_{18} 100 Å (Part no: 00f-4462-AN) column (150 x 2.1 mm) fitted with a C_{18} guard column and eluted with a gradient of: 0-3 min isocratic 45% ACN; to 100% ACN over the next 10 min; hold at 100% ACN for 3 min with a return to 45% ACN over the next 2 min at a flow rate of 0.12 mL* min^{-1} (25°C). Following passage through a dual channel UV/VIS detector (280 and 315 nm), the

eluent was deposited onto a moving nickel wire and the [^{14}C]-DBC$_{eq}$ converted to $^{14}CO_2$ prior to AMS analysis[47]. Multiple channels allow for the simultaneous determination of A_{280} and A_{315} as well as counts of ^{12}C and ^{14}C. Only the ^{14}C profile is shown here. The use of unlabeled parent DBC and standards (DBC-(±)-11,12-diol and DBC-(±)-11,12,13,14-tetraol) allow for tentative identification of ^{14}C peaks. The polar putative metabolite eluting between 2-2.5 min is currently unknown. It should be noted that this is the first samples run by UHLPC and is from plasma 0.75 h post-dosing from volunteer #6 (see Table 3).

Extraction at later time points (or pooling of some time points) and from higher volumes of plasma should allow us to definitively quantify these putative metabolites. We compared the human [^{14}C]-DBC$_{eq}$ pharmacokinetic profile with the previously published PBPK model for rats and mice [168]. Note that the rodent model reliably predicts the actual human data (Figure 3.5).

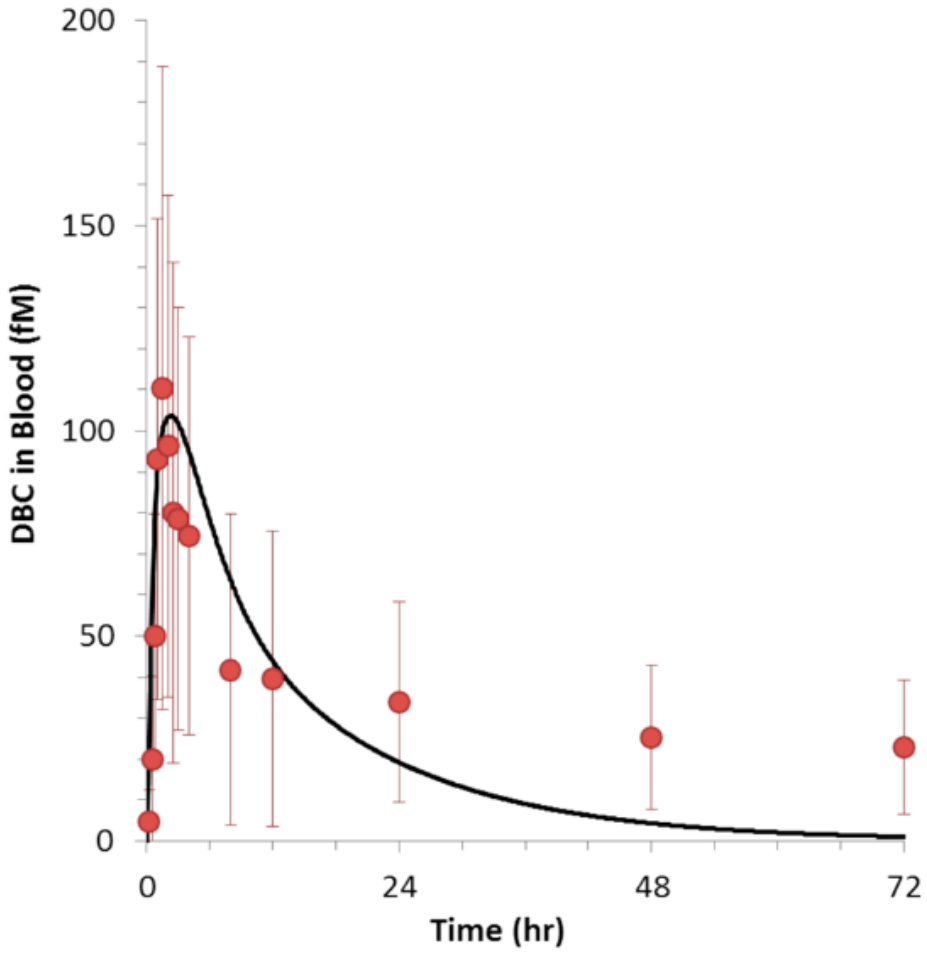

Figure 3.5: Pharmacokinetic Profile of [^{14}C]-DBC$_{eq}$ in Humans: Comparison to Rat and Mouse PBPK Models.

The ● symbols are plasma levels over time of [^{14}C]-DBC$_{eq}$ following micro-dosing of humans with 5 nCi (29 ng) of [^{14}C]-DBC. The solid curves are PBPK model predictions from rat and mouse as calculated by Crowell et al.

The pharmacokinetics of phenanthrene (a 3 ring PAH) and its diol and tetraol metabolites has been conducted in humans following oral or inhalation exposure to 10 µg of [D_{10}]-phenanthrene and analysis of plasma and urine over time by GC-electron impact-MS/MS [171-173]. Phenanthrene can act as a surrogate for larger molecular weight carcinogenic PAHs [174] as it has a bay region and is metabolized in a similar

manner as BaP but regarded as a class C PAH by IARC [14] and has been given an RPF of 0 by EPA [2]. In our subsequent studies characterizing the pharmacokinetics of BaP and its metabolites by UHPLC-AMS following micro-dosing with 46 ng, we hope to examine the impact of genetic polymorphisms in BaP-metabolizing enzymes as was done by Wang et al.[172].

The ability to determine the pharmacokinetic parameters, safely in humans, of carcinogenic chemicals found in the environment and their metabolites is an advancement in risk assessment. Further development and application of this technology could have a major impact in the arena of human environmental health.

ACKNOWLEDGEMENTS

The authors would like to acknowledge the pharmaceutical expertise and contribution of materials provided by Dr. Mark Christensen (College of Pharmacy, Oregon State University). This study was funded by PHS grants P42ES016465, K.C. Donnelly Supplement P42ES016465, P41GM103483 and T32ES07060. AMS was performed at the Research Resource for Biomedical AMS which is operated at LLNL under the auspices of the U.S. Department of Energy under contract DE-AC52-07NA27344 and National Institute of General Medical Sciences 8P41 GM103483-14.

Chapter 4

Environmentally Relevant *in vivo* Human Pharmacodynamics of Polycyclic Aromatic Hydrocarbon Dibenzo[*def*,*p*]chrysene, Liquid Sample-AMS Applications for Risk Assessment

Erin P. Madeen[1,2], Ted Ognibene[3], Rick Corley[4], Mark Christensen[5], Tammie McQuistan[2], Ken Turteltaub[6], David E. Williams[1,2].

[1]Department of Environmental and Molecular Toxicology, Oregon State University, Corvallis, Oregon 97330
[2]Superfund Research Program, Oregon State University, Corvallis, Oregon 97330
[3]Center for Accelerator Mass Spectrometry, Lawrence Livermore National Laboratory, Livermore, California
[4]Systems Toxicology & Exposure Science, Pacific Northwest National Laboratory, Richland, Washington 99354, United States
[5]College of Pharmacy, Oregon State University, Corvallis, Oregon 97330
[6]Biology and Biotechnology Research Division, Lawrence Livermore National Laboratory, Livermore, California 94550, United States

4.1 Abstract

Dibenzo[def,p]chrysene (DBC) is not included in the list of priority pollutants, however it has an accepted BaP equivalence of 30 with a range of 10-40 BaPeq by route of exposure and is a class 2A carcinogen, defined by IARC as a compound likely to be carcinogenic to humans. Metabolism is a key factor in health risk from PAH exposures, including that of DBC. PAHs are procarcinogens, requiring enzymatic activation to a reactive metabolite capable of DNA adduction or redox cycling. Plasma was collected by time points 0, 0.25, 0.5, 0.75, 1.0, 1.5, 2.0, 2.5, 3, 4, 8, 12, 24, 48 and 72 hours. All urine voided during the 72-hour cycle was collected. Urine was pooled by 0– 6, 6– 12, 12-24, 24-48 and 48-72 hr batches for homogenized sampling and volume record by pool. The major plasma product from DBC exposure is parent DBC. There is a large range of plasma concentrations, likely related to absorption and volume of distribution in a heterogeneous population. The cumulative pool of DBC metabolites were more consistent between volunteers than were the concentrations of parent compound, indicating that DBC is removed from the system, likely through biliary excretion, instead of cycling as metabolites in plasma and that metabolic rate is not determined by absorption of parent alone. The major known plasma metabolite is diol. DBC tetrols were not present in the plasma fraction. The lack of free tetrol in plasma, while conjugated tetrol is the major urine species, indicates that tetrol is rapidly conjugated, filtered from plasma and eliminated renally. Several unknown species of DBC product were detected, including a high concentration ^{14}C peak in the mobile phase solvent front. Additionally, DBC products with polarity between DBC and DBC diol were present. Putatively, these compounds

are quinones. When the AUC of each metabolite was normalized as a percent of the DBC AUC, the percent relative standard deviation increased between 2 to 5 fold. There was no central tendency for metabolite formation based as a percentage of DBC distributed in plasma. This indicates that the metabolism rate is limited more so by enzyme kinetics than absorption rate as the metabolite profile is not dependent upon uptake rate, and that kinetics are more similar between individuals than is uptake between individuals.

4.2 Introduction

PAHs

Polycyclic aromatic hydrocarbons (PAHs) are ubiquitous environmental pollutants produced by combustion, often originating from industrial activity, automotive exhaust, and forest fires. Oral exposure occurs in humans from contamination to crops or soils that crops are grown in [13, 147]. Additionally, PAHs are added to preserve or flavor foods through smoking or storing liquids in smoke charred containers. The largest source of PAH exposure in non-smokers is through the diet, contributing up to 95% of PAH intake [24, 151].

Of the 126 EPA priority pollutants, 16 are PAHs [46]. Dibenzo[*def,p*]chrysene (DBC) is not included in the list of priority pollutants, however it has an accepted BaP equivalence of 30 with a range of 10-40 BaPeq by route of exposure [2, 175] and is a class 2A carcinogen, defined by IARC as a compound likely to be carcinogenic to humans [14]. Rarely is data available on the DBC content of food products, likely due to exclusion from analytical library programs as DBC is not an EPA priority pollutant. DBC has been found in common food sources from markets [7, 13]. DBC has been found to be a potent DNA mutagen in *in vitro* studies [27, 169, 176-178] and has been found to yield a variety of cancers and morbidities in several animal models, including mouse offspring following transplacental exposure [32, 33, 38, 44].

PAHs occur in highly variable mixtures in a variety of occupational or environmental exposures due to combustion dynamics, making pharmacokinetic studies from most high concentration human exposures inconsistent and challenging for risk assessment. Traditional instrumentation has not been sensitive enough to safely evaluate an administered dose in human volunteers. A recent challenge to human risk assessment modelers was the limited data available from low dose studies, studies of human exposure, or animal high dose studies of DBC [47].

Metabolic Activation of PAHs

Metabolism is a key factor in health risk from PAH exposures, including that of DBC. PAHs are procarcinogens, requiring enzymatic activation to a reactive metabolite capable of DNA adduction or redox cycling (Figure 4.1). PAHs are metabolized by cytochrome P450 (CYP)-dependent epoxygenation, hydroxylation or formation of quinones [25, 179, 180] or peroxidase-mediated production of radical cations[27, 181]. Penning and colleagues have demonstrated that PAH *trans*-dihydrodiols (DHDs, formed by hydrolysis of the epoxide) are substrates for aldo-keto reductase (AKR) production of catechols which generate oxidative stress through redox cycling between the catechol, semi-quinone and quinone [121]. Hydroxylated PAHs are also substrates for UDP-glucuronosyl transferases (UGT) and sulfotransferases (SULT); “phase two” reactions that enhance excretion [182, 183]. The carcinogenicity of the larger PAHs such as BaP and DBC, especially those containing a “bay” and/or “fjord” region is thought to be due mostly to CYP1A1 and CYP1B1 epoxygenation followed by epoxide hydrolase (EH) hydrolysis to the dihydrodiol [26, 184, 185]. A

second epoxygenation of the dihydrodiol produces the ultimate carcinogen, the dihydrodiol-epoxide (DHDE). CYP can epoxygenate the aromatic rings on PAHs above or below the plane of the molecule, resulting in two DHD *trans* sterioisomers following EH hydrolysis. Both DHDs can then be epoxygenated a second time by CYPs 1A1 and 1B yielding 4 possible dihydrodiol-epoxides; in the case of DBC this produces 4 enatiomers of 11,12-dihydrodiol-13,14-epoxide [186, 187]. DBC dihydrodiol-epoxides are electrophilic and readily form DNA adducts, the most potent is the (-)-*anti-trans-11,12*-diol-13,14-epoxide), primarily with dA followed by dG producing mutations [188]. The enzymatic rates for these reactions are known and are incorporated into the rodent PBPK model for human DBC metabolism [189].

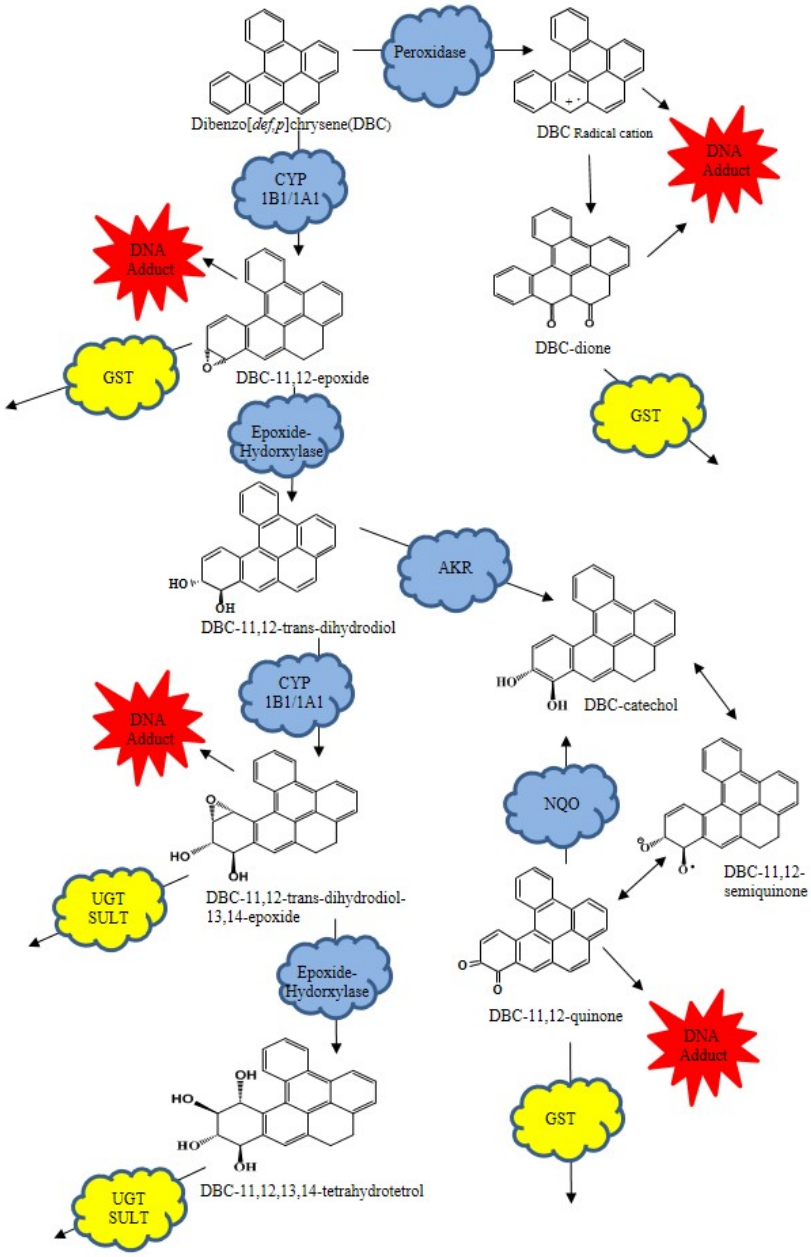

Figure 4.1: Metabolic Activation of DBC

AMS

Accelerator mass spectrometry (AMS) is used to detect and quantify rare isotopes. More recently, AMS instruments have been dedicated to the biomedical study of pharmaceuticals, biological molecules, and pollutant metabolism through human *in vivo* and cell based *in vivo* experiments [170, 190]. Endogenous ^{14}C content can be utilized as a marker of age and cell turn over relative to the ^{14}C bomb pulse background present from nuclear arms testing. Exogenous molecules are labeled with an isotope such as ^{14}C or ^{3}H and are assessed at various endpoints from a variety of tissues. The sensitivity of the Lawrence Livermore National Laboratory (LLNL) Center for Mass Spectrometry (CAMS) 1MV Bio-AMS, in the attomole range for ^{14}C, [170] allows for the administration and subsequent detection of a microdose, defined as a dosage at least two orders of magnitude below that of which would be expected to yield a pharmacologic effect [63]. This sensitivity allows for the administration of carcinogenic compounds to humans at dosages predicted to yield *de minimus* health risks, with reliable detection.

Aims

Previously, we addressed the pharmacokinetics of DBC absorption and elimination in urine and plasma of human volunteers [191]. The aim of this work is to address the pharmacodynamics of *in vivo* human metabolism of DBC following a controlled environmentally relevant dose representing a *de minimus* risk to human volunteers. This is the first application of online HPLC-AMS ^{14}C isotope detection from a controlled human *in vivo* biological sample set.

4.2 Materials and Methods:

Human Volunteers:

The recruitment and inclusion of human volunteers was approved by the Oregon State University Institutional Review Board in cooperation with the Oregon State University Radioactive User Agreement under the oversight of the Oregon Health Authority. Volunteers were recruited from 2011 to 2012 to participate in a pharmacokinetic study of the elimination of DBC in plasma and urine [191], with additional samples archived, per volunteer informed consent agreements, to be analyzed for pharmacodynamics as the technology to do so was developed at LLNL. Archived sample processing and analysis occurred in several batches from 2013 to 2014. Volunteer inclusion criteria included good general health with exclusion in any of the following scenarios: smoking, using medications that can affect gut motility, history of gastrointestinal surgeries, kidney or liver disease, or GI diseases such as Crohn's, ulcerative colitis, or gastritis. Women pregnant or capable of becoming pregnant were excluded from this study out of extreme caution due to proven transplacental toxicity in high dose rodent models [32, 38]. Volunteer demographics are included in Table 4.1.

Table 4.1 Volunteer Demographics

Volunteer	Gender	Ethnicity	Age	BMI
V5	F	Caucasian	65	34
V8	M	Caucasian	26	24
V9	F	Caucasian	56	32
V10	M	Caucasian	20	23
V11	M	Caucasian	43	35

V13	M	Caucasian	36	34

Dosage selection, preparation, and QA:

DBC, ^{14}C labeled on the U ring, with a specific activity of 51.4 mCi/mg was donated by the Midwest Research Institute (Kansas). Metabolism of DBC, and bay region containing PAHs in general, includes dihydrodiols and epoxide formation about the bay region, without alteration of the carbon backbone (Figure 4.1). As such, all metabolites of DBC are traceable and quantifiable via ^{14}C-DBC equivalent isotopes detected. As previously described [191], a dosage solution, ±98% radio and chemical purity, was adjusted to 29 ng DBC, containing 5 nCi ^{14}C, per 26 µL ethanol, delivered to overnight fasted volunteers via oral capsule with water.

Plasma:

Plasma was collected at time points of 0, 0.25, 0.5, 0.75, 1.0, 1.5, 2.0, 2.5, 3, 4, 8, 12, 24, 48 and 72 hours. Archived aliquots of 1 mL plasma were thawed from $^{-}80^{o}C$ storage and prepared by the methods previously described [47]. Briefly, plasma was treated with 0.75 mL of 1 M H_2SO_4, vortexed, combined with 0.75 g of K_2SO_4, and extracted thrice with 1 mL of ethyl acetate. Extracts were shipped to LLNL on dry ice and subsequently stored at $^{-}80^{o}C$ until preparation for HPLC. Samples were dried by speed vap at room temperature, reconstituted with 100 µL ethyl acetate, transferred to HPLC inserts, dried under vacuum and reconstituted with 50 µL acetonitrile. They were then stored at $^{-}80^{o}C$ until HPLC injection. All containers were single use glass to reduce the risk of adsorption to plastic.

Urine

All urine voided during the 72-hour cycle was collected. Urine was pooled by 0– 6, 6– 12, 12-24, 24-48 and 48-72 hr batches for homogenized sampling and volume recording by pool. Urine was prepared pairwise as 1 mL aliquots from archived storage at $^{-}80^{o}$C as β-glucuronidase cleaved experimental or non-enzyme treated control samples. Sample pH was adjusted to 7 with 0.063 M H_2SO_4 and 0.12 M NaOH. Experimental samples were treated with 2,000 Fleischman units of β-Glucuronidase (St. Louis, MO). All samples were vortexed and placed in a shaking water bath at 37^{o}C for 18 hours. Samples were extracted thrice with 1 mL ethyl acetate and the organic phase transferred to a separate culture tube for nitrogen evaporation at 35^{o}C to dryness. Samples were stored at 4^{o}C for overnight shipping to LLNL for analysis, at which time they were stored at $^{-}80^{o}$C until reconstitution with 50 µL acetonitrile for HPLC. All containers were single use glass.

HPLC:

A Waters Aquity H Series HPLC was utilized with a C18, 150 x 2.10 mm, 2.6 µm, 100 angstrom column (Phenomenex 00F-4462-AN) and 2.1 mm guard column (Phenomenex AJ0-8782) at 25^{o}C. The gradient solvent program was ACN:Water, 0-3 min 45:55 isocratic, 3-33 min 45:55 to 100:0, 33-36 min 100:0, 36-38 min 100:0 to 45:55. The flow rate was 0.12 mL·min^{-1}. DBC standards were found to elute as follows: DBC 20.5 minutes, DBC 11,12-diol 12.5 minutes, DBC racemic tetrols 6.5,7.5, and 11 minutes, (Figure 4.2).

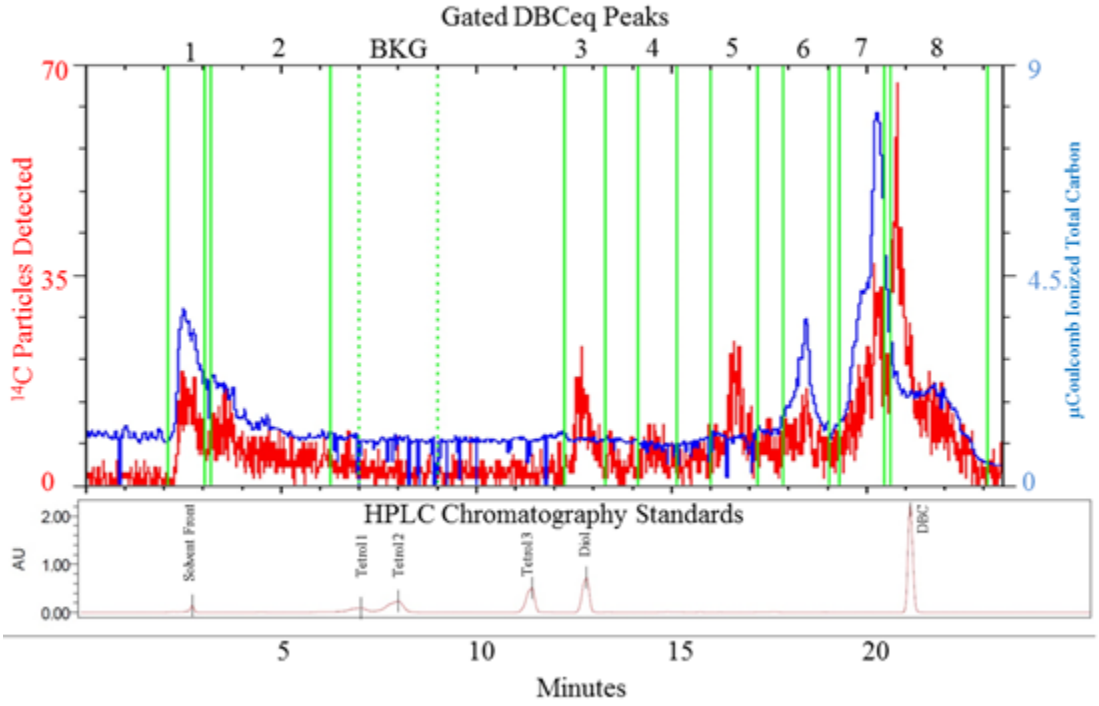

Figure 4.2: ^{14}C-DBC Plasma Tracing and HPLC Standards

Non-labeled DBC HPLC standards provided retention time data by PDA detection (bottom). ^{14}C particles were detected by AMS, which are then related to the specific activity of DBC to provide quantitative data (top left axis). To account for the endogenous ^{14}C content of a biological material and potential carbon spikes from elution of biological material across the gradient, the concentration of total carbon was quantited during the AMS run (top right axis). This allows for the removal of ^{14}C endogenous background from the ^{14}C detected.

HPLC-AMS:

HPLC eluent is converted to CO_2 in the method described [170]. Briefly, a moving nickel wire with evenly spaced indentations transfers eluent as discrete droplets to a 140^{o}C drying oven to evaporate solvent, prior to a 750^{o}C combustion oven, converting available carbon to CO_2. Helium carries the CO_2 generated to the cesium sputter ionization source.

A faraday cup detector provides quantitative data on total carbon measurements pre-acceleration online with ^{14}C particle detection post-acceleration (Figure 4.2 top right axis). Endogenous carbon contains 97.89 zmol ^{14}C/µg total carbon, or 1 Modern, allowing endogenous ^{14}C to be independently quantified and removed from downstream ^{14}C particle counts in a single HPLC-AMS sample run, Figure (4.2). This is an advantage over traditional HPLC methods as the AMS system allows distinction of matrix noise from analyte, reducing the need for inefficient or complex cleanup of low concentration samples, such as solid phase extraction or QuEChERS methods. All ^{14}C data reported is post adjustment for removal of endogenous ^{14}C contributions.

Data Quality Assurance

Error in precision of AMS data values are known for each tracing as accuracy standards are analyzed prior to each HPLC injection. Error considered is total error, propagated from errors around precision, endogenous carbon (faraday cup), and ^{14}C particle detection, as AMS-chromatography data is adjusted for these factors detected within a sample analysis run. Total error is determined utilizing a non-linear uncertainty propagation method. Error tolerance was limited to 30% RSD of total error. The remaining 339 plasma data points (of 445 points analyzed), (Table 4.2) contained 24 data points above 20% RSD and the RSD averaged 12±5%. All plasma values containing error ≥ 30% detected values were reported as >%RSD and were eliminated from data interpretation (Table 4.2).

The lower limit of quantitation (LLOQ) was determined by the signal to noise method [192, 193]. Background is determined from a gate representing the system noise in counts/second. Signal is total ^{14}C particle counts less (background + endogenous ^{14}C contributions). Noise is defined as $2 \cdot \sigma$ baseline mean. The LLOQ was determined to be S/N $\geq$ 5, all data points below this value were reported as <S/N and were eliminated from data interpretation. Of the 339 plasma data point remaining from the 445 analyzed, 85 data points were below S/N 10. The S/N of the 339 included data points averaged 33 with a unimodal SD of 55 and mode of 18 (Table 4.2).

Accuracy was determined with a reference ^{14}C sucrose solution (ANU), determined to have 300 ng total carbon/µL and 147.52 zmol ^{14}C particles/µg C [194]. Analytes are detected as ^{14}C particles and are related to the target molecule through specific activity. As such, ANU serves as a surrogate to research compounds for efficiency of combustion, ionization, molecular stripping, and ultimately detection. CO_2 from combustion is carried via helium through a disposable ionization target that is replaced with each HPLC run. Discrete drops of 2 µL ANU are applied to the moving wire prior to every HPLC run to determine the ionization efficiency of each target, and accuracy of the system as a whole for accuracy adjustments and error determination [170].

Pharmacokinetic (PK) analysis of data utilized an Excel based add-on developed at Allergan, Inc. (Irvine, CA) [195]. Metabolite peaks are assessed individually or as the sums of peaks of a given time point. PK formulae rely on non-compartmental

analysis of six functions: peak concentrations in plasma (C_{max}), time of peak plasma concentration (T_{max}), plasma elimination half-life ($T_{1/2}$), apparent elimination rate constant (k_{el}) and area under the plasma concentration curve (AUC_{0-t}) using standard regression techniques [165]. Alpha phase classification primarily 0-8h, while beta phase was considered from 8 to 12 h.

4.4 Results

Plasma:

DBCeq of parent and metabolite concentrations by volunteer and time point are reported in Table 4.2 and Figure 4.3. The major plasma product from DBC exposure is parent DBC. There is a large range of plasma DBC concentrations, likely related to differing absorption and volume of distribution in a heterogeneous population. The cumulative pool of DBC metabolites were more consistent between volunteers than were the concentrations of parent compound, indicating that metabolism is rate limited by enzyme kinetics more so than DBC uptake at an environmentally relevant dosage (Figure 4.3, Table 4.4).

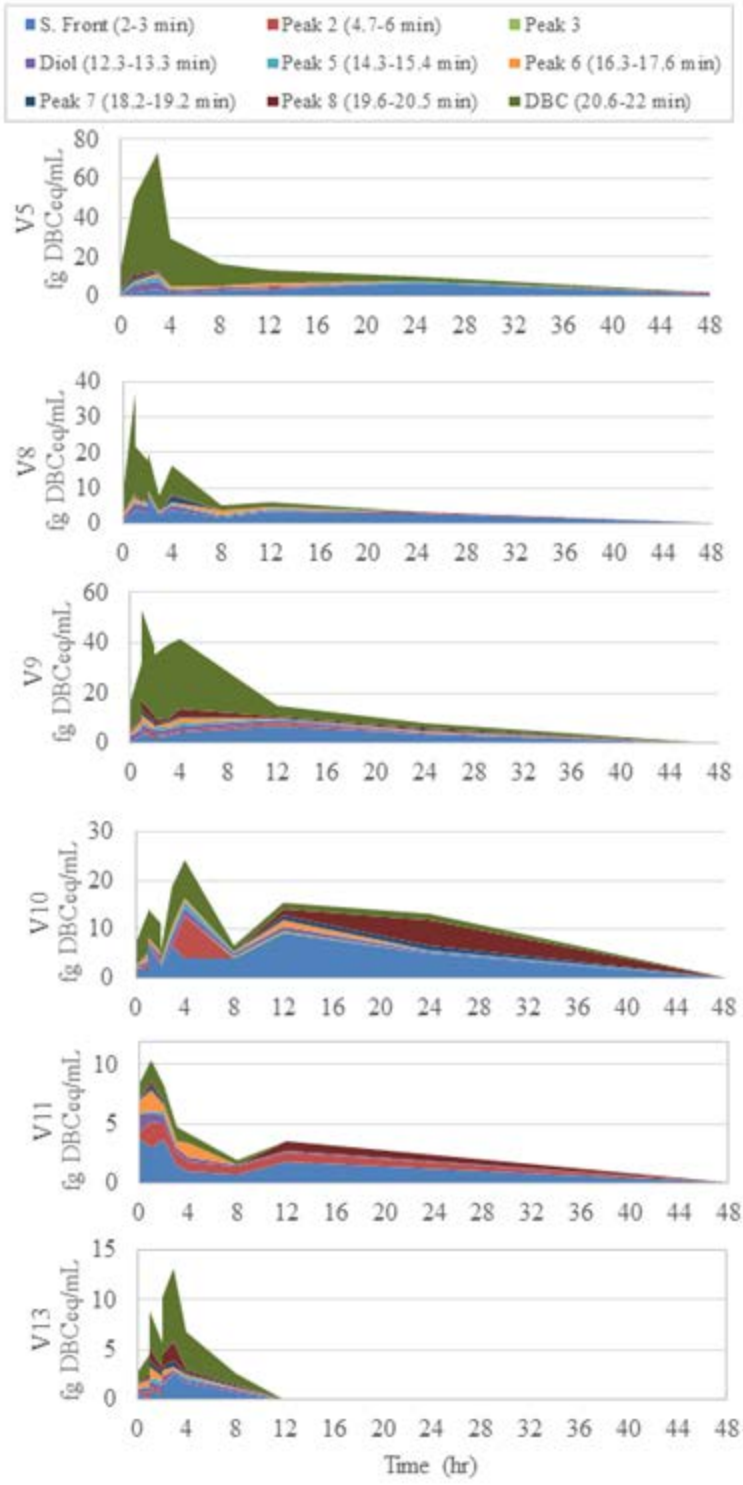

Figure 4.3. : ^{14}C-DBC Metabolite Appearance in Plasma

The concentration of ^{14}C-DBC in plasma was plotted as concentration over time by metabolite. The most abundant product was parent DBC, with species from the polar solvent front (more polar than tetrols), likely being conjugates of DBC metabolites.

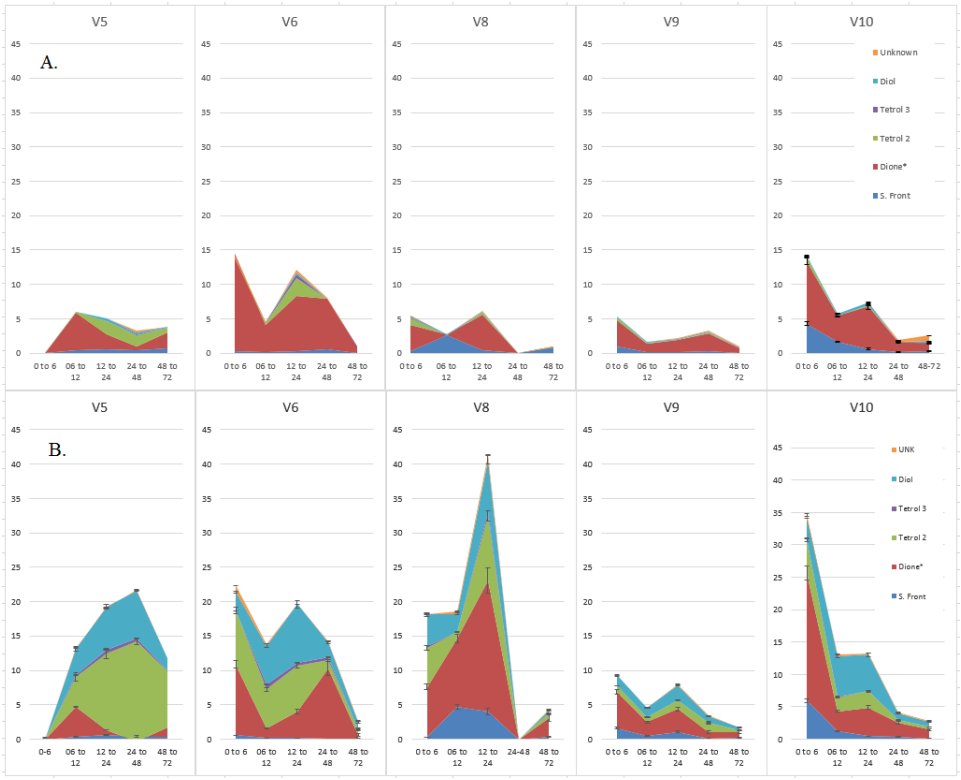

Figure 4.4: Metabolite Profile of ^{14}C-DBC in Urine (fg/urine pool)

The DBC metabolite profile in urine was assessed from native urine extracts (A) or from β-glucuronidase, with sulfatase activity, treated urine extracts (B). The diol is only present following enzyme treatment, indicating that it is in a conjugated form in urine. The putative dione concentration is increased following enzyme treatment only slightly, while other metabolite fractions were mostly present only following enzymatic cleavage, indicating that they exist in the conjugated form in urine.

The major known plasma metabolite is diol. DBC tetrols were not present in the plasma fraction, however unknown metabolites with a polarity higher than diols (determined by retention time and mobile solvent) eluting in peaks at 4.7-6 minutes

and 9.25 to 10.25 minutes, indicating further metabolism of diol products (Figure 4.3) The lack of free tetrol in plasma, while conjugated tetrol is the major urine species, indicates that tetrol is rapidly conjugated in plasma and eliminated renally. Isotopic labeling allows for the detection of metabolites other than those for which standards are available (Figure 4.2). Several unknown species of DBC product were detected, including a high concentration ^{14}C peak in the mobile phase solvent front. Additionally, DBC products with polarity between DBC and DBC diol are present. Putatively, these compounds are quinones and other intermediate metabolites between parent and diol (Figure 4.1 and Figure 4.3).

HPLC-AMS Peak Data

		Retention Times (min)								
		2.0-3.0	4.7-6	12.3-13.3	14.3-15.4	16.3-17.6	18.2-19.2	19.6-20.5	20.6-22	Total
Volunteer	Time Point									
V10	h	S. Front	Peak 2	Diol	Peak 4	Peak 5	Peak 6	Peak 7	DBC	Sum
	0.5	1.40	ND	0.26	<S/N	<S/N	<S/N	<S/N	1.08	2.74
	0.75	1.94	ND	0.43	<S/N	>%RSD	<S/N	>%RSD	4.55	6.92
	1	1.72	0.89	0.79	0.38	1.19	0.39	>%RSD	8.05	13.41
	1.5	6.86	ND	0.79	<S/N	0.54	<S/N	<S/N	6.07	14.49
	2	2.79	0.94	0.87	0.42	0.40	<S/N	<S/N	5.82	11.24
	2.5	2.19	ND	0.57	0.22	0.28	<S/N	<S/N	2.28	5.55
	3	6.60	ND	1.92	1.07	0.99	<S/N	<S/N	8.05	18.61
	4	4.11	8.77	1.52	1.25	0.62	<S/N	<S/N	8.09	24.37
	8	3.87	ND	0.66	0.36	>%RSD	<S/N	<S/N	1.47	6.36
	12	9.09	ND	1.00	ND	ND	0.95	1.26	1.56	13.86
	24	4.88	ND	0.28	0.44	<S/N	0.93	5.35	1.29	13.18
V11		S. Front	Peak 2	Diol	Peak 4	Peak 5	Peak 6	Peak 7	DBC	Sum
	0.5	3.11	ND	1.38	0.29	0.70	0.40	0.38	1.40	7.67
	0.75	3.76	0.49	1.57	<S/N	1.09	<S/N	<S/N	1.28	8.20
	1.5	3.02	2.15	0.79	0.19	1.70	0.45	0.32	1.79	10.41
	2	3.63	1.39	0.73	<S/N	0.71	0.26	<S/N	1.39	8.11
	3	1.54	1.09	0.39	<S/N	0.55	<S/N	>%RSD	1.17	4.98
	4	1.00	0.78	0.37	<S/N	1.23	<S/N	<S/N	0.84	4.22
	8	0.70	0.65	0.19	0.11	>%RSD	ND	<S/N	0.38	2.03
	12	1.76	0.77	0.22	<S/N	>%RSD	ND	0.75	<QC	3.51
	48	4.17	ND	<S/N	<S/N	>%RSD	ND	>%RSD	<S/N	4.30
V13		S. Front	Peak 2	Diol	Peak 4	Peak 5	Peak 6	Peak 7	DBC	Sum
	0.75	0.61	ND	0.47	<S/N	0.49	<S/N	>%RSD	1.05	2.73
	1	0.18	0.52	0.44	0.22	0.61	0.28	0.45	1.92	4.62
	1.5	0.90	0.25	0.65	0.30	1.17	0.70	1.15	3.71	8.85
	2	0.65	0.18	0.49	0.15	0.49	0.28	0.46	2.58	5.29
	2.5	1.36	0.35	0.59	0.12	0.61	0.43	1.25	5.64	10.34
	3	2.71	<S/N	0.27	<S/N	0.36	0.55	1.94	7.32	13.15
	4	1.63	0.15	0.45	0.18	0.25	0.21	0.28	3.74	6.90
	8	0.78	<S/N	0.25	<QC	0.18	0.13	0.24	1.05	2.75

HPLC-AMS Peak Data
Retention Times (min)
(Continued)

		2.0-3.0	4.7-6	12.3-13.3	14.3-15.4	16.3-17.6	18.2-19.2	19.6-20.5	20.6-22	Total
Volunteer	Time Point									
V5		S. Front	Peak 2	Diol	Peak 4	Peak 5	Peak 6	Peak 7	DBC	Sum
	0.25	0.31	ND	<S/N	<S/N	<S/N	<S/N	>%RSD	<S/N	0.45
	0.5	0.51	ND	0.27	<S/N	<S/N	>%RSD	0.50	1.62	2.90
	0.75	0.24	ND	0.95	0.61	0.61	0.25	0.61	12.41	15.69
	1	1.74	<S/N	3.45	1.42	1.45	1.61	1.20	39.33	50.46
	3	3.83	ND	3.65	2.68	1.96	0.55	0.50	59.88	73.05
	4	1.44	ND	1.34	0.95	1.21	<S/N	<S/N	24.31	29.40
	8	3.20	ND	1.01	0.36	0.39	<S/N	<S/N	11.28	16.24
	12	3.71	0.61	1.00	0.31	0.44	<S/N	<S/N	6.30	12.37
	24	6.77	0.21	0.54	0.41	<S/N	<S/N	>%RSD	2.72	10.94
	48	1.59	ND	<S/N	<S/N	<S/N	<S/N	<S/N	>%RSD	1.59
V8		S. Front	Peak 2	Diol	Peak 4	Peak 5	Peak 6	Peak 7	DBC	Sum
	0.5	1.39	0.44	0.51	<S/N	<S/N	<S/N	<S/N	3.22	5.70
	0.75	0.78	ND	0.57	0.13	1.08	>%RSD	0.25	5.02	7.83
	1	3.41	ND	2.45	1.13	1.25	0.66	>%RSD	27.86	36.76
	1.5	3.86	ND	1.50	0.69	0.73	0.60	<S/N	14.18	21.56
	2	3.03	ND	1.56	0.55	0.76	0.42	>%RSD	11.09	17.41
	2.5	6.90	ND	1.34	0.41	0.43	<S/N	<S/N	11.03	20.34
	3	2.20	ND	0.68	0.20	0.27	<S/N	<S/N	4.29	7.74
	4	3.77	ND	1.37	0.47	0.47	0.42	0.30	8.11	14.92
	8	1.32	0.33	0.44	0.21	1.25	>%RSD	<S/N	1.64	5.20
	12	3.21	0.29	0.43	0.24	1.10	>%RSD	<S/N	1.47	6.74
	24	2.70	0.53	<S/N	<S/N	<S/N	<S/N	<S/N	<S/N	3.23
V9		S.Front	Peak 2	Diol	Peak 4	Peak 5	Peak 6	Peak 7	DBC	Sum
	0.75	1.11	ND	1.56	0.39	1.05	0.63	0.77	11.63	17.13
	1	3.16	ND	2.58	1.10	2.53	0.85	0.72	21.34	32.29
	1.5	3.32	0.62	3.14	1.28	2.75	1.97	3.97	35.88	52.94
	2	2.62	0.85	2.28	0.65	1.34	1.81	2.39	27.36	39.30
	2.5	2.23	0.53	2.31	0.75	1.10	1.01	1.82	25.46	35.21
	3	2.90	0.66	1.91	0.69	1.76	0.93	0.72	29.51	39.08
	4	4.12	0.91	1.91	1.24	1.45	1.11	2.80	27.99	41.53
	12	6.84	1.02	1.19	0.56	0.37	0.49	0.41	4.46	15.35
	24	3.34	0.25	0.45	0.37	0.40	0.65	0.55	1.95	7.97

Table 4.2: Raw ^{14}C-DBC HPLC-AMS Metabolite Data

The quality control of sample data included elimination of samples that were below the limit of detection (<LOD), defined as a signal to noise ratio of 5 or higher. Samples failing to meet the quality standard of a %RSD of ≥ 30 were also eliminated to maintain data quality (>%RSD).

As single points dependent upon an individual's specific ADME, T_{max} and C_{max} can be highly variable in heterogeneous populations. Metabolite plasma concentrations were compared as Area Under the Curve (AUC, $fg*h*mL^{-1}$) for the alpha phase (peak to trough), and beta phase (trough-24 h). The percent relative standard deviation (%RSD) of the AUC by phase is used to compare plasma concentration of metabolites by time across volunteers (Table 4.4 A).

Table 4.3: Plasma Pharmacokinetic Data by Volunteer and HPLC-AMS Peak

HPLC-AMS Peak PK Data

		Retention Times (min)								
		2.0-3.0	4.7-6	12.3-13.3	14.3-15.4	16.3-17.6	18.2-19.2	19.6-20.5	20.6-22	Total
V10		S. Front	Peak 2	Diol	Peak 4	Peak 5	Peak 6	Peak 7	DBC	Sum
T_{max}	fg/mL	1.50	4.00	3.00	4.00	1.00	N.A.	N.A.	1.00	4.00
C_{max}	fg/mL	6.86	8.77	1.92	1.25	1.19	N.A.	N.A.	8.05	24.37
α AUC	$fg \cdot h \cdot mL^{-1}$	30.19	N.A.	8.13	5.16	1.96	N.A.	N.A.	10.80	110.33
$T_{1/2}$	h	0.61	N.A.	3.28	2.22	0.75	N.A.	N.A.	0.91	2.06
k_{el}	$fg \cdot h^{-1}$	1.14	N.A.	0.21	0.31	0.92	N.A.	N.A.	0.77	0.34
V11		S. Front	Peak 2	Diol	Peak 4	Peak 5	Peak 6	Peak 7	DBC	Sum
T_{max}	fg/mL	0.75	1.50	0.75	N.A.	1.50	N.A.	N.A.	1.50	1.50
C_{max}	fg/mL	3.76	2.15	1.57	N.A.	1.70	N.A.	N.A.	1.79	10.41
α AUC	$fg \cdot h \cdot mL^{-1}$	12.33	6.91	3.71	N.A.	3.39	N.A.	N.A.	7.00	37.23
$T_{1/2}$	h	2.77	4.42	2.68	N.A.	1.02	N.A.	N.A.	3.01	2.92
k_{el}	$fg \cdot h^{-1}$	0.25	0.16	0.26	N.A.	0.68	N.A.	N.A.	0.23	0.24
V13		S. Front	Peak 2	Diol	Peak 4	Peak 5	Peak 6	Peak 7	DBC	Sum
T_{max}	fg/mL	3.00	1.00	1.50	1.50	1.50	1.50	3.00	3.00	3.00
C_{max}	fg/mL	2.71	0.52	0.65	0.30	1.17	0.70	1.94	7.32	13.15
$T_{1/2}$	h	3.01	0.67	1.41	0.73	2.92	3.18	2.21	1.88	2.40
k_{el}	$fg \cdot h^{-1}$	0.23	1.04	0.49	0.96	0.24	0.22	0.31	0.37	0.29
V5		S. Front	Peak 2	Diol	Peak 4	Peak 5	Peak 6	Peak 7	DBC	Sum
T_{max}	fg/mL	3.00	N.A.	3.00	3.00	3.00	1.00	N.A.	3.00	3.00
C_{max}	fg/mL	3.83	N.A.	3.65	2.68	1.96	1.61	N.A.	3.00	73.05
α AUC	$fg \cdot h \cdot mL^{-1}$	17.93	N.A.	14.99	8.79	8.47	N.A.	N.A.	220.70	277.04
$T_{1/2}$	h	0.71	N.A.	3.39	1.96	2.24	0.93	N.A.	2.36	2.70
k_{el}	$fg \cdot h^{-1}$	0.98	N.A.	0.20	0.35	0.31	0.75	N.A.	0.29	0.26
V8		S. Front	Peak 2	Diol	Peak 4	Peak 5	Peak 6	Peak 7	DBC	Sum
T_{max}	fg/mL	2.50	N.A.	1.00	1.00	1.00	1.00	N.A.	1.00	1.00
α AUC	$fg \cdot h \cdot mL^{-1}$	22.28	N.A.	8.12	3.02	0.25	1.08	N.A.	57.02	99.62
$T_{1/2}$	h	3.09	N.A.	3.32	3.66	0.96	0.73	N.A.	0.87	1.09
k_{el}	$fg \cdot h^{-1}$	0.22	N.A.	0.21	0.19	0.72	0.95	N.A.	0.80	0.63
V9		S. Front	Peak 2	Diol	Peak 4	Peak 5	Peak 6	Peak 7	DBC	Sum
T_{max}	fg/mL	1.50	2.00	1.50	1.50	1.50	1.50	1.50	1.50	1.50
C_{max}	fg/mL	3.32	0.85	3.14	1.28	2.75	1.97	3.97	35.88	52.94
α AUC	$fg \cdot h \cdot mL^{-1}$	9.64	1.79	13.46	2.94	5.72	4.04	6.40	153.34	299.04
$T_{1/2}$	h	1.73	0.74	4.98	2.04	0.75	1.22	0.64	2.05	8.63
k_{el}	$fg \cdot h^{-1}$	0.40	0.94	0.14	0.34	0.92	0.57	1.08	0.34	0.08

The pharmacokinetic parameters of plasma ^{14}C-DBC HPLC-AMS data was determined using non-compartmental computational models. Several peaks did not have enough detectable, quality data points to generate a full PK curve or regression and parameter analysis (N.A.).

The solvent front (peak 1) and 11,12-diol (Peak 3) had the most consistency between volunteers with 48.59% and 57.55%, respectively in the alpha phase (T0-trough).

These two metabolite fractions were also the most consistent in the beta phase, with 31.32% and 13.41 % RSD respectively. When the AUC for each metabolites was normalized as a percent of DBC AUC (Table 4.4 B), the % RSD increased between 2 to 5 fold and, there was no central tendency for metabolite formation based as a percentage of DBC distributed in plasma. This indicates that the metabolism rate is limited more so by enzyme kinetics than absorption rate as the metabolite profile is not dependent upon uptake rate, and that kinetics are more similar between individuals than is uptake between individuals. As the plasma DBC concentration is not accounted for by plasma metabolites, other mechanisms of elimination from plasma must be present. Biliary excretion has previously been proposed as a mechanism for eliminating parent PAHs. DBC may be eliminated via biliary excretion in the liver prior to enzymatic activation.

Table 4.4: Relative AUC of ^{14}C-DBC and Metabolites by Volunteer

Table A. AUC DBCeq Plasma (fg*h*mL^{-1})

		Peak 1	Peak 2	Diol	Peak 4	Peak 5	Peak 6	Peak 7	DBC
V5	α-AUC	17.93	na	14.99	8.79	8.47	na	na	220.70
V8	α-AUC	22.28	na	8.12	3.02	0.25	1.08	na	57.02
V9	α-AUC	9.64	1.79	13.46	2.94	5.72	4.04	6.40	153.34
V10	α-AUC	30.19	na	8.13	5.16	1.96	na	na	10.80
V11	α-AUC	12.33	6.91	3.71	na	3.39	na	na	7.00
V13	α-AUC	9.26	1.14	2.92	0.58	2.69	1.97	4.18	23.75
	RSD	48.59	96.25	57.55	75.20	78.10	64.37	29.70	112.09
V5	β-AUC	76.73	6.15	13.25	5.70	5.94	na	na	89.32
V9	β-AUC	146.14	16.55	14.47	na	na	na	na	54.82
V10	β-AUC	109.75	na	11.05	na	na	na	na	23.15
	RSD	31.32	64.76	13.41	na	na	na	na	59.35

Table B. Metabolite α-AUC Relative To DBC AUC (%)

		Peak 1	Peak 2	11,12-Diol	Peak 4	Peak 5	Peak 6	Peak 7	DBCeq (fg*mL)/h
V5	α-AUC$_{(0\text{-}8h)}$	8.12	na	0.07	3.98	3.84	na	na	220.70
V8	α-AUC$_{(0\text{-}8h)}$	39.07	na	0.14	5.30	0.44	1.89	na	57.02
V9	α-AUC$_{(0\text{-}8h)}$	6.29	1.17	0.09	1.92	3.73	2.64	4.18	153.34
V10	α-AUC$_{(0\text{-}8h)}$	74.42	na	0.20	12.73	4.83	na	na	10.80
V11	α-AUC$_{(0\text{-}8h)}$	175.98	98.66	0.53	na	48.41	na	na	7.00
V13	α-AUC$_{(0\text{-}8h)}$	38.99	4.81	0.12	2.42	11.34	8.31	17.61	23.75
	RSD	110.86	228.40	89.49	101.68	149.99	150.95	194.13	112.08
V5	β-AUC$_{(8\text{-}24h)}$	85.90	6.89	14.84	6.39	6.65	na	na	89.32
V9	β-AUC$_{(8\text{-}24h)}$	266.58	30.20	26.40	na	na	na	na	54.82
V10	β-AUC$_{(8\text{-}24h)}$	474.15	na	47.75	na	na	na	na	23.15
	RSD	70.51	88.87	56.29	na	na	na	na	59.35

The AUC was determined for plasma α and β phases (A). The AUC of each metabolite was divided by the AUC of parent DBC to determine if there was a relationship to the relative abundance of DBC and DBC metabolites (B). The %RSD of metabolites AUC normalized by DBC AUC across volunteers was several fold higher than the % RSD of the AUC of the metabolite alone, indicating that there was not a correlation of DBC AUC to metabolite AUC across volunteers (B).

Urine:

In urine (Figure 4.3), parent DBC was not present. The only consistent metabolites present in native (non-β-glucuronidase treated) urine extracts were the solvent front and a putative dione with a retention time of 3.75-6.3 minutes that was homologous to peak 3 in plasma with a retention of 4.7 to 6 minutes that was only evident in volunteer 10 at the 8 and 12 hour time points. In β-glucuronidase/sulfatase deconjugated urine extracts, metabolites were freed from polar conjugate groups, allowing metabolites to extracted and separated in non-polar enzyme systems. Enzyme deconjugation released tetrols and diol as well as increased putative dione concentrations.

4.5 Discussion

DBC metabolites appeared rapidly in plasma, suggesting gut CYP enzymatic activation and absorption as has previously been demonstrated in mouse models to be critical to generate plasma concentration levels [196]. Previously the mice null, heterozygote, and homozygote for wild-type Cyp enzymes that were exposed to BaP had a drastic variance in circulating plasma concentrations of PAHs with a 25-fold increase in null mice [196]. This is a potential explanation for why the circulating plasma concentrations are highly variable among volunteers. There appears to be a

marked difference in the absorption of parent DBC between volunteers as the plasma concentrations of parent DBC vary greatly by volunteer. DBC is known to be poorly absorbed. In a radiolabeled mouse study, only about 3% of an orally administered dose of DBC in a DMSO vehicle was recovered in urine, with the great majority eliminated in feces [197].

Utilizing the specificity of a radiolabel and the sensitivity of AMS, we were able to determine the metabolites profile of DBC in human volunteers. We were able to identify and quantify metabolites seen previously in high dose rodent studies, such as diols and tetrols in plasma and urine respectively. Additionally, we identified several novel metabolite peaks that occur to a lesser extent and that may be important in understanding the process of metabolism in humans. As DBC is a procarcinogen, the type and extent of metabolites formed determine the risk from exposure. We observed a rapid appearance and elimination of metabolites from plasma and from urine, with the majority eliminated within 24 hours of dosing.

Funding:

This study was funded by PHS grants P42ES016465, K.C. Donnelly Supplement P42ES016465, P41GM103483 and T32ES07060 (E.P.M). AMS was performed at the Research Resource for Biomedical AMS which is operated at LLNL under the auspices of the U.S. Department of Energy under contract DE-AC52-07NA27344 and National Institute of General Medical Sciences 8P41 GM103483-14.

Chapter 5. General Discussion:

Addressing Specific Aim 1: *Determine the effects of Cyp1b1 genotype status of wild-type, null, or transgenic-humanized on carcinogenesis and tumogenesis in a in utero exposure following a maternal oral dose of 6.5 mg/kg DBC or 12 mg/kg DBC.* Murine models of DBC administered orally as a single PAH to pregnant mice, generated several tissue specific diseases, including leukemia/lymphoma, lung adenoma/carcinoma, liver tumors (primarily in males), reproductive morphological aberrations, and splenomegaly. The disease type and extent of toxicity relies upon dose administered, timing of dosage, and genotype of PAH bioactivating enzymes.

The toxicity of DBC is tissue specific, likely determined by the availability of PAH activating and detoxifying enzymes available. The role of Cyp1b1, the bioactiving enzyme with highest affinity to generate DBC-epoxides, was investigated in multiple target tissues (chapter 2, appendix 1 and 2) following *in utero* DBC exposure in mice. Cyp1b1 wild-type mice were 59% more likely to succumb to T-cell Acute Lymphoblastic Leukemia (T-ALL) than Cyp1b1 null (chapter 2, Fig 2.7). The *AhR* genotype was not a significant factor in lung tumor incidence, multiplicity, or mortality (Fig 2.7 and 2.8). While, gender was not a significant factor in lung tumor incidence or mortality (Fig 2.7), males exhibited a significantly greater lung tumor

multiplicity. The h*CYP1B1* genotype did not impact lung tumor multiplicity, but lung tumor incidence was greater in *Cyp1b1*-nulls compared to wild-type mice. *CYP1B1*-humanzied mice were more likely to develop lung tumors than *mCyp1b1* wild-type mice but this did not reach statistical significance ($p = 0.07$).

There is little data available on the expression of Cyp enzymes during different stages of development in tissue and specific cell types. Considering that the fetal plasma concentrations from a single maternal dose of DBC were two orders of magnitude below that of the dam [37, 198], and the magnitude of the effects in mice exposed as fetuses, understanding *in utero* metabolism is critical to determining risk from PAH exposure. Many adult on-set diseases are idiopathic in origin, meaning that we simply do not know how they were initiated. There is likely a role in humans for PAH exposure initiated adult on-set disease from *in utero* exposures.

To further the translation between high dose rodent laboratory models to human risk assessment, human volunteer metabolism of DBC and BaP were determined from environmentally relevant doses. Previously, a PB/PK model of human metabolism of DBC and BaP was developed [47], scaled from high dose exposures in rat and mouse. However, models are based on assumptions that need to be validated. Our human studies were designed to generate data on the metabolism of human, oral, environmentally relevant exposures. This is the data that the models are built to simulate, allowing validation of model accuracy.

Specific Aim 2 (Chapter 3): *Determine the human pharmacokinetics of an environmentally relevant oral dose of 26 ng DBC utilizing the sensitivity of AMS* and Specific Aim 3 (Chapter 4): *Utilize a novel HPLC-AMS interface to determine the pharmacodynamics of DBC from human volunteers administered an environmentally relevant dose* were complementary aims to generate PK and PD data with instrumentation sensitive enough to generate environmentally relevant human metabolite data.

Human PK from DBC oral dosing demonstrated a rapid uptake/elimination alpha phase of ^{14}C-DBCeq, followed by a slower beta phase appearance and elimination. The majority of ingested DBC is likely eliminated in feces, we identified approximately 2% of the ^{14}C-DBC administered in urine when corrected for volume of elimination (Table 3.2). The plasma C_{max} was 68.8 ± 44.3 fg*mL^{-1} with a T_{max} of 2.25 ± 1.04 h. Elimination occurred in two distinct phases; a rapid (α)-phase, with a $T_{1/2}$ of 5.8 ± 3.4 h and apparent elimination rate constant (K_{el}) of 0.17 ± 0.12 fg*h^{-1} followed by a slower (β)-phase, with a $T_{1/2}$ of 41.3 ± 29.8 h and apparent K_{el} of 0.03 ± 0.02 fg*h^{-1} (Table 3.3) The pharmacokinetic curve from human volunteers closely matched that of the model prediction scaled from rodents (Fig 3.4).

Human PD from DBC exposure provides more detail on the specific enzymatic metabolic transformations of DBC from a procarcinogen to all potentially toxic and non-toxic intermediates. Again, the dosage administered represents an average oral dose of PAH BaPeq exposure in humans, the risk of potentially toxic intermediate

formation is considered *de minimus* as it adds no additional risk beyond that of daily exposure.

Previously, in high exposure rodent studies, the major metabolites of oral DBC exposure, as determined by HPLC-PDA were the diol and tetrol components in plasma and urine [37]. A limitation to UV detection, such as PDA, is that it is targeted to the optical properties of metabolites that are expected based on the properties of known standards. AMS relies on a specific radiolabel that allows detection of all species present in a biological samples, regardless of the specific metabolite properties from bio-transformation (Fig 4.2). Relying on the ^{14}C radiolabel, we were able to identify a substantial polar fraction in plasma from the HPLC solvent front (Fig 4.3). This fraction demonstrates that metabolism is very rapid as it appears early in the PK curve and has a polarity greater than DBC-tetrol, three separate bio-transformations of DBC must occur (Fig 4.1). Parent DBC was found to a varying extent in plasma by volunteer, indicating that absorption may not be similar among volunteers (Fig 4.2). Metabolite AUC data was more consistent across volunteers than DBC AUC, with the major known peak being DBC diol in plasma (Fig 4.4).

The PD data suggests that in circulating plasma, tetrols and downstream intermediates with adduction potential, such as epoxides, were not present in free from in the plasma (Fig 4.3). The unknown peaks less polar than the diol and that elute before DBC are potentially dione metabolites capable of redox cycling or future

transformation to tetrols and downstream metabolites (Fig 4.2). The lack of tetrols suggests in that in circulating plasma, tetrols are rapidly eliminated.

Urine data indicates that the majority of most metabolites were present as a conjugates, with the exception of a putative dione (Fig 4.4). The putative dione is the major peak in urine, the concentration of dione did increase, but to a minor extent, with the addition of β-glucuronidase/sulfatase. Enzymatic cleavage freed tetrol metabolites from polar conjugates, allowing them to be organically extracted from urine and quantitated.

The urine metabolites were primarily polar metabolites generated by at least two biotransfomations of DBC (Fig 4.1). The conjugation status of the diol and tetrols demonstrates that detoxification enzymes conjugated these DBC species for elimination, preventing further biotransformations to more toxic intermediates such as expoxides. As only 2% of the dose administered was recovered in urine (Table 3.2), there is concern for tissue burden of DBC or DBC adducts. Recently, a high dose ^{14}C-DBC dosed mouse model experiment examined the tissue specific distribution of DBC over time [197]. The PK indicated that lung is a target for DBC, but that DBC was eliminated rapidly from lung. Ovary was determined to be the ultimate target for DBC as the PK curve was found to persist past the three week final time point [197]. A recruitment requirement for human volunteers was that women who were pregnant or capable of becoming pregnant were excluded due to the reproductive toxicity in high dose rodent studies. The ovarian toxicity of DBC in humans is unknown. The

environmentally relevant DBC dose utilized in this study is expected to be no appreciable additional risk to participants.

The role of bioactivating enzyme status in human environmentally relevant exposure to PAHs as mixtures is a translational goal (Fig 4.1). PAHs occur in a wide variety of mixtures. To determine the relative risk from exposures to mixtures, a risk assessment approach needed to be developed. The EPA relative potency factor (RPF) approach relates the carcinogenicity of each PAH component in a mixture to that of BaP (BaPeq), then it relates the concentration multiplied by the BaPeq of each PAH in a mixture and adds them for the total BaPeq hazard from a mixture. This is similar to the approach used for dioxins and dibenzofurans. This assumes that PAH risk is additive and that there is no synergy or competition among PAH components for bioactivating enzyme systems or detoxification enzymes. This also assumes that non-carcinogenic PAHs have no impact on the risk from the carcinogenic PAHs in a mixture.

Currently, we are administering ^{14}C-BaP as a single environmentally relevant dose (46 ng) or administering ^{14}C-BaP plus a serving of smoked fish containing a complex mixture of PAHs (460 ng BaPeq) to human volunteers to identify gene/exposure PD as well as to address the (RPF) approach to PAH risk. The volunteers who ingest a ^{14}C-BaP capsule will then be asked to ingest a ^{14}C-BaP capsule plus a smoked fish meal (Table A3.4). If the ^{14}C-BaP PK/PD does not change with the addition of the mixture of PAHs contained in the fish meal, the RPF is validated. If the PK/PD

profile changes, the RPF approach may not accurately reflect the risk from exposure to dynamic PAH mixtures.

Volunteers are being genotyped for the status of CYP1B1, a PAH bioactivation enzyme for which there are polymorphisms that exist in prevalent percentages of the population, as well as for GSTM1, a detoxifying enzyme which also has a high percentages of polymorphisms in populations. Currently, we have several volunteers enrolled with one or both polymorphisms (Table 4.2). The PK/PD profiles will be compared by genotype to assess the impacts of genetic polymorphisms in PAH metabolism and PK/PD.

The objective of this work is to add to the body of translational data between high dose animal model research and the environmentally relevant human metabolism of the persistent pollutant dibenzo[*def,p*]chrysene (DBC). We furthered the knowledge of gene/exposure interactions by determining the carcinogenesis risk based on Cyp1b1 genotype following *in utero* DBC exposure in mice, finding no difference in lung carcinogesis, but a lack of susceptibility T-Cell Lymphoblastic Leukemia in mice null for Cyp1b1.

In addition, sensitive AMS was utilized to detect the metabolism of DBC (and BaP) by human volunteers from environmentally relevant exposures. The human PK data from DBC exposure validated model predictions of human metabolism scaled from rodent exposure data. DBC appeared quickly in plasma, with the majority eliminated

quickly over 24 hours and a slower elimination period to 72 hours. The PD of DBC provided evidence that DBC is rapidly biotransformed to metabolites circulating in plasma. The three transformation products and higher (tetrols and beyond) were not present in the plasma, indicating that they are quickly converted to conjugated species and eliminated from the plasma compartment. Urine contained primarily DBC metabolites that had undergone two transformations or more (diols, tetrols, and a putative dione). The majority of these species exist as conjugated metabolites in urine.

Continuing work includes a more detailed PD analysis of DBC from human samples and sample generation and analysis of samples from humans who ingested BaP as we address gene/environment interactions and the RPF approach. Additionally, the reproductive effects of DBC from fetally exposed mice will continue as we strive to address mechanism of toxicity.

This body of work furthers the field of PAH translation by addressing ethically addressing disease and disease prevention endpoints from PAH exposure in rodent laboratory research models. Additionally, we are addressing human risk by removing the translational uncertainty and directly measuring PAH metabolism in humans from the oral route of exposure by taking a FDA IND “phase 0” approach to PK/PD.

ABBREVIATIONS

AA, amino acid; AAALAC, Association for Assessment and Accreditation of Laboratory Animal Care; ACN, acetonitrile; Ahr, aryl hydrocarbon receptor; ALL, acute lymphoblastic leumekia; AMS, Accelerator Mass Spectrometry; ATSDR, Agency for Toxic Substances and Disease Registry; AUC, area under the curve; BaP, benzo[*a*]pyrene; BMI, body mass index; CAMS, center for accelerator mass spectometry; C_{max}, maximum concentration; CYP, human cytochrome P450; Cyp, mouse cytochrome P450; DBC, dibenzo[*def,p*]chrysene; DBCDE, dibenzo[*def,p*]chrysene-11,12-dihydrodiol-13,14-epoxide; DBC_{eq}, dibenzo[*def,p*]chrysene equivalents (DBC plus metabolites); DDT, 1,1,1-trichloro-2,2-di(4-chlorophenyl)ethane; FMO, flavin-containing mono-oxygenase; GSTs, glutathione-*S*-transferases; HPLC, high pressure liquid chromatography; IACUC, Internal Animal Care and Use Committee; IARC, International Agency for Research on Cancer; I3C, indole-3-carbinol; IQ, imidazo[4,5-*f*]quinolone; JECFA, Joint FAO/WHO Expert Committee on Food Additives; K_{el}, elimination rate constant; LLNL, Lawrence Livermore National Laboratory; LLOQ, lower limit of quantitation; Log K_{ow}, octinal-water coeffecient reported in log scal; MeIQ, 2-amino-3,4-dimethylimidazo[4,5-*f*]quinoline; MeIQx, 2-amino-3,8-dimethylimidazo[4,5-*f*]quinoxaline; ORF, open reading frame; OSU, Oregon State University; PAH, polycyclic aromatic hydrocarbon; PBPK, physiologically based pharmacokinetic

model; PhIP, 2-amino-1-methyl-6-phenylimidazo[4,5-*b*]pyridine; PCBs, polychlorinated biphenyls; q-rt-PCR, quantitative reverse transcription polymerase chain reaction; RIN, RNA index number; % RSD, percent relative standard deviation; SD., standard deviation; S/N, signal to noise ratio; SRS, substrate recognition site; SULTs, sulfotransferases; T-All, T-cell lymphoblasitic leukemia; TCDD, 2,3,7,8-tetrachlorodibenzo-*p*-dioxin; T_{max}, time of maximum concentration; $T_{1/2}$, half life; UGTs, UDP-glucuronosyltransferases; UPLC, ultra high pressure liquid chromatography

Chapter 6. Bibliography

1. Thompson, H.S., *Fear and Loathing: On the Campaign Trail '72*. 1985, Grand Central Publishing. p. 512.
2. EPA, U.S., *Development of a relative potency factor (RPF) approach for polycyclic aromatic hydrocarbon (PAH) mixtures*. 2010, United States Environmental Protection Agency.
3. Katz, A.K., H.L. Carrell, and J.P. Glusker, *Dibenzo a,l pyrene (dibenzo def,p chrysene): fjord-region distortions.* Carcinogenesis, 1998. **19**(9): p. 1641-1648.
4. *Dibenzo(def,p)chrysene*. 08/29/2003; Available from: Toxnet.nlm.nih.gov.
5. Amin, S., et al., *Tumorigenicity in newborn mice of fjord region and other sterically hindered diol epoxides of benzo[g]chrysene, dibenzo[a,l]pyrene (dibenzo[def,p]chrysene), 4H-cyclopenta[def]chyrsene and fluoranthene.* Carcinogenesis, 1995. **16**(11): p. 2813-2817.
6. Cavalieri, E.L., et al., *Comparative dose-response tumorigenicity studies of dibenzo[a,l]pyrene versus 7,12-dimethylbenz[a]anthrocene, benzo[a]pyrene, and 2-dibenzo[a,l]pyrene dihydrodiols in mouse skin and rat mammary gland.* Carcinogenesis, 1991. **12**(10): p. 1939-1944.
7. Veyrand, B., et al., *Human dietary exposure to polycyclic aromatic hydrocarbons: Results of the second French Total Diet Study*. Environment International, 2013. **54**: p. 11-17.
8. Oanh, N.T.K., et al., *Emission of particulate matter and polycyclic aromatic hydrocarbons from select cookstove-fuel systems in Asia.* Biomass & Bioenergy, 2005. **28**(6): p. 579-590.
9. Oanh, N.T.K., L.B. Reutergardh, and N.T. Dung, *Emission of polycyclic aromatic hydrocarbons and particulate matter from domestic combustion of selected fuels.* Environmental Science & Technology, 1999. **33**(16): p. 2703-2709.
10. Boffetta, P., N. Jourenkova, and P. Gustavsson, *Cancer risk from occupational and environmental exposure to polycyclic aromatic hydrocarbons.* Cancer Causes & Control, 1997. **8**(3): p. 444-472.
11. Bostrom, C.E., et al., *Cancer risk assessment, indicators, and guidelines for polycyclic aromatic hydrocarbons in the ambient air*. Environmental Health Perspectives, 2002. **110**: p. 451-488.
12. Kazerouni, N., et al., *Analysis of 200 food items for benzo a pyrene and estimation of its intake in an epidemiologic study*. Food and Chemical Toxicology, 2001. **39**(5).
13. Jakszyn, P., et al., *Development of a food database of nitrosamines, heterocyclic amines, and polycyclic aromatic hydrocarbons.* Journal of Nutrition, 2004. **134**(8).
14. IARC, *Monographs on the Evaluation of Carcinogenic Risks to Humans*, in *Some non-heterocyclic polycyclic aromatic hydrocarbons and some exposures*. 2010, World Health Organization International Agency for Research on Cancer: Lyon, France.
15. Whyatt, R.M., et al., *Biomarkers of polycyclic aromatic hydrocarbon-DNA damage and cigarette smoke exposures in paired maternal and newborn blood samples as a measure of differential susceptibility*. Cancer Epidemiology Biomarkers & Prevention, 2001. **10**(6): p. 581-588.
16. Perera, F.P., et al., *Biomarkers in maternal and newborn blood indicate heightened fetal susceptibility to procarcinogenic DNA damage.* Environmental Health Perspectives, 2004. **112**(10): p. 1133-1136.

17. Perera, F., et al., *DNA damage from polycyclic aromatic hydrocarbons measured by benzo a pyrene-DNA adducts in mothers and newborns from Northern manhattan, the World Trade Center area, Poland, And china.* Cancer Epidemiology Biomarkers & Prevention, 2005. **14**(3): p. 709-714.
18. Perera, F.P., et al., *Molecular epidemiologic research on the effects of environmental pollutants on the fetus.* Environmental Health Perspectives, 1999. **107**: p. 451-460.
19. Lederman, S.A., et al., *The effects of the World Trade Center event on birth outcomes among term deliveries at three lower Manhattan hospitals.* Environmental Health Perspectives, 2004. **112**(17): p. 1772-1778.
20. Bocskay, K.A., et al., *Chromosomal aberrations in cord blood are associated with prenatal exposure to carcinogenic polycyclic aromatic hydrocarbons.* Cancer Epidemiology Biomarkers & Prevention, 2005. **14**(2): p. 506-511.
21. Orjuela, M.A., et al., *Prenatal PAH exposure is associated with chromosome-specific aberrations in cord blood.* Mutation Research-Genetic Toxicology and Environmental Mutagenesis, 2010. **703**(2): p. 108-114.
22. Peterson, B.S., et al., *Effects of Prenatal Exposure to Air Pollutants (Polycyclic Aromatic Hydrocarbons) on the Development of Brain White Matter, Cognition, and Behavior in Later Childhood.* Jama Psychiatry, 2015. **72**(6): p. 531-540.
23. Buu-HoÎ, N.P., O. Périn-Roussel, and P. Jacquignon, *On the new synthesis of dibenzo(a,l)pyrene.* Bull. Soc. chim. F, 1969. **5**(36): p. 3566-3568.
24. IARC, *Monographs on the Evaluation of Carcinogenic Risks to Humans*, in *Polynuclear aromatic compounds, Part 1: chemical, environmental, and experimental data*. 1983, World Health Organization International Agency For Research On Cancer: Lyon, France.
25. Shimada, T. and Y. Fujii-Kuriyama, *Metabolic activation of polycyclic aromatic hydrocarbons to carcinogens by cytochromes P450 1A1 and 1B1.* Cancer Science, 2004. **95**(1): p. 1-6.
26. Shimada, T., et al., *Metabolic activation of polycyclic aromatic hydrocarbons and other procarcinogens by cytochromes P450 1A1 and P4501B1 allelic variants and other human cytochromes P450 in Salmonella typhimurium NM2009.* Drug Metabolism and Disposition, 2001. **29**(9): p. 1176-1182.
27. Melendez-Colon, V.J., et al., *Comparison of cytochrome P450- and peroxidase-dependent metabolic activation of the potent carcinogen dibenzo a,l pyrene in human cell lines: Formation of stable DNA adducts and absence of a detectable increase in apurinic sites.* Cancer Research, 1999. **59**(7): p. 1412-1416.
28. Straif, K., et al., *Carcinogenicity of polycyclic aromatic hydrocarbons.* Lancet Oncology, 2005. **6**(12): p. 931-932.
29. *Luekemia-Acute Lymphocytic*. 2015 [cited 2015 July 20]; Available from: http://www.cancer.org/cancer/leukemia-acutelymphocyticallinadults/detailedguide/leukemia-acute-lymphocytic-key-statistics.
30. Ross, M.E., et al., *Classification of pediatric acute lymphoblastic leukemia by gene expression profiling.* Blood, 2003. **102**(8): p. 2951-2959.
31. Maser, R.S., et al., *Chromosomally unstable mouse tumours have genomic alterations similar to diverse human cancers.* Nature, 2007. **447**(7147): p. 966-U3.
32. Castro, D.J., et al., *Lymphoma and lung cancer in offspring born to pregnant mice dosed with dibenzo a,l pyrene: The importance of in utero vs. lactational exposure.* Toxicology and Applied Pharmacology, 2008. **233**(3): p. 454-458.
33. Yu, Z., et al., *In utero exposure of mice to dibenzo a,l pyrene produces lymphoma in the offspring: Role of the aryl hydrocarbon receptor.* Cancer Research, 2006. **66**(2): p. 755-762.
34. FitzGerald, C.T., et al., *Differential regulation of mouse Ah receptor gene expression in cell lines of different tissue origins.* Archives of Biochemistry and Biophysics, 1996. **333**(1): p. 170-178.
35. Denison, M.S., et al., *Exactly the same but different: promiscuity and diversity in the molecular mechanisms of action of the aryl hydrocarbon (Dioxin) receptor.* Toxicological Sciences, 2011. **124**(1): p. 1-22.
36. Hahn, M.E., *Aryl hydrocarbon receptors: diversity and evolution.* Chemico-Biological Interactions, 2002. **141**(1-2): p. 131-160.

37. Crowell, S.R., et al., *Impact of pregnancy on the pharmacokinetics of dibenzo[def,p]chrysene in mice.* Toxicological Sciences, 2013. **135**(1): p. 48-62.
38. Shorey, L.E., et al., *Transplacental carcinogenesis with dibenzo def,p chrysene (DBC): Timing of maternal exposures determines target tissue response in offspring.* Cancer Letters, 2012. **317**(1): p. 49-55.
39. Castro, D.J., et al., *Chemoprevention of dibenzo a,l pyrene transplacental carcinogenesis in mice born to mothers administered green tea: primary role of caffeine.* Carcinogenesis, 2008. **29**(8): p. 1581-1586.
40. Hankinson, O., *The aryl-hydrocarbon receptor complex.* Annual Review of Pharmacology and Toxicology, 1995. **35**: p. 307-340.
41. Castro, D.J., et al., *Identifying efficacious approaches to chemoprevention with chlorophyllin, purified chlorophylls and freeze-dried spinach in a mouse model of transplacental carcinogenesis.* Carcinogenesis, 2009. **30**(2): p. 315-320.
42. Yu, Z., et al., *Indole-3-carbinol in the maternal diet provides chemoprotection for the fetus against transplacental carcinogenesis by the polycyclic aromatic hydrocarbon dibenzo a,l pyrene.* Carcinogenesis, 2006. **27**(10): p. 2116-2123.
43. Shorey, L.E., et al., *Differential modulation of dibenzo def,p chrysene transplacental carcinogenesis: Maternal diets rich in indole-3-carbinol versus sulforaphane.* Toxicology and Applied Pharmacology, 2013. **270**(1): p. 60-69.
44. Castro, D.J., et al., *Fetal mouse Cyp1b1 and transplacental carcinogenesis from maternal exposure to Dibenzo(a,l)pyrene.* Cancer Prevention Research, 2008. **1**(2): p. 128-134.
45. Niziolek-Kierecka, M., et al., *gamma H2AX, pChk1, and Wip1 as Potential Markers of Persistent DNA Damage Derived from Dibenzo a,l pyrene and PAH-Containing Extracts from Contaminated Soils.* Chemical Research in Toxicology, 2012. **25**(4): p. 862-872.
46. EPA, *Code of Federal Regulations PART 423 - Steme electric power generating point of source category*, in *Title 40 - Protection of Environment. Chapter 1 - Environmental protection agency subchapter N - Effluent guidelines and standards*, E.P. Agency, Editor. 2007.
47. Crowell, S.R., et al., *Preliminary physiologically based pharmacokinetic models for benzo a pyrene and dibenzo def,p chrysene in rodents.* Toxicology and Applied Pharmacology, 2011. **257**(3).
48. Elmore, D. and F.M. Phillips, *Accelerator mass-spectrometry for measurement of long-lived radioisotopes.* Science, 1987. **236**(4801): p. 543-550.
49. Bard, E., *Geochemical and geophysical implications of the radiocarbon calibration.* Geochimica Et Cosmochimica Acta, 1998. **62**(12): p. 2025-2038.
50. Salazar, G. and T. Ognibene, *Design of a secondary ionization target for direct production of a C- beam from CO2 pulses for online AMS.* Nuclear Instruments & Methods in Physics Research Section B-Beam Interactions with Materials and Atoms, 2013. **294**: p. 300-306.
51. Ognibene, T.J., et al., *A new accelerator mass spectrometry system for C-14-quantification of biochemical samples.* International Journal of Mass Spectrometry, 2002. **218**(3): p. 255-264.
52. Mauthe, R.J., et al., *Distribution and metabolism of 2-amino-1-methyl-6-phenylimidazo 4,5-b pyridine (PhIP) in female rats and their pups at dietary doses.* Carcinogenesis, 1998. **19**(5): p. 919-924.
53. Garner, R.C., et al., *Comparative biotransformation studies of MeIQx and PhIP in animal models and humans.* Cancer Letters, 1999. **143**(2): p. 161-165.
54. Dingley, K.H., et al., *Covalent binding of 2-amino-3,8-dimethylimidazo 4,5-f quinoxaline to albumin and hemoglobin at environmentally relevant doses - Comparison of human subjects and F344 rats.* Drug Metabolism and Disposition, 1998. **26**(8): p. 825-828.
55. Dingley, K.H., et al., *DNA and protein adduct formation in the colon and blood of humans after exposure to a dietary-relevant dose of 2-amino-1-methyl-6-phenylimidazo 4,5-b pyridine.* Cancer Epidemiology Biomarkers & Prevention, 1999. **8**(6): p. 507-512.
56. Malfatti, M.A., et al., *The urinary metabolite profile of the dietary carcinogen 2-amino-1-methyl-6-phenylimidazo 4,5-b pyridine is predictive of colon DNA adducts after a low-dose exposure in humans.* Cancer Research, 2006. **66**(21): p. 10541-10547.
57. Bacon, J.R., et al., *Sulforaphane and quercetin modulate PhIP-DNA adduct formation in human HepG2 cells and hepatocytes.* Carcinogenesis, 2003. **24**(12): p. 1903-1911.

58. Dingley, K.H., et al., *Effect of dietary constituents with chemopreventive potential on adduct formation of a low dose of the heterocyclic amines PhIP and IQ and phase II hepatic enzymes.* Nutrition and Cancer-an International Journal, 2003. **46**(2): p. 212-221.
59. Cheng, Y., et al., *Inhibition of nicotine-DNA adduct formation in mice by six dietary constituents.* Food and Chemical Toxicology, 2003. **41**(7): p. 1045-1050.
60. Cupid, B.C., et al., *The formation of AFB(1)-macromolecular adducts in rats and humans at dietary levels of exposure.* Food and Chemical Toxicology, 2004. **42**(4): p. 559-569.
61. Jubert, C., et al., *Effects of chlorophyll and chlorophyllin on low-dose aflatoxin B-1 pharmacokinetics in human volunteers.* Cancer Prevention Research, 2009. **2**(12): p. 1015-1022.
62. Lappin, G., R. Noveck, and T. Burt, *Microdosing and drug development: past, present and future.* Expert Opinion on Drug Metabolism & Toxicology, 2013. **9**(7): p. 817-834.
63. Kimmelman, J., *Ethics at phase 0: Clarifying the issues.* Journal of Law Medicine & Ethics, 2007. **35**(4): p. 727.
64. Lappin, G., et al., *Comparative pharmacokinetics between a microdose and therapeutic dose for clarithromycin, sumatriptan, propafenone, paracetamol (acetaminophen), and phenobarbital in human volunteers.* European Journal of Pharmaceutical Sciences, 2011. **43**(3): p. 141-150.
65. Lin, T.H., et al., *Assessment of the absorption, metabolism and excretion of C-14 pasireotide in healthy volunteers using accelerator mass spectrometry.* Cancer Chemotherapy and Pharmacology, 2013. **72**(1): p. 181-188.
66. Bowers, G.D., et al., *Disposition and metabolism of GSK2251052 in humans: a novel boron-containing antibiotic.* Drug Metabolism and Disposition, 2013. **41**(5): p. 1070-1081.
67. Chen, J., et al., *Biphasic Elimination of Tenofovir Diphosphate and Nonlinear Pharmacokinetics of Zidovudine Triphosphate in a Microdosing Study.* Jaids-Journal of Acquired Immune Deficiency Syndromes, 2012. **61**(5): p. 593-599.
68. Dave, M., et al., *Disposition and Metabolism of Darapladib, a Lipoprotein-Associated Phospholipase A2 Inhibitor, in Humans.* Drug Metabolism and Disposition, 2014. **42**(3): p. 415-430.
69. Zollinger, M., et al., *Absorption, distribution, metabolism, and excretion (ADME) of C-14-sonidegib (LDE225) in healthy volunteers.* Cancer Chemotherapy and Pharmacology, 2014. **74**(1): p. 63-75.
70. Hoffmann, E., et al., *Pharmacokinetics and tolerability of SRT2104, a first-in-class small molecule activator of SIRT1, after single and repeated oral administration in man.* British Journal of Clinical Pharmacology, 2013. **75**(1): p. 186-196.
71. Miyaji, Y., et al., *Novel comb-shaped PEG modification enhances the osteoclastic inhibitory effect and bone delivery of osteoprotegerin after intravenous administration in ovariectomized rats.* Pharmaceutical Research, 2012. **29**(11): p. 3143-3155.
72. Gordi, T., et al., *Pharmacokinetic analysis of C-14-ursodiol in newborn infants using accelerator mass spectrometry.* Journal of Clinical Pharmacology, 2014. **54**(9): p. 1031-1037.
73. Ikeda, T., et al., *Microdose pharmacogenetic study of C-14-tolbutamide in healthy subjects with accelerator mass spectrometry to examine the effects of CYP2C9*3 on its pharmacokinetics and metabolism.* European Journal of Pharmaceutical Sciences, 2013. **49**(4): p. 642-648.
74. Blanchard, J. and S.J.A. Sawers, *The absolute bioavailability of caffeine in man.* European Journal of Clinical Pharmacology, 1983. **24**(1): p. 93-98.
75. Boulton, D.W., et al., *Simultaneous oral therapeutic and intravenous 14C-microdoses to determine the absolute oral bioavailability of saxagliptin and dapagliflozin.* British Journal of Clinical Pharmacology, 2013. **75**(3): p. 763-768.
76. Schwab, D., et al., *A novel double-tracer technique to characterize absorption, distribution, metabolism and excretion (ADME) of C-14 tofogliflozin after oral administration and concomitant intravenous microdose administration of C-13 tofogliflozin in humans.* Clinical Pharmacokinetics, 2013. **52**(6): p. 463-473.
77. Duchateau, G., et al., *Absolute oral bioavailability and metabolic turnover of beta-sitosterol in healthy subjects.* Drug Metabolism and Disposition, 2012. **40**(10): p. 2026-2030.

78. Leonowens, C., et al., *Concomitant oral and intravenous pharmacokinetics of trametinib, a MEK inhibitor, in subjects with solid tumours.* British Journal of Clinical Pharmacology, 2014. **78**(3): p. 524-532.
79. Graham, R.A., et al., *Single and multiple dose intravenous and oral pharmacokinetics of the hedgehog pathway inhibitor vismodegib in healthy female subjects.* British Journal of Clinical Pharmacology, 2012. **74**(5): p. 788-796.
80. Graham, R.A., et al., *A single dose mass balance study of the hedgehog pathway inhibitor vismodegib (GDC-0449) in humans using accelerator mass spectrometry.* Drug Metabolism and Disposition, 2011. **39**(8): p. 1460-1467.
81. Malfatti, M.A., et al., *Use of microdosing and accelerator mass spectrometry to evaluate the pharmacokinetic linearity of a novel tricyclic GyrB/ParE inhibitor in rats.* Antimicrobial Agents and Chemotherapy, 2014. **58**(11): p. 6477-6483.
82. Tse, S., et al., *Disposition and metabolic profiling of C-14 cerlapirdine using accelerator mass spectrometry.* Drug Metabolism and Disposition, 2014. **42**(12): p. 2023-2032.
83. King, C.L., et al., *Debio 0507 primarily forms diaminocyclohexane-Pt-d(GpG) and -d(ApG) DNA adducts in HCT116 cells.* Cancer Chemotherapy and Pharmacology, 2012. **69**(3): p. 665-677.
84. Ghosh, D., et al., *Intercalation and induction of strand breaks by adriamycin and daunomycin: a study with human genomic DNA.* DNA and Cell Biology, 2012. **31**(3): p. 377-386.
85. Henderson, P.T., et al., *A microdosing approach for characterizing formation and repair of carboplatin-DNA monoadducts and chemoresistance.* International Journal of Cancer, 2011. **129**(6): p. 1425-1434.
86. Scharadin, T.M., et al., *Accelerator mass spectrometry for quantifying Gemcitabine DNA incorporation and identifying Gemcitabine chemosensitivity.* Abstracts of Papers of the American Chemical Society, 2014. **248**.
87. Yamazaki, H., et al., *Zone analysis by two-dimensional electrophoresis with accelerator mass spectrometry of in vivo protein bindings of idiosyncratic hepatotoxicants troglitazone and flutamide bioactivated in chimeric mice with humanized liver.* Toxicology Research, 2015. **4**(1): p. 106-111.
88. Brown, K., et al., *Tamoxifen forms DNA adducts in human colon after administration of a single C-14 -labeled therapeutic dose.* Cancer Research, 2007. **67**(14): p. 6995-7002.
89. Brown, K., *Is tamoxifen a genotoxic carcinogen in women?* Mutagenesis, 2009. **24**(5): p. 391-404.
90. Schebb, N.H., et al., *Metabolism of the antibacterial triclocarban by human epidermal keratinocytes to yield protein adducts.* Journal of Biochemical and Molecular Toxicology, 2012. **26**(6): p. 230-234.
91. Neuwirth, C., et al., *Furan carcinogenicity: DNA binding and genotoxicity of furan in rats in vivo.* Molecular Nutrition & Food Research, 2012. **56**(9): p. 1363-1374.
92. Weng, Z., et al., *Differential genotoxic effects of subchronic exposure to ethyl tertiary butyl ether in the livers of Aldh2 knockout and wild-type mice.* Archives of Toxicology, 2012. **86**(4): p. 675-682.
93. Walton, J.R., *Chronic aluminum intake causes alzheimer's disease: applying Sir Austin Bradford Hill's causality criteria.* Journal of Alzheimers Disease, 2014. **40**(4): p. 765-838.
94. Malfatti, M.A., et al., *Determining the pharmacokinetics and long-term biodistribution of SiO2 nanoparticles in vivo using accelerator mass spectrometry.* Nano Letters, 2012. **12**(11): p. 5532-5538.
95. Wang, B., et al., *Applying accelerator mass spectrometry for low-level detection of complex engineered nanoparticles in biological media.* Journal of Pharmaceutical and Biomedical Analysis, 2014. **97**: p. 81-87.
96. Dong, K., et al., *Study on bone resorption behavior of osteoclast under drug effect using Ca-41 tracing.* Nuclear Instruments & Methods in Physics Research Section B-Beam Interactions with Materials and Atoms, 2013. **294**: p. 671-674.
97. Etminan, N., et al., *Cerebral aneurysms: formation, progression, and developmental chronology.* Translational Stroke Research, 2014. **5**(2): p. 167-173.

98. Etminan, N., et al., *Exploring the age of intracranial aneurysms using carbon birth dating preliminary results.* Stroke, 2013. **44**(3): p. 799-802.
99. Cappuccio, J.A., et al., *C-14 Analysis of protein extracts from Bacillus spores.* Forensic Science International, 2014. **240**: p. 54-60.
100. Qiao, J., et al., *Sequential injection approach for simultaneous determination of ultratrace plutonium and neptunium in urine with accelerator mass spectrometry.* Analytical Chemistry, 2013. **85**(18): p. 8826-8833.
101. Nelson, M.A., et al., *Contemporary fraction of bis[2-ethylhexyl]phthalate in Stilton cheese by accelerator mass spectrometry.* Radiocarbon, 2013. **55**(2-3): p. 686-697.
102. Goldman, R., et al., *Quantitation of benzo a pyrene-DNA adducts by postlabeling with C-14-acetic anhydride and accelerator mass spectrometry.* Chemico-Biological Interactions, 2000. **126**(3): p. 171-183.
103. Buchholz, B.A., et al., *Free flow electrophoresis separation and AMS quantitation of C-14-naphthalene-protein adducts.* Nuclear Instruments & Methods in Physics Research Section B-Beam Interactions with Materials and Atoms, 2010. **268**(7-8): p. 1324-1327.
104. Lightfoot, T.J., et al., *Analysis of DNA adducts by accelerator mass spectrometry in human breast tissue after administration of 2-amino-1-methyl-6-phenylimidazo 4,5-b pyridine and benzo a pyrene.* Mutation Research-Genetic Toxicology and Environmental Mutagenesis, 2000. **472**(1-2): p. 119-127.
105. Sutter, T.R., et al., *Complete cDNA sequence of a human dioxin-inducible messenger-RNA identifies a new gene subfamily of cytochrome-P450 that maps to cytochrome-2.* Journal of Biological Chemistry, 1994. **269**(18): p. 13092-13099.
106. Huang, Z.Q., et al., *Expression of cytochromes P450 in human breast tissue and tumors.* Drug Metabolism and Disposition, 1996. **24**(8): p. 899-905.
107. Shimada, T., et al., *Activation of chemically diverse procarcinogens by human cytochrome P-450 1B1.* Cancer Research, 1996. **56**(13): p. 2979-2984.
108. Hakkola, J., et al., *Expression of CYP1B1 in human adult and fetal tissues and differential inducibility of CYP1B1 and CYP1A1 by Ah receptor ligands in human placenta and cultured cells.* Carcinogenesis, 1997. **18**(2): p. 391-397.
109. Vadlamuri, S.V., et al., *Regiospecific expression of cytochrome P4501A1 and 1B1 in human uterine tissue.* Cancer Letters, 1998. **122**(1-2): p. 143-150.
110. Tang, Y.M., et al., *Development of an antipeptide antibody that binds to the C-terminal region of human CYP1B1.* Drug Metabolism and Disposition, 1999. **27**(2): p. 274-280.
111. Muskhelishvili, L., et al., *In situ hybridization and immunohistochemical analysis of cytochrome P4501B1 expression in human normal tissues.* Journal of Histochemistry & Cytochemistry, 2001. **49**(2): p. 229-236.
112. Stoilov, I., A.N. Akarsu, and M. Sarfarazi, *Identification of cytochrome P4501B1 as the gene mutated in primary congenital glaucoma families linked to the GLC3A locus on 2p21.* American Journal of Human Genetics, 1997. **61**(4): p. A21-A21.
113. Gajjar, K., P.L. Martin-Hirsch, and F.L. Martin, *CYP1B1 and hormone-induced cancer.* Cancer Letters, 2012. **324**(1): p. 13-30.
114. Spink, D.C., et al., *The effects of 2,3,7,8-tetrachlorodibenzo-p-dioxin on estrogen metabolism in MCF-7 breast-cancer cells, evidence for induction fo a novel 17-beta-estradiol 4-hydroxylase.* Journal of Steroid Biochemistry and Molecular Biology, 1994. **51**(5-6): p. 251-258.
115. Liehr, J.G., et al., *4-hydroxylation of estradiol by human uterine myometrium and myoma microsomes, implications for the mechanism of uterine tumorigenesis.* Proceedings of the National Academy of Sciences of the United States of America, 1995. **92**(20): p. 9220-9224.
116. Hayes, C.L., et al., *17 beta-estradiol hydroxylation catalyzed by human cytochrome P450 1B1.* Proceedings of the National Academy of Sciences of the United States of America, 1996. **93**(18): p. 9776-9781.
117. Shimada, T., *Xenobiotic-metabolizing enzymes involved in activation and detoxification of carcinogenic polycyclic aromatic hydrocarbons.* Drug Metabolism and Pharmacokinetics, 2006. **21**(4): p. 257-276.
118. Pfeifer, G.P., et al., *Tobacco smoke carcinogens, DNA damage and p53 mutations in smoking-associated cancers.* Oncogene, 2002. **21**(48): p. 7435-7451.

119. Baird, W.M., L.A. Hooven, and B. Mahadevan, *Carcinogenic polycyclic aromatic hydrocarbon-DNA adducts and mechanism of action.* Environmental and Molecular Mutagenesis, 2005. **45**(2-3): p. 106-114.
120. Melendez-Colon, V.J., et al., *Cancer initiation by polycyclic aromatic hydrocarbons results from formation of stable DNA adducts rather than apurinic sites.* Carcinogenesis, 1999. **20**(10): p. 1885-1891.
121. Penning, T.M., et al., *Generation of reactive oxygen species during the enzymatic oxidation of polycyclic aromatic hydrocarbon trans-dihydrodiols catalyzed by dihydrodiol dehydrogenase.* Chemical Research in Toxicology, 1996. **9**(1): p. 84-92.
122. Nebert, D.W., et al., *Role of the aromatic hydrocarbon receptor and Ah gene battery in the oxidative stress response, cell cycle control, and apoptosis.* Biochemical Pharmacology, 2000. **59**(1): p. 65-85.
123. Harper, P.A., et al., *Polymorphisms in the human AH receptor.* Chemico-Biological Interactions, 2002. **141**(1-2): p. 161-187.
124. Moriguchi, T., et al., *Distinct response to dioxin in an arylhydrocarbon receptor (AHR)-humanized mouse.* Proceedings of the National Academy of Sciences of the United States of America, 2003. **100**(10): p. 5652-5657.
125. Gonzalez, F.J., *CYP3A4 and pregnane X receptor humanized mice.* Journal of Biochemical and Molecular Toxicology, 2007. **21**(4): p. 158-162.
126. Yu, A.M., J.R. Idle, and F.J. Gonzalez, *Polymorphic cytochrome p450 2D6: Humanized mouse model and endogenous substrates.* Drug Metabolism Reviews, 2004. **36**(2): p. 243-277.
127. Hwang, D.Y., et al., *Xenobiotic response in humanized double transgenic mice expressing tetracycline-controlled transactivator and human CYP1B1.* Archives of Biochemistry and Biophysics, 2001. **395**(1): p. 32-40.
128. Li, F., et al., *Lipidomics reveals a link between CYP1B1 and SCD1 in promoting obesity.* Journal of Proteome Research, 2014. **13**(5): p. 2679-2687.
129. Zhang, L.Y., et al., *Characterization of the mouse Cyp1B1 gene - Identification of an enhancer region that directs aryl hydrocarbon receptor-mediated constitutive and induced expression.* Journal of Biological Chemistry, 1998. **273**(9): p. 5174-5183.
130. Tang, W.M., et al., *Isolation and characterization of the human cytochrome p450 CYP1B1 gene.* Journal of Biological Chemistry, 1996. **271**(45): p. 28324-28330.
131. Savas, U. and C.R. Jefcoate, *Dual regulation of cytochrome-P450EF expression via the aryl-hydrocarabon receptor and protein stabilization in C3H/10T1/2 cells.* Molecular Pharmacology, 1994. **45**(6): p. 1153-1159.
132. Stoilov, I., et al., *Sequence analysis and homology modeling suggest that primary congenital glaucoma on 2p21 results from mutations disrupting either the hinge region or the conserved core structures of cytochrome P4501B1.* American Journal of Human Genetics, 1998. **62**(3): p. 573-584.
133. Choudhary, D., et al., *Metabolism of retinoids and arachidonic acid by human and mouse cytochrome P4501B1.* Drug Metabolism and Disposition, 2004. **32**(8): p. 840-847.
134. Guengerich, F.P., *Analysis and characterization of Enzymes*, ed. A.W. Hayes. 1989, New York: Raven Press.
135. Vidal, J.D., et al., *2,3,7,8-Tetrachlorodibenzo-p-dioxin induces CYP1B1 expression in human luteinized granulosa cells.* Archives of Biochemistry and Biophysics, 2005. **439**(1): p. 53-60.
136. Breslow, N.E., *Analysis of survival data under proportional hazards model.* International Statistical Review, 1975. **43**(1): p. 45-58.
137. Hope, A.C.A., *A simplified Monte Carlo significance test procedure.* Journal of the Royal Statistical Society Series B-Statistical Methodology, 1968. **30**(3): p. 582-&.
138. Hothorn, T., F. Bretz, and P. Westfall, *Simultaneous inference in general parametric models.* Biometrical Journal, 2008. **50**(3): p. 346-363.
139. Miller, M.S., et al., *Role of the maternal environment in determining susceptibility to transplacentally induced chemical carcinogenesis in mouse fetuses.* Carcinogenesis, 1990. **11**(11): p. 1979-1984.

140. Miller, M.S., et al., *The formation of 3-methylcholanthrene-initiated lung-tumors correlates with induction of cytochrome-p4501A1 by the carcinogen in fetal but not adult mice.* Toxicology and Applied Pharmacology, 1990. **104**(2): p. 235-245.
141. Crowell, S.R., et al., *In vitro metabolism of benzo a pyrene and dibenzo def, p chrysene in rodent and human hepatic microsomes.* Toxicology Letters, 2014. **228**(1): p. 48-55.
142. Donehower, L.A., et al., *Effects of genetic background on tumorigenesis in p53-deficient mice.* Molecular Carcinogenesis, 1995. **14**(1): p. 16-22.
143. Zhang, F., Y. Wen, and X. Guo, *CRISPR/Cas9 for genome editing: progress, implications and challenges.* Human Molecular Genetics, 2014. **23**: p. R40-R46.
144. Schober, W., et al., *On the species-specific biotransformation of dibenzo a,l pyrene.* Chemico-Biological Interactions, 2006. **161**(1): p. 37-48.
145. Liu, J.Y., et al., *Association between the CYP1B1 polymorphisms and risk of cancer: a meta-analysis.* Molecular Genetics and Genomics, 2015. **290**(2): p. 739-765.
146. ATSDR, *Priority list of hazardous substances*. 2011, Agency for Toxic Substances and Disease Registry: Center for Disease Control.
147. Dennis, M.J., et al., *Factors Affecting the Polycyclic Aromatic Hydrocarbon Content of Cereals, Fats and Other Food-Products.* Food Additives and Contaminants, 1991. **8**(4).
148. Santodonato, J., P. Howard, and D. Basu, *Health and Ecological Assessment of Polynuclear Aromatic Hydrocarbons.* Journal of Environmental Pathology and Toxicology, 1981. **5**(1): p. 1-364.
149. Hattemerfrey, H.A. and C.C. Travis, *Benzo(a)pyrene Environmental Partitioning and Human Exposure.* Toxicology and Industrial Health, 1991. **7**(3).
150. JEFCA, *Sixty-fourth International Meeting Abstracts*. 2005, Joint Food and Agriculture Organization/World Health Organization Expert Committee on Food Additives: Rome, Italy.
151. Menzie, C.A., B.B. Potocki, and J. Santodonato, *Exposure to Carcinogenic PAHs in the Environment.* Environmental Science & Technology, 1992. **26**(7).
152. Brown, K., E.M. Tompkins, and I.N.H. White, *Applications of accelerator mass spectrometry for pharmacological and toxicological research.* Mass Spectrometry Reviews, 2006. **25**(1): p. 127-145.
153. Forsgard, N., M. Salehpour, and G. Possnert, *Accelerator mass spectrometry in the attomolar concentration range for (14)C-labeled biologically active compounds in complex matrixes.* Journal of Analytical Atomic Spectrometry, 2010. **25**(1): p. 74-78.
154. Dueker, S.R., et al., *Early human ADME using microdoses and microtracers: bioanalytical considerations.* Bioanalysis, 2010. **2**(3): p. 441-454.
155. Dueker, S.R., et al., *Quantifying exploratory low dose compounds in humans with AMS.* Advanced Drug Delivery Reviews, 2011. **63**(7): p. 518-531.
156. Penner, N., L. Xu, and C. Prakash, *Radiolabeled Absorption, Distribution, Metabolism, and Excretion Studies in Drug Development: Why, When, and How?* Chemical Research in Toxicology, 2012. **25**(3): p. 513-531.
157. Lang, N.P., et al., *In vivo human metabolism of 2-C-14 2-amino-1-methyl-6-phenylimidazo-4,5-b pyridine (PhIP).* Cancer Letters, 1999. **143**(2): p. 135-138.
158. BinSamat, S., S. Green, and A.H. Beddoe, *The K-40 activity of one gram of potassium.* Physics in Medicine and Biology, 1997. **42**(2): p. 407-413.
159. Savarino, V., S. Vigneri, and G. Celle, *The C-13 urea breath test in the diagnosis of Helicobacter pylori infection.* Gut, 1999. **45**: p. I18-I22.
160. 97/43/Euratom, C.D., *On health protection of individuals against the damages of ionizing radiation in relation to medical exposure, and repealing Directive 84/466/Eurotom.* 1997, Council of Federal Regulations 10 part 20.10003.
161. Ognibene, T.J., et al., *A high-throughput method for the conversion of CO2 obtained from biochemical samples to graphite in septa-sealed vials for quantification of C-14 via accelerator mass spectrometry.* Analytical Chemistry, 2003. **75**(9): p. 2192-2196.
162. Ognibene, T.J., et al., *The LLNL accelerator mass spectrometry system for biochemical C-14-measurements.* Nuclear Instruments & Methods in Physics Research Section B-Beam Interactions with Materials and Atoms, 2004. **223**: p. 12-15.

163. Ognibene, T.J. and G.A. Salazar, *Installation of hybrid ion source on the 1-MV LLNL BioAMS spectrometer.* Nuclear Instruments & Methods in Physics Research Section B-Beam Interactions with Materials and Atoms, 2013. **294**: p. 311-314.
164. Usansky, J., Desai, A, And Tang-Liu, D., *PK Functions for Microsoft Excel.* 2005, Department of Pharmacokinetics and Drug metabolism, Allergan, Irvine, Ca.
165. Perrier, D. and M. Gibaldi, *General derivation of the equation for time to reach a certain fraction of steady-state.* Journal of Pharmaceutical Sciences, 1982. **71**(4): p. 474-475.
166. Rahman, A., J.A. Barrowman, and A. Rahimtula, *The influence of bile on the bioavailability of polynuclear aromatic-hydrocarbons from the rat intestine.* Canadian Journal of Physiology and Pharmacology, 1986. **64**(9): p. 1214-1218.
167. Jongeneelen, F.J., C.M. Leijdekkers, and P.T. Henderson, *Urinary-excretion of 3-hyoxy-benzo(a)pyrene after percutaneous penetration and oral absorption of Benzo[a] pyrene in rats.* Cancer Letters, 1984. **25**(2): p. 195-201.
168. Bouchard, M. and C. Viau, *Urinary excretion of benzo a pyrene metabolites following intravenous, oral, and cutaneous benzo a pyrene administration.* Canadian Journal of Physiology and Pharmacology, 1997. **75**(3): p. 185-192.
169. Mahadevan, B., et al., *Mutations induced by (-)-anti-11R, 12S-dihydrodiol 13S,14R-epoxide of dibenzo a,l lpyrene in the coding region of the hypoxanthine phosphoribosyltransferase (Hprt) gene in Chinese hamster V79 cells.* Environmental and Molecular Mutagenesis, 2003. **41**(2): p. 131-139.
170. Thomas, A.T., et al., *Directly Coupled High-Performance Liquid Chromatography-Accelerator Mass Spectrometry Measurement of Chemically Modified Protein and Peptides.* Analytical Chemistry, 2013. **85**(7): p. 3644-3650.
171. Zhong, Y., et al., *Metabolism of D-10 Phenanthrene to Tetraols in Smokers for Potential Lung Cancer Susceptibility Assessment: Comparison of Oral and Inhalation Routes of Administration.* Journal of Pharmacology and Experimental Therapeutics, 2011. **338**(1): p. 353-361.
172. Wang, J., et al., *Phenanthrene Metabolism in Smokers: Use of a Two-Step Diagnostic Plot Approach to Identify Subjects with Extensive Metabolic Activation.* Journal of Pharmacology and Experimental Therapeutics, 2012. **342**(3): p. 750-760.
173. Hecht, S.S., et al., *Longitudinal study of D-10 phenanthrene metabolism by the diol epoxide pathway in smokers.* Biomarkers, 2013. **18**(2): p. 144-150.
174. Hecht, S.S., et al., *Analysis of Phenanthrene and Benzo a pyrene Tetraol Enantiomers in Human Urine: Relevance to the Bay Region Diol Epoxide Hypothesis of Benzo a pyrene Carcinogenesis and to Biomarker Studies.* Chemical Research in Toxicology, 2010. **23**(5): p. 900-908.
175. Luch, A., *Molecular, clinical and Environmental Toxicology: Volume 1: Molecular Toxicology*, ed. A. Luch. Vol. 1. 2009: Springer Science and Business Media.
176. Guttenplan, J.B., et al., *Mutagenesis and carcinogenesis induced by dibenzo a,l pyrene in the mouse oral cavity: a potential new model for oral cancer.* International Journal of Cancer, 2012. **130**(12): p. 2783-2790.
177. John, A., et al., *Analysis of GSH Conjugates of Bay- and Fjord-Region Dihydrodiol Epoxides of Benzo a pyrene and Dibenzo a,l pyrene and their Transport in Enterocyte-like Caco-2 Cells.* Polycyclic Aromatic Compounds, 2012. **32**(2): p. 221-237.
178. DeMarini, D.M., et al., *Association between mutation spectra and stable and unstable DNA adduct profiles in Salmonella for benzo a pyrene and dibenzo a,l pyrene.* Mutation Research-Fundamental and Molecular Mechanisms of Mutagenesis, 2011. **714**(1-2): p. 17-25.
179. Conney, A.H., et al., *Studies on the metabolism of Benzo[a]pyrene and dose-dependent differences in the mutagenic profile of its ultimate carcinogenic metabolite.* Drug Metabolism Reviews, 1994. **26**(1-2): p. 125-163.
180. Shou, M.G., et al., *Metabolic activation of the potent carcinogen dibenzo a,l pyrene by human recombinant cytochromes P450, lung and liver microsomes.* Carcinogenesis, 1996. **17**(11): p. 2429-2433.
181. Cavalieri, E.L. and E.G. Rogan, *Central role of radical cations in metabolic-activation of polycyclic aromatic hydrocarbons.* Xenobiotica, 1995. **25**(7): p. 677-688.

182. Meinl, W., et al., *Sulfotransferase forms expressed in human intestinal Caco-2 and TC7 cells at varying stages of differentiation and role in benzo a pyrene metabolism.* Drug Metabolism and Disposition, 2008. **36**(2): p. 276-283.
183. Olson, K.C., et al., *Characterization of Dibenzo a,l pyrene-trans-11,12-diol (Dibenzo def,p chrysene) Glucuronidation by UDP-Glucuronosyltransferases.* Chemical Research in Toxicology, 2011. **24**(9): p. 1549-1559.
184. Shimada, T., et al., *Oxidation of xenobiotics by recombinant human cytochrome P450 1B1.* Drug Metabolism and Disposition, 1997. **25**(5): p. 617-622.
185. Buters, J.T.M., et al., *Cytochrome p450 1B1 determines susceptibility to dibenzo a,l pyrene-induced tumor formation.* Chemical Research in Toxicology, 2002. **15**(9): p. 1127-1135.
186. Ralston, S.L., et al., *Stereoselective activation of Dibenzo a,l pyrene and its trans-11,12-dihydrodiol to Fjord region 11,12-diol 13,14-epoxides in a human mammary carcinoma MCF-7 cell-mediated V79 cell mutation assay.* Chemical Research in Toxicology, 1997. **10**(6): p. 687-693.
187. Zhang, S.M., et al., *Identification and quantification of DNA adducts in the oral tissues of mice treated with the environmental carcinogen dibenzo a, l pyrene (DB a, l P) by liquid chromatography-tandem mass spectrometry (LC-MS/MS).* Abstracts of Papers of the American Chemical Society, 2012. **244**.
188. Prahalad, A.K., et al., *Dibenzo a,l pyrene-induced DNA adduction, tumorigenicity, and Ki-ras oncogene mutations in strain A/J mouse lung.* Carcinogenesis, 1997. **18**(10): p. 1955-1963.
189. EPA, U.S., *Proposed guidelines for carcinogen risk assessment.* 2006, Federal Register. p. 17960-18011.
190. Seymour, M., *Accelerating Clinical Insights: How to Use Accelerator Mass Spectrometry to Make Better Early Development Decisions.* Atla-Alternatives to Laboratory Animals, 2010. **38**: p. 15-20.
191. Madeen, E., et al., *Human in Vivo Pharmacokinetics of C-14 Dibenzo def,p chrysene by Accelerator Mass Spectrometry Following Oral Microdosing.* Chemical Research in Toxicology, 2015. **28**(1): p. 126-134.
192. Dolan, J.W., *The role of the signal-to-noise ratio in precision and accuracy.* Lc Gc Europe, 2006. **19**(1): p. 12-+.
193. Tiwari, G. and R. Tiwari, *Bioanalytical method validation: An updated review.* Pharm. Methods, 2010. **1**(1): p. 25-38.
194. Thomas, A.T., et al., *Ultrahigh Efficiency Moving Wire Combustion Interface for Online Coupling of High-Performance Liquid Chromatography (HPLC).* Analytical Chemistry, 2011. **83**(24): p. 9413-9417.
195. Usansky, J., A. Desai, and D. Tang-Liu, *PK Functions for Microsoft Excel*. Department of Pharmacokinetics and Drug Metabolism, Allergan: Irvine, CA.
196. Nebert, D.W., et al., *Oral Benzo a pyrene: Understanding Pharmacokinetics, Detoxication, and Consequences-Cyp1 Knockout Mouse Lines as a Paradigm.* Molecular Pharmacology, 2013. **84**(3): p. 304-313.
197. Sun, Y.-W., et al., *Tissue distribution, excretion, and pharmacokinerics of the environmental pollutant dibenzo[def,p]pyrene in mouse.* Chemical Research in Toxicology, 2015. **28**(7): p. 1427-1433.
198. Shorey, L.E. and D.E. Williams, *Distribution of C-14-Dibenzo a,l pyrene in a Transplacental Model.* International Journal of Toxicology, 2009. **28**(1).